Ministry of Higher Education and Scientific Research

Hassiba Benbouali University of Chlef

Faculty of Technology

Department of Mechanical Engineering

THESIS

Submitted in fulfillment of the requirements for the degree of

DOCTORATE (LMD)

Field: Mechanical Engineering

Specialty: mechanical construction

By

Chaaben ARROUSSI

Title:

Damage under Thermo-mechanical Behavior of Tubular Structures

Defended on…../…../….., in front of the committee members:

Pr. Ali KHELIL	Professor	UHB-Chlef	President
Pr. Mohammed HADJ MELIANI	Professor	UHB-Chlef	Supervisor
Dr. Azeddine BELALIA	MCA	UHB-Chlef	Co- Supervisor
Pr. Abdelkader HOCINE	Professor	UHB-Chlef	Examiner
Pr. Laid AMINALLAH	Professor	UMS-Mascara	Examiner
Dr. Souad MAKHFI	MCA	UIK-Tiaret	Examiner
Dr. Omar BOULEDROUA	MCB	CRD-Sonatrach	Invited

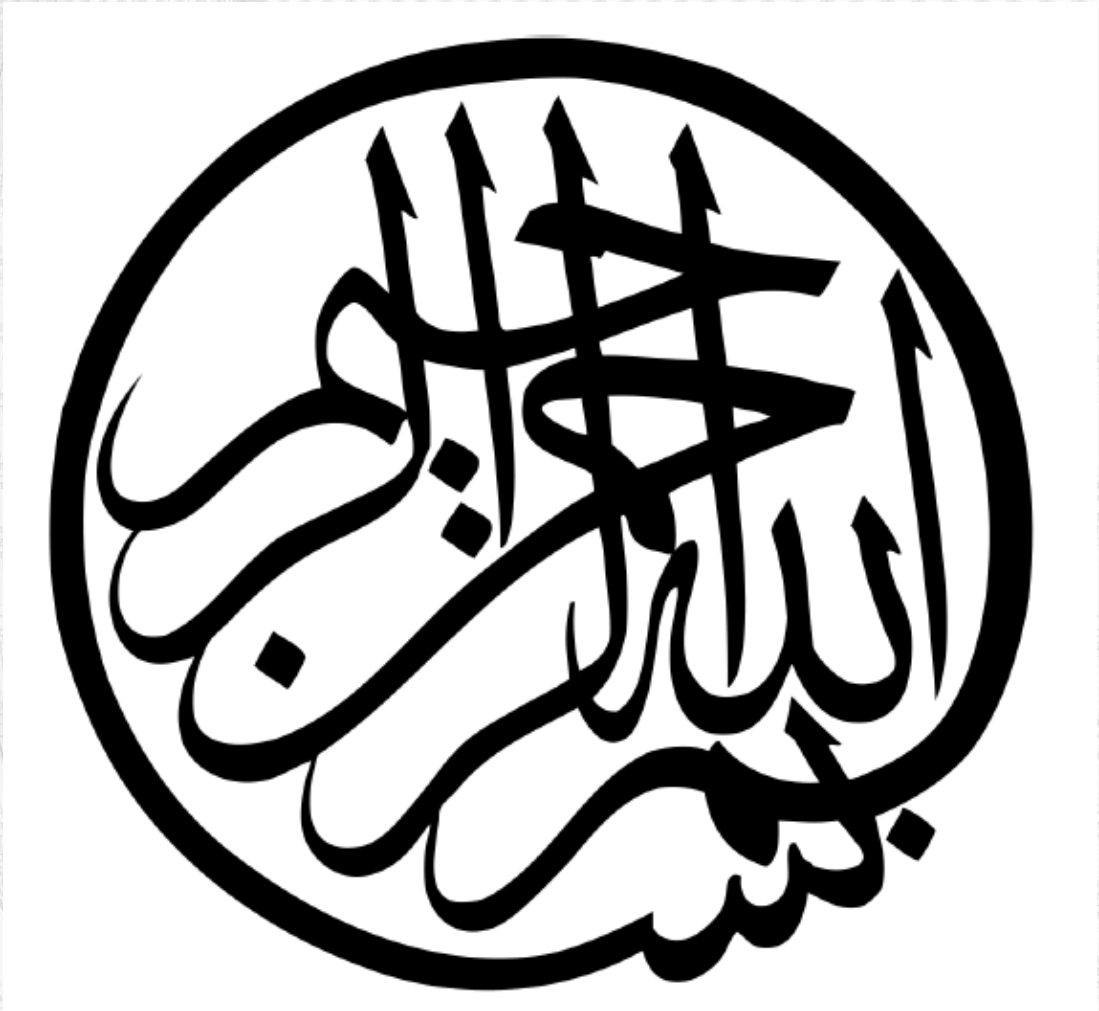
بسم الله الرحمن الرحيم

DEDICATIONS

To

My greatest mother, my greatest father, my dear brothers and my dear sisters.

My wonderful big family "uncles, aunts and cousins"

My earliest teachers who inspired me a desire for lifelong learning.

My best friends and colleagues

ACKNOWLEDGEMENTS

Firstly, I express my gratitude to the Almighty for granting me the strength to successfully complete this humble research endeavor.

I extend warm thanks to my thesis supervisor, **Pr. Mohammed HADJ MELIANI** and my co-supervisor **Dr. Azeddine BELALIA**, for entrusting me with a prestigious and captivating research topic. Despite their busy schedules, they willingly guided me throughout this journey, turning challenges into valuable experiences. I am appreciative of their unwavering support and mentorship, allowing me to discover my own path.

I would also like to acknowledge the committee chair, **Pr. Ali KHELIL**, and the members, **Pr.Abdelkader HOCINE**, **Pr. Laid AMINALLAH**, and **Dr. Souad MAKHFI**, for their esteemed role in evaluating this doctoral thesis. I sincerely appreciate the time and effort they dedicated to examining, analyzing, and providing feedback on my work. Additionally, I would like to express my gratitude to **Dr. Omar BOULEDROUA** for graciously serving as an invited committee member during the defense ceremony.

Words cannot adequately convey my appreciation to my beloved father, mother, and brothers, who have continuously encouraged me and provided unwavering affection and love. They have been the pillars of my efforts.

I cannot conclude without acknowledging the friendly and warm support of my dear friends who have stood by me throughout this doctoral journey. Although the list is extensive, I would like to mention Mr. Belkacem Yagoubi, Dr.Bssam Muthanna, Mr. Abdelilah Bouragba, Mr. Mohammed Teldjoune, Mr. Khaled Madani Kouadria, Mr. Abdelwahab Khledj, Mr. Adel Hadj Amar, Mr. Louza Abdelkader and Ms. Didouh Hadjer, Ms. Khedim Fatima Zohra who deserve special recognition for their advice and support.

I extend my thanks to all the teachers at the University of Chlef, as well as the administrators, for their contributions.

Finally, I would like to specify that this research was conducted at the LPTPM laboratory of the University of Chlef, resulting in the drafting of several published articles and others currently undergoing the publication process.

Chaaben

Abstract

Pipelines play a crucial role in the transportation of petroleum products, including gas, oil, and hydrogen, within the oil industry. However, their operation carries significant risks, including potential material and human damage as well as environmental harm. Among the components of pipeline networks, pipe elbows are particularly critical and susceptible due to stress intensification and bend curvature. They are more prone to various corrosion failure modes compared to straight pipes.

The main objective of this thesis was to employ the Extended Finite Element Method (XFEM) to predict the damage occurring in pipe elbows with defects located at different positions. The analysis focused on the combined effects of internal pressure and in-plane bending moments, both in the closing and opening directions. The study was structured into three distinct sections:

The first section aimed to predict the damage in pipe elbows with defects situated at various positions on the internal wall of the extrados.

In the second section, the influence of service temperature on the damage of pipe elbows was investigated under combined internal pressure and opening bending moments. End-rotation curves were plotted for different service temperatures.

The third section examined the effectiveness of two repair methods for critical defect positions: composite patch, and metallic patch. A parametric analysis was conducted to assess the impact of geometric parameters such as patch thickness, adhesive properties, and patch material on the repair's efficiency.

The findings obtained from the study revealed that the damage in pipe elbows is primarily governed by the bending moment and the proximity of the defect to the critical elbow zone or maximum bending moment. Additionally, the behavior of the elbows under varying temperatures depends on the surrounding environment, which can lead to either brittle or ductile failure modes. The utilization of composite bonding, with different quantities of composite patches, enhances the critical moment, offering greater benefits in comparison to metallic patches. Furthermore, the research validates the precision of the suggested approach in forecasting the performance of the repairs.

Résumé

Les pipelines jouent un rôle crucial dans le transport des produits pétroliers tels que le gaz, le pétrole et l'hydrogène au sein de l'industrie pétrolière. Cependant, leur fonctionnement présente des risques importants, notamment des dommages matériels et humains potentiels ainsi que des impacts sur l'environnement. Parmi les composants des réseaux de pipelines, les coudes de tuyaux sont particulièrement critiques et sensibles en raison de l'intensification des contraintes et de la courbure. Ils sont plus sujets à divers modes de défaillance par corrosion par rapport aux tuyaux droits.

L'objectif principal de cette thèse était de prédire les dommages sur les coudes de tuyaux présentant des défauts situés à différentes positions en utilisant la méthode des éléments finis étendus (XFEM). L'analyse s'est concentrée sur les effets combinés de la pression interne et des moments fléchissant dans le plan, à la fois en fermeture et en ouverture. L'étude était structurée en trois sections distinctes :

La première section visait à prédire les dommages sur les coudes de tuyaux avec des défauts situés à différentes positions sur la paroi interne de l'extrados.

Dans la deuxième section, l'influence de la température de service sur les dommages des coudes de tuyaux a été étudiée sous l'effet combiné de la pression interne et des moments fléchissant d'ouverture. Des courbes de rotation finale ont été tracées pour différentes températures de service.

La troisième section examinait l'efficacité de deux méthodes de réparation pour les positions critiques des défauts : le patch composite et le patch métallique. Une analyse paramétrique a été réalisée pour évaluer l'impact des paramètres géométriques tels que l'épaisseur du patch, les propriétés de l'adhésif et le matériau du patch sur l'efficacité de la réparation.

Les résultats obtenus à partir de l'étude ont révélé que les dommages sur les coudes de tuyaux sont principalement régis par le moment fléchissant et la proximité du défaut par rapport à la zone critique du coude ou au moment fléchissant maximal. De plus, le comportement des coudes en fonction des températures varie en fonction de l'environnement, ce qui peut conduire à des modes de défaillance fragiles ou ductiles. L'utilisation de patch composite, avec différents nombres de patches, améliore le moment critique, offrant ainsi de nombreux avantages par rapport aux patches métalliques. De plus, la recherche valide la précision de l'approche recommandée dans la prévision des performances des réparations.

الملخص

الأنابيب هي وسيلة النقل الأكثر استخدامًا في صناعة النفط لنقل المنتجات البترولية مثل الغاز والنفط والهيدروجين. ومع ذلك، فإن استخدامها يشكل مخاطر كبيرة، بما في ذلك الأضرار المحتملة على المواد والبشر وتأثيراتها على البيئة. ومن بين مكونات شبكات الأنابيب، تُعتبر المرفقات أو الأكواع أجزاء حساسة وحرجة بسبب تكثيف الإجهاد والتأثيرات الناجمة عن الانحناء. فهي أكثر عرضة لأنماط فشل التآكل المتنوعة مقارنة بالأنابيب المستقيمة

كان الهدف الرئيسي لهذه الأطروحة هو التنبؤ بالأضرار في المرفقات أو الأكواع التي تحتوي على عيوب في مواقع مختلفة باستخدام طريقة العنصر المحدود الموسع (XFEM) تحت تأثير الضغط الداخلي المجتمع مع لحظة الثني في الاتجاه الداخلي والخارجي. تم تقسيم هذا العمل إلى ثلاثة أقسام:

القسم الأول كان يهدف إلى تنبؤ الأضرار في المرفقات أو الأكواع التي تحتوي على عيوب في مواقع مختلفة على الجدار الداخلي للخارج

في القسم الثاني، تم دراسة تأثير درجة حرارة الخدمة على الأضرار في المرفقات أو الأكواع تحت تأثير الضغط الداخلي المجتمع ولحظة الثني في الاتجاه الخارجي. تم رسم منحنيات الانحراف النهائي لدرجات الحرارة المختلفة

القسم الثالث كان يدرس فعالية طريقتين للإصلاح في المواقع الحرجة للعيوب: الرقعة المركبة، والرقعة المعدنية. تم إجراء تحليل معلمي لتقييم تأثير المعلمات الهندسية مثل سمك الرقعة والمادة اللاصقة ومواد الرقعة على كفاءة الإصلاح

أظهرت النتائج المستنتجة من الدراسة أن الأضرار في المرفقات أو الأكواع تتحكم فيها بشكل كبير لحظة الثني وموقع العيب قرب أو بعيد عن لحظة الثني القصوى أو المنطقة الحرجة للمرفق. تأثير درجة الحرارة يتم تحكمه بواسطة البيئة حيث تصبح المرفقات هشة أو مطيلة اعتمادًا على هذه البيئة, استخدام الإصلاح المركب، بأعداد مختلفة من الرقع المركبة، يعزز اللحظة الحرجة، مما يوفر فوائد أكبر مقارنةً بالرقع المعدنية. علاوة على ذلك، يؤكد البحث دقة النهج المقترح في توقع أداء الإصلاحات.

TABLE OF CONTENTS

LIST OF FIGURES

CHAPTER I: LITERATURE REVIEW OF PIPELINES

CHAPTER II: METHODS OF SAFETY ASSESSMENT OF PIPE ELBOW

CHAPTER III: Damage predicting of pipe elbows containing single defects for different positions under combined bending and pressure loading

CHAPTER IV: Proposal Engineering Methods to Repair Bend Elbow Pipe Contain Internal Corrosion Defect

LIST OF TABLES

List of Symbols

A	Parametric angle of elliptical crack (°)
Ai	Additional degrees of freedom associated with the Heaviside function
C	Half-length of surface crack (mm)
D_{ext} or D	Outer diameter of pipe (mm)
D_m	Mean diameter of pipe (mm)
E	Young's modulus (MPa)
$F_j(x)$	Singular enrichment functions located at the fracture front
$H(x)$	The Heaviside enrichment function that represents the jump in displacement at the crack
$I_{intrados}$	Decrease in wall thickness
$I_{extrados}$	Increase in wall thickness
K_{eq}	Equivalent stress intensity factor (MPa√m)
K_I, K_{II}, K_{III}	Stress intensity factors for mode one, two and three (MPa√m)
K_{IC} , K_{IIC} , K_{IIIC}	Fracture toughness for mode one, two and three (MPa√m)
L	Longitudinal corrosion defect length (m)
Lf	Lorenzo factor
M	Moment at collapse (N.mm)
M	Moment at instability (N.mm)
M_0	Limit Moment of defect free elbow (N.mm)
M_L	Limit Moment (N.mm)
N	Number of layer
$N_i(x)$	Standard finite element interpolation functions
P	Internal pressure (MPa)
T	Temperature (°C)
X	Weakening factor

A	Depth of defect (mm)
f_P	Failure pressure (MPa)
H	bends characteristics
n	The strain hardening exponent
R	Rotation at collapse (rad)

r^*	Rotation at instability (rad)
t	Pipe wall thickness (mm)
t_a	Thickness of adhesive (mm)
t_p	Thickness of patch (mm)
ε	True strain
θ	Total crack angle (°)
θ	Position of defect at the wall of elbow(°)
σ	True stress (MPa)
$\sigma_1, \sigma_2, \sigma_3$	Principal stresses (MPa)
σ_f	Flow stress (MPa)
σ_l	Longitudinal stress (MPa)
σ_r	Radial stress (MPa)
σ_{ult}	Ultimate stress (MPa)
σ_{VM}	Von Mises Stress (MPa)
σ_y	Yield stress (MPa)
σ_θ	Hoop stress (MPa)

List of Acronyms and Abbreviations

API	American Petroleum Institute
ASME	American Society of Mechanical Engineers
FE	Finite Element
FEA	Finite Element Analysis
FEM	Finite Element Method
XFEM	Extended Finite Element Method
SIF	Stress Intensity Factors
TES	Twice Elastic Slope
UTS	Ultimate Strength
CEA	French Alternative Energies and Atomic Energy Commission
DEMT	Department of Materials Studies for Transport

INTRODUCTION

INTRODUCTION

Pipelines play a crucial role in the petrochemical industry by facilitating the transportation of crude oil and gas. However, as pipelines age, they become susceptible to corrosion, which can lead to catastrophic accidents. Corrosion can manifest on both the internal and external surfaces of the pipeline. Typically, corrosion results in the loss of metal, thereby reducing the thickness of the pipe and compromising its strength. Consequently, the likelihood of pipe failure increases. Therefore, addressing failure due to corrosion-related issues has become a significant concern in maintaining pipeline integrity [1, 2].

The failure of pipelines is considered a significant problem as it results in substantial energy loss and has a direct impact on the economy. However, the consequences of pipeline failure extend beyond energy loss and also affect the environment and human lives, sometimes resulting in fatalities [3, 4]. Corrosion stands out as one of the main factors contributing to pipeline failure. Statistics from North America indicate that corrosion accounts for 41% of oil and gas pipeline failures in Canada. Additionally, there are other phenomena, such as cracking and fatigue, which pose threats to pipelines. These factors increase the risk of leaks and explosions, thereby adversely affecting the reliability and performance of pipelines [5-10]. What we need to do is first predict damage before it happens and before it gets worse. In this work, we present a numerical study by the Extended Finite Element Method (XFEM).

Predicting defects doesn't guarantee their avoidance; instead, it marks the beginning of examining the damage and its repercussions on the pipeline's strength. Within this domain, we investigate the vulnerability level of a composite elbow when a defect is present, employing the XFEM method. If the damage is beyond repair, pipeline replacement becomes necessary. However, if it's reparable, multiple repair methods are available. Many researchers have demonstrated the significance of employing composite materials for repairing damaged pipelines. This approach plays a crucial role in rehabilitating the strength of the affected sections and has proven to be effective in repairing bends and elbows, thereby extending the overall lifespan of the pipeline [11-15].

Bonding composite materials to the damaged section of the pipe is a commonly employed method of repair utilized by numerous pipeline companies. In addition to this approach, alternative repair methods include replacing the damaged section or elbows with undamaged ones, or reinforcing the strength by bonding a metal plate onto the affected area of the pipe or bends.

The objective of this study is to investigate and numerically predict thermo-mechanical damage in pipelines, considering the influence of internal fluid pressure, temperature gradients, external factors, and the effectiveness of various repair methods on the pipeline's resistance capacity

In the following chapters we have studied numerical models to solve our problems of thermo-mechanical damage in tubular structures.

The first chapter focuses on a literature review concerning pipe elbows, exploring the various types of damage that pipelines can undergo, as well as different methods employed for repairing damaged pipelines. .

The second chapter provides an overview of the different techniques utilized for assessing the integrity of corroded pipelines. It discusses the mathematical equations employed in these methods, as well as the experimental and numerical approaches used to calculate the limit load of the pipeline.

The third chapter consists of two main sections that examine the bearing capacity of API X60 pipe elbows. The first section investigates the limit load of elbows with single defects positioned at various locations on the internal wall using the Extended Finite Element Method (XFEM). The second part examines the impact of different temperature values on the limit load of damaged pipe elbows using the XFEM method.

The fourth chapter focuses on evaluating the effectiveness of various repair methods in enhancing the limit load of damaged pipe elbows. These methods include repairing with composite materials, metallic patches, and replacement of the damaged pipe bend. The study assesses the impact of these repair techniques on the overall strength and performance of the damaged pipe elbows.

REFERENCES

[1] Y.K. Lee, Y.P. Kim, M.-W. Moon, the Prediction of Failure Pressure of Gas Pipeline with Multi Corroded Region, Materials Science Forum, 2005, 475:479, pp. 3323-3326

[2] Geon Ho Lee, Hassan Pouraria, Jung Kwan Seo and Jeom Kee Paik. Burst strength behaviour of an aging subsea gas pipeline elbow in different external and internal corrosion-damaged positions, Int. J. Nav. Archit. Ocean Eng. 2015; 7:435~451.http://dx.doi.org/10.1515/ijnaoe-2015-0031.

[3] Y.F. Cheng, Monitor safety of aged fuel pipelines, Nature 2016; 529:156.

[4] J.G. Ramírez-Camacho, F. Carbone, E. Pastor, R. Bubbico, J. Casal, Assessing the consequences of pipeline accidents to support land-use planning, Saf. Sci. 2017; 97:34–42.

[5] Canadian Energy Pipeline Association (CEPA), Pipeline Performance Report, Canada, Calgary, Alberta, 2019.

[6] Pipeline and Hazardous Materials Safety Administration (PHMSA), Pipeline Incident 20 Year Trends, Department of Transportation, Washington DC, US, 2020.

[7] A. Cosham, P. Hopkins, The assessment of corrosion in pipelines–guidance in the pipeline defect assessment manual (PDAM), in: Pipeline Pigging & Integrity Management Conf., Amsterdam, The Netherlands, May 17-18, 2004.

[8] Chattopadhyay J, Tomar AKS. New plastic collapse moment equations of defect-free and throughwall circumferentially cracked elbows subjected to combined internal pressure and in-plane bending moment. Eng Fract Mech 2006; 73:829–54.

[9] Zhixiang D, Shiming S. Analysis and experiments on the plastic limit pressure of elbows. Int J Press Vessels Pip 2006; 83:707–13.

[10] Kim JW, Na MG, Park CY. Effect of local wall thinning on the collapse behavior of pipe elbows subjected to a combined internal pressure and in-plane bending load. Nucl Eng Des 2008; 238:1275–85.

[11] Gerhardus, H.K., Brongers, M.P.H., Thompson, N.G., Virmani, Y.P., Payer, J.H., Corrosion costs and preventive strategies in the United States, Summary 2002;1–12.

[12] Mokhtari, M., Alavi Nia, A., The influence of using CFRP wraps on performance of buried steel pipelines under permanent ground deformations, J. Soil Dynamics and Earthquake Engineering 2015;73:29–41.

[13] Greenwood, C., Composite pipe repair method shows versatility, long-lasting, J. Pipeline Gas 2001; 228:58.

[14] Alexander, C., Wilson, F., Development and testing of the Armor plate pipeline repair system, in: Proceedings of the ASME Energy Sources Technology Conference, American Society of Mechanical Engineers, Petroleum Division, Houston 1999.

[15] Alexander, C., Ochoa, O., Extending onshore pipeline repair to offshore steel risers with carbon–fiber reinforced composites, J. Composite Structures., 2010;92:499–507.

CHAPTER I

Literrateur Review on pipeline

I.1 INTRODUCTION

Elbows are important components of pipelines as they can not only change the direction of a pipeline but also absorb high loads and thermal expansion during service [1]. They are widely used in pipeline engineering, petrochemical engineering, and engineering machinery.

Depending on the specifications, bending can be performed either cold or hot. In cold bending, a bending force is applied, while in hot bending, an electromagnetic current is simultaneously applied to heat a small section of the tube. This provides flexibility in terms of angle, radius, or bending plane, while also reducing the risk of wall-thinning and elastic recovery, resulting in inherently better bending accuracy [2].

The integrity of both the elbow and the entire pipeline may be compromised by various defects that can occur during manufacturing, installation, or operating conditions [3]. The fabrication of pipe elbows by bending the pipeline to the required geometric forms is a frequent requirement in piping systems [4].

Many external defects in pipelines, such as cracks or corrosion, lead to increased energy costs. Traditionally, pipelines with severe corrosion problems have required cutting and removing damaged sections, followed by welding replacement joints or reinforcing them with casing repairs or prefabricated steel casings. This process involves two parts that are placed over the pipe and then welded or bolted together along the damaged section [5]. Recently, repairs using fiber-reinforced polymer composites have emerged and proven effective. The use of composite materials for repairs and reinforcement offers clear advantages over traditional methods. These advantages include reduced repair time and the ability to maintain product transmission during the repair process without causing damage to the system [6].

I.2 PIPE BEND MANUFACTURING

Pipe elbows can be manufactured using various methods, such as forging, casting, or cold bending. In the case of cold bending, the permissible bending radius is approximately 10 times the outside diameter of the pipe.

For high-pressure applications, the most common and reliable method for creating bends is induction bending. In this process, the tube is heated at the bending zone using an induction coil, reaching temperatures of approximately 750 to 900 degrees Celsius. Then, the machine gradually bends the tube to the required radius and angle [7], as shown in Figure I.1.

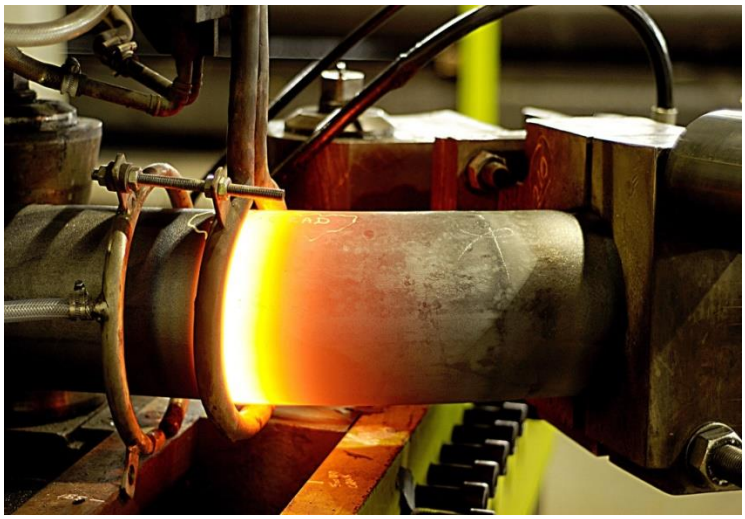

Figure I.1: Induction Bending Process (Courtesy of Induction Bend pipe UK) [7]

It should be noted, however, that the transition from a straight to a bent tube causes changes in both the mechanical properties of the material and the shape of the tube's cross-section [7].

In such cases, a normalization and annealing heat treatment is typically performed to achieve the required material properties for the final product.

As for the change in shape, it involves a geometric transition from a circle to an ellipse. In fact, the curvature in the middle of the bend and the initial ovality of the straight tube increase proportionally as the bending progresses.

Pipes and elbows are not perfectly round; they exhibit ovalization, which refers to the deformation of circularity in each pipe.Ovalization is determined by assessing the ratio between the difference in diameter from the upper (Maximum Diamter) to the lower limits(Minimum Diamter) and the nominal diameter.

$$\text{Ovality} = \frac{D_{\text{upper bound}} - D_{\text{Lower bound}}}{D_{\text{Nominal}}} \qquad \textbf{(I.1)}$$

Figure I.2 gives an idea about the circularity of the initial tube and the ovality of the bent tube.

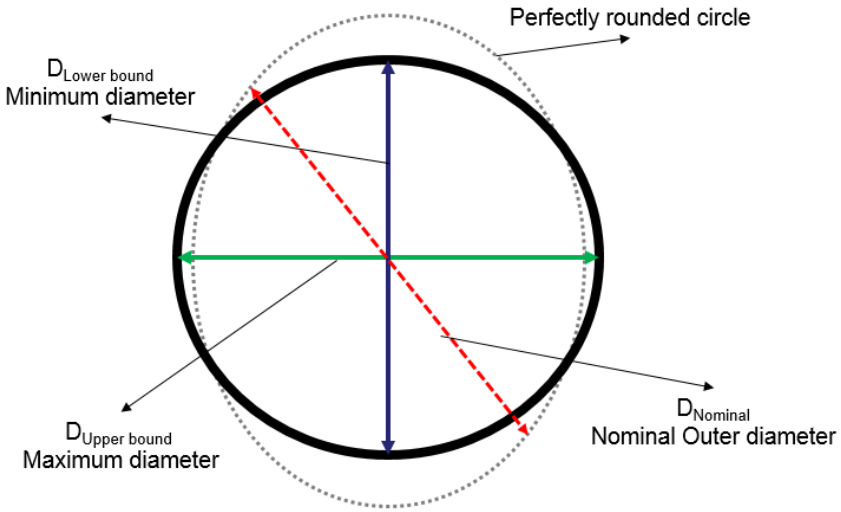

Figure I.2: Pipeline Ovality Diagram [7]

It is generally stated that the ovality at the end and center of the elbow is less than 2.5%. Based on the experience, the elbow manufacturer can provide products with a maximum ovality of 0.9% for pipes with a diameter to thikness ratio (D/t) as low as 15 [7].

Thinning and thickening of the wall thickness is another phenomenon that occurs when bending pipes. The lower side of the pipe intrados becomes shorter while the upper surface extrados - becomes longer, Figure I.3. ASME B31.3 provides formulas to calculate the decrease and increase in wall thickness for one and for the other respectively due to the bending process [7].

$$I_{intrados} = \frac{4\left(\frac{R1}{D}\right)-1}{4\left(\frac{R1}{D}\right)-2} \qquad \textbf{(I.2)}$$

$$I_{extrados} = \frac{4\left(\frac{R1}{D}\right)+1}{4\left(\frac{R1}{D}\right)+2} \qquad \textbf{(I.3)}$$

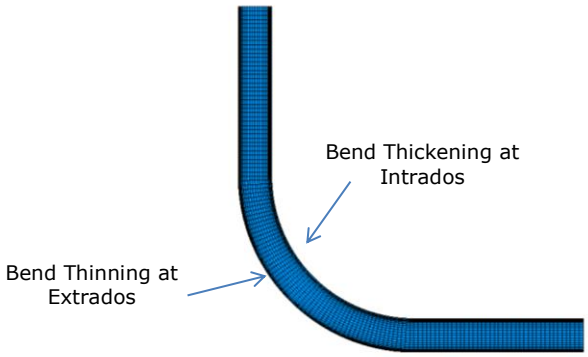

Figure I.3: Pipe bends illustration for intrados and extrados [7]

I.3 EFFECT OF INTERNAL PRESSURE AND BENDING MOMENT ON PIPE BENDS

I.3.1 Pipe bend subject to internal pressure

Elbows are commonly utilized to alter the direction of pipes. The positioning of elbows within piping systems often exposes them to high levels of stress. This increase in stress arises from the high bending flexibility of the cross-section, which causes ovalization when subjected to bending or internal pressure. Furthermore, the surface geometry of the bend can generate significant unbalanced thrust resulting from internal pressure. This internal pressure generates an outward force that tends to straighten the bend, leading to heightened levels of stress and strain [8]. These levels must be predicted and evaluated to ensure that the structure's burst or collapse resistance remains below the maximum allowable working pressure. Lee et al. [9] have conducted assessments and analyses using both design formulas and numerical methods. They identified the most critical corrosion site in the aging elbow API 5L X42 by evaluating various locations of corrosion to ascertain its operational viability. The results revealed that the elbow fails upon reaching its maximum load when exhibiting defects. This approach illustrated that the failure of the pipe elbow is primarily influenced by global instability. The burst pressure of the compromised elbow can be determined by multiplying the Lorentz factor (L_f) with the burst pressure calculated according to the industrial code, as outlined in the subsequent equation:

$$L_f = \frac{Burst\ pressure\ of\ \ straight\ pipe\ with\ defect\ calculated\ by\ industrial\ code}{Burst\ pressure\ of\ \ elbow\ with\ defect} \quad \textbf{(I.4)}$$

Additionally, a new method for calculating the plastic limit pressure of elbows has been developed and evaluated by Lee et al. [10]. This method takes into account elbows without defects and those with multiple localized areas of thinning. The evaluation involved using finite element analysis (FEA) in conjunction with the Goodall formula [11]. The findings showed that the results obtained from the new formula align with those obtained through FEA, indicating the effectiveness of the modeling approach. This new formula is applicable for determining the maximum load that elbows can withstand under internal pressure, even when defects are present.

The FEA analysis revealed significant variations in the ultimate load of elbows with defects, depending on factors such as the mean angle, bend angle, and size of the defect. Notably, if the defect is situated on the extrados and is smaller than half the material thickness, it behaves as a standard structural failure on the bottom surface of the elbow. In such cases, the final rupture of the defective elbow is equivalent to that of an undamaged elbow. Compared to the existing formula, which is known for its conservative nature, the new formula provides more accurate predictions. The Goodall formula and the newly developed formula can be expressed using the following equation:

- Goodall formula:

$$P_{fd} = \frac{\sigma_f\, t}{R_m} \frac{1-\frac{R_m}{R_b}}{1-\frac{R_m}{2R_b}} \bullet DF \bullet MF \bullet BF \qquad \textbf{(I.5)}$$

New formula:

$$\text{If } \begin{cases} a \le \sqrt{100 R_m}\, t \\ c < 0.5t \\ \alpha \ge 0° \end{cases}, \; P_{fd} = \frac{\sigma_f\, t}{R_m} \frac{1-\frac{R_m}{R_b}}{1-\frac{R_m}{2R_b}} \qquad \textbf{(I.6)}$$

Where P_f plastic limit pressure of elbow without defect, P_{fd} plastic limit pressure of elbow with defect, a is depth of defect and c is the length of defect and α circumferential mean angle from the crown of the elbow, and R_b elbow bending radius, R_m elbow mean radius.

Otherwise

$$P_{fd} = \frac{\sigma_f\, t}{R_m} \frac{1-\frac{R_m}{R_b}}{1-\frac{R_m}{2R_b}} \bullet DF \bullet MF \bullet BF \qquad \textbf{(I.7)}$$

Where

$$\mathrm{DF} = \left(1 - \left[\left(\frac{a}{2\pi R_b}\right)^{1.5} + \left(\frac{b}{2\pi R_m}\right)^{1.5} + \left(\frac{c}{t}\right)^{3.2}\right]\right) \qquad \textbf{(I.8)}$$

$$\begin{cases} M_F = \dfrac{\frac{R_b}{R_m} + \sin\alpha}{\frac{R_b}{R_m} + \frac{\sin\alpha}{1.502}} \\ B_F = 1 + \sin\dfrac{\beta}{24} \end{cases} \qquad \textbf{(I.9)}$$

Where *BF* bending angle factor, *DF* defect size factor, *MF* mean angle factor, β circumferential bending angle from the crown of the elbow

Khalajastani et al. [12] have presented a comprehensive solution in the form of a tabular artificial neural network that predicts the ultimate corrosion pressure for elbows under internal pressure. They have collected a Large Database Collection (LDC) of limit pressure capacities by conducting over 1200 3D finite element analyses. These analyses encompass various bend and defect geometries, accounting for both geometric and material nonlinearities. The gathered database is utilized to train a Multi-Layer Perceptron (MLP) neural network, consisting of two

hidden layers with seven neurons in the first layer and 14 neurons in the second layer. The authors have demonstrated that their results align well with experimental data, the DNV prediction (2015) [13], and the Goodall formula [11].

The depth and longitudinal extent of the defect were identified as having the most significant detrimental effect on the load-carrying capacity, while the width of the defect and the radius of curvature of the elbow have minimal impact. Additionally, the circumferential position of the defects was found to be crucial, with the defects closest to the lower surfaces being the most detrimental. The DNV solution (2015) [13] was modified to accommodate elbow corrosion. The new prediction method shows a mean relative difference of -0.067 compared to the FEA results, with a standard deviation of 0.07. Figure I.4 represent the sechmatic view of pipe elbow with defect subject to internal pressure

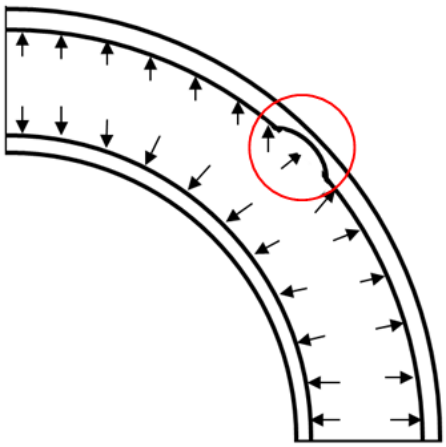

Figure I.4: Pipe elbow with single defect subject to internal pressure.

I.2.2 Pipe bend subject to bending moment

Pipe elbows have the capability to undergo plastic deformation across extensive areas when a system is subjected to excessive stress, due to their unique deformation behavior beyond the elastic limit. In order to better understand the effect of bending moment on the limit load, Shalaby & Younan [14] have explored the phenomena of plastic deformation in elbows subjected to combined bending moments and internal pressure. They utilized finite element analysis with specialized elbow elements but encountered challenges in accurately modeling the initial ovality in the bend and variations in pipe thickness around its circumference. The study primarily focuses on the plastic deformation of the bend and the evolution of plasticity with increasing bending moments. It validates that the bend exhibits a higher capacity for opening than for closing. Full plasticity throughout the thickness at the crown of the bend precedes instability, while complete plasticity around the circumference occurs before structural instability leading to collapse under the opening bending moment. Shuai et al. [15] have investigated the buckling behavior of pipes and determined the critical bending moment for a corroded X80 steel pipe with a corrosion defect under a bending force. They developed a nonlinear finite element model, considering geometric factors such as the shape, depth, length, and width of the corrosion defect, as well as pipe

geometry (outer diameter and wall thickness) and operating pressure. The analysis reveals that pipeline buckling at the corrosion defect is influenced by the shape of the defect.

Abdulhameed et al. [16] have used FEA software to model bends with various nominal pipe diameters, bending angles, and different ratios of bend radius to pipe cross-section radius. The study aimed to cover the behavior of initially circular cross-sections and smooth bends of uniform thickness under in-plane opening/closing bending moments and assess the applicability of the SIF (Stress Intensity Factor) factor provided in the design code for different loading scenarios. A comparison between the CSA-Z662 code [17] and the FEA data was conducted. The research discovered that the direction of the in-plane bending moment acting on the pipe has a significant impact on the stress distribution and flexibility of the pipe bend. Additionally, changes in bend angle and radius were found to have a significant impact on maximum stress, thus necessitating their consideration as parameters in flexibility and SIF factors. Furthermore, depending on the bend angle and direction of the applied bending moment, the CSA-Z662 code [17] values were shown to be non-conservative in certain circumstances. Figure I.15 represents a schematic view of the elbow with internal defect subject to bending moment.

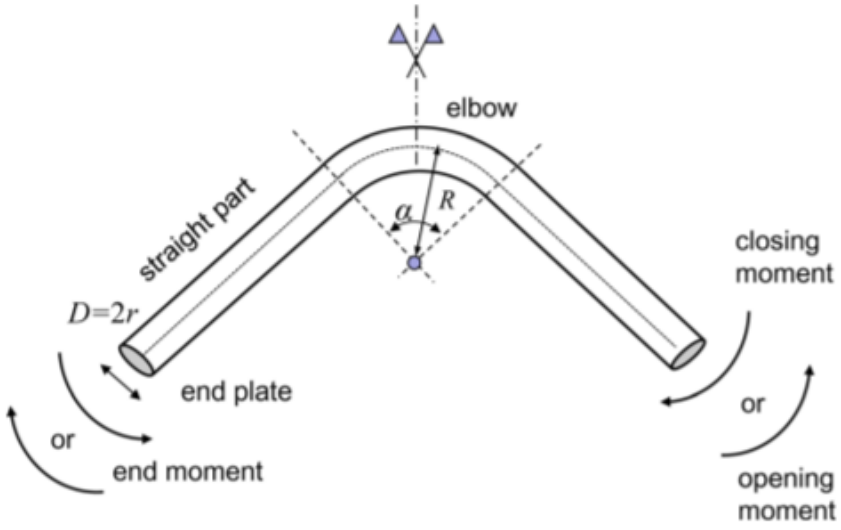

Figure I.5: Pipe elbow subject to bending Moment [18].

I.2.3 Pipe bend subject to interanal pressure and bending moment

Pipe bends are extensively employed in various industrial applications and everyday life as a significant pipeline component. They serve the dual purpose of altering the pipeline's direction and accommodating high loads and thermal expansions during operation [19]. The bending region of the pipeline typically experiences the highest levels of stress due to factors like internal pressure, bending moment, torsion, and weight, making it a potential weak point of the system [20]. Failure of pipe bends commonly occurs through plastic damage controlled by the limit load or ductile rupture resulting from substantial deformation, making the investigation of elbow failures predominantly focused on ultimate load control [21].Figure I.6 represents a schematic

view of a pipe elbow with a defect subject to combined internal pressure and in-plane bending moment.

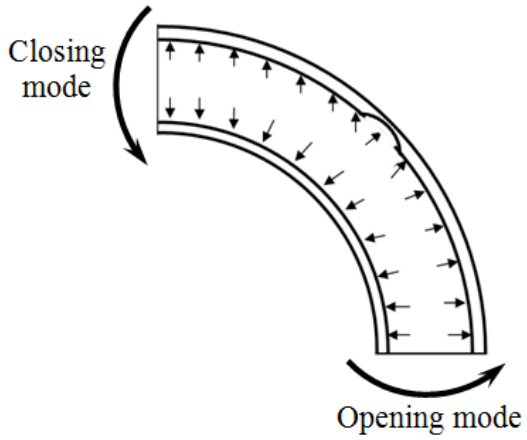

Figure I.6: Pipe elbow subject to combined internal pressure and bending Moment.

To determine the limit load of a pipe elbow under in-plane bending moment and internal pressure, Shalaby and Younan [22] conducted a study using nonlinear finite element analysis. Their objective was to investigate the influence of internal pressure and the geometry of the pipe elbow on its limit load. The results revealed that the limit load initially increases with increasing internal pressure up to a critical value, after which it decreases. This phenomenon, known as the internal pressure hardening effect, is directly associated with the geometric non-linearity caused by the neglect of large displacements. Additionally, the bending stiffness of the elbow cross-section plays a role in plastic instability and collapse loads, which increase with the pipe bending coefficient (h). The effect of internal pressure is dependent on the diameter-to-thickness ratio (D/t) of the bend, with more pronounced effects observed for higher values of (D/t) or lower values of (h).

Chattopadhyay [23] has presented a comprehensive overview of the equations used to determine the bending capacity of pipes. The focus of the discussion is on the difference between opening and closing the elbow, while out-of-plane bending is not addressed. The bending moment of the elbow is derived from the bending moment of a straight pipe but is adjusted to account for the elbow's stiffness, resulting in a reduction factor. The bending moment capacity of a straight pipe is determined by its yield strength, diameter, and wall thickness, and the reduction factor is influenced by the characteristic parameter of the bend and a calibration factor. On the other hand, Chattopadhyay et al. [24] have conducted finite element analysis in the elasto-plastic domain to assess the collapse moments of six bends with diverse bending coefficients, ranging from 0.24 to 0.6. They explored various loading conditions, including in-plane closing/opening moments and varying levels of internal pressure. As a result, they derived two closed-form equations designed to calculate the collapse moment of the bend when subjected to a combination of internal pressure and opening or closing bending moments.

Li et al. [25] have focused on determining the limit loads for pipe bends subjected to combined internal pressure and out-of-plane bending moments. Finite element modeling was employed, considering both small displacement analysis and large displacement analysis. The study explored the impact of internal pressure on limit loads. Significant displacement research revealed that the yield strain (ε_0) significantly influences the limit load. Based on finite element results, engineering evaluation equations for limit loads in pipe bends under combined loads were developed. These proposed equations were validated using experimental data and are considered a suitable choice for assessing limit loads.

Yun et al [26] introduced a novel method, the Deep Fuzzy Neural Network (DFNN), for estimating the bending moments of thin-walled pipes, particularly bends and elbows. The model features a streamlined structure where fuzzy neural network modules are interconnected and iteratively optimized using least squares and genetic algorithms. The Finite Element Analysis (FEA) results serve as the dataset for training the DFNN model, considering various loading conditions and wall-thinning defects at upper, lower, and top positions [26]. The developed model undergoes rigorous training and validation processes using distinct development and test datasets. A cross all defects, the relative Root Mean Square (RMS) error for both the development and test data falls within the range of approximately 0.25% to 0.5%, with values of 0.21% each. The DFNN-based model demonstrates accurate estimations of the collapse moment for thin-walled pipes and bends. Consequently, the proposed DFNN model proves to be an effective tool for promptly and efficiently estimating the thinning condition of bends and elbows and predicting the collapse time.

Hammadi et al. [27] employed the Finite Element Method (FEM) and the XFEM technique to assess structural damage using solid elements. Their study focused on a specific research scenario and revealed that the critical moment ranged from 65 kNm to 85 kNm when the pressure varied between 20 bars and 40 bars. This finding differed by 11 kN from the work of Karamanos [17], who investigated a structure with a thickness of 3 mm and a diameter of 270 mm. The efficiency and applicability of the X-FEM technology and damage criteria were demonstrated, irrespective of the mesh structure. Notably, pre-cracking was not required in their case. It was observed that the purely pressurized tubular structure exhibited higher circumferential stresses compared to other stresses. These stresses were significant and could alter the nature of the compressive stress depending on the load and geometric conditions, as illustrated in Figure I.7. The buckling mode supported by the horizontal elliptical plane of the bend influenced its behavior. Ovalization occurred in the middle of the bend and the damaged area, while the presence of pressure and bending moment led to temperature weakening. This accumulation of mechanical load accelerated structural damage.

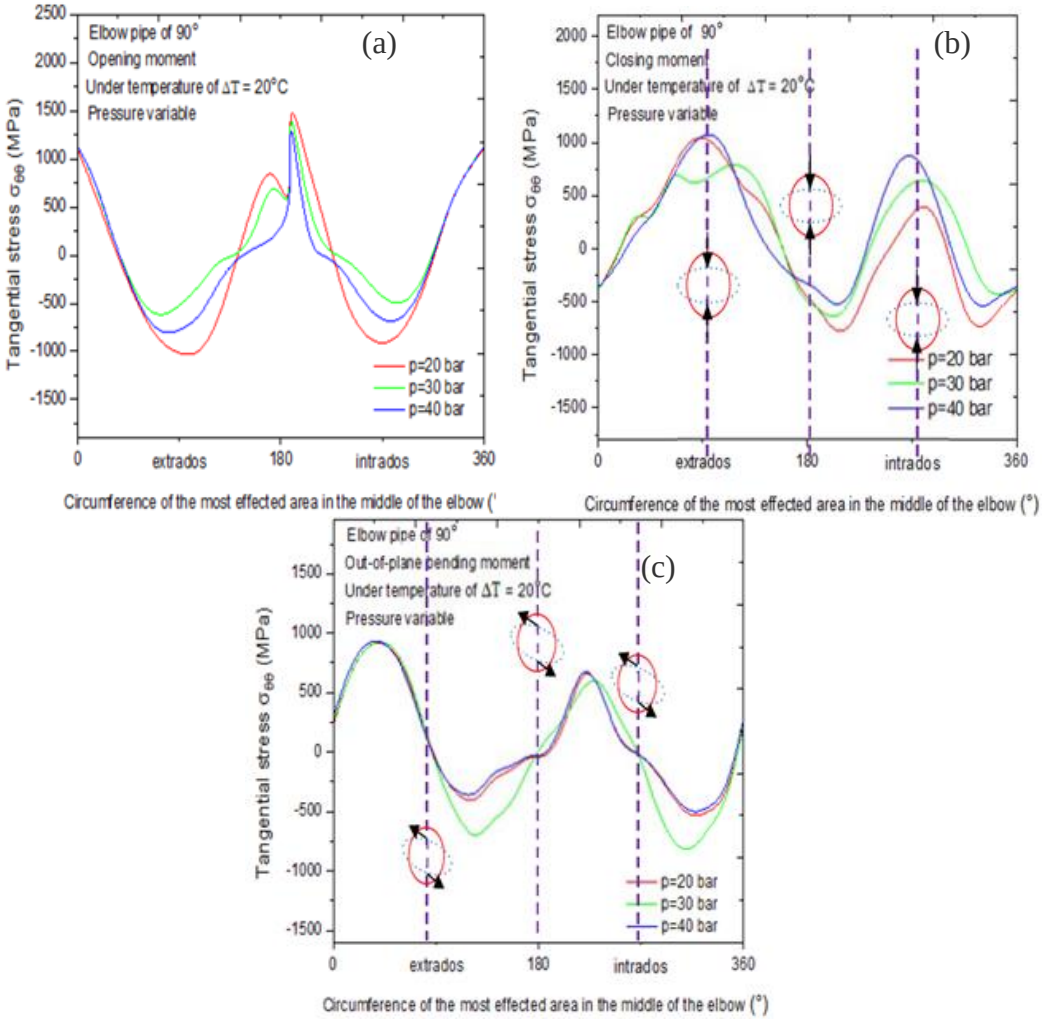

Figure I.7: Tangential stress just before damage with pressure effect in the case of 90° angular elbows and 40°C temperature under opening (a), closing (b), and out-of-plan flexion moment (c) [27].

The phenomenon of the Water hammer is one of the causes of generating the bending moment on the pipe elbow because of the non-permanent flow of liquid, accompanied by a substantial change in pressure, which can endanger the pipe. These changes are the result of permanent interference with the flow conditions. When an incompressible liquid such as water stops in the pipe, it is called a hydraulic shock wave. In other words, it is the sudden stop of water flow when the tap (or any other device) is closed, many researchers have studied this phenomenon and their effect on the pipe system, Hadj Taieb et al [28] have studied the transient response of the metal-polymer combination network, the different states of the network and the different combinations of cast iron, and High-Density Polyethylene (HDPE) pipes are considered for numerical analysis. However, Essaidi and Triki [29] and Oinonen [30] have suggested that the employment of a plastic pipe wall material-based pumping system offers a considerable attenuation impact of the initial pressure-head increase and drop, connected with an expansion effect of the period of pressure-wave oscillations, for a pump failure-initiated transient scenario. Furthermore, when

using a Low-Density Polyethylene (LDPE) pipe-wall material against an HDPE material, the pressure attenuation and period expansion effects are more significant.

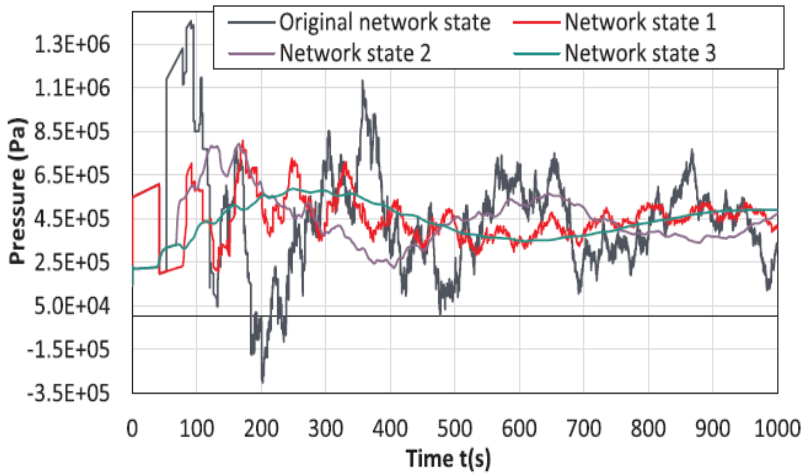

Figure I.8: Variation of pressure in pipe [30].

I.4 DAMAGE OF PIPELINES DURING OPERATION

The pipeline is being transported to the construction site for commissioning. As a result, so-called damages started to appear. Research has been conducted to control the risk of pipeline surface defects [31, 32].

- During transportation, the pipeline oscillates, which may cause microscopic cracks by weakening the material mesh.
- During pipe joining, welds (butt welds) made in the field can crack because they are sometimes made under difficult conditions and may not need to be inspected (insufficient material permeability).
- During maintenance operations, due to the robustness of the machine, the machine hits the pipe and produces a deformation called "deformation" (scratch, dent or fusion (scratch + dent))
- Depending on the condition of the pipeline (buried/submerged or elevated), the environment will have an impact.

For pipelines, damage is caused by the following reasons: corrosion pitting, cracks, dents, scratches and so-called combined defects (dents + scratches). Figure I.9 and Table I.1 summarize the differents damages of pipelines during service and their shape and causes.

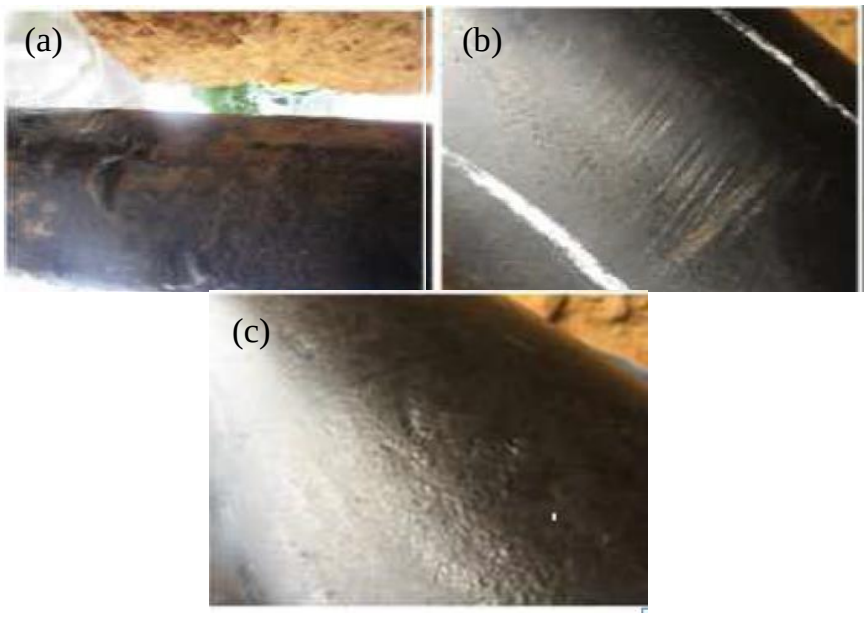

Figure I.9 Coating degradation(a), mechanical scratches(b), and surface pittings(c) [33].

Table I.1: Damage of pipelines during operation

Type of damage	Causes	Consequences	Ref
Cracks	– Hydrogen generated by the welding process. – A hard brittle structure which is susceptible to cracking. – Tensile stresses acting on the welded joint.	– Reduces the integrity of the material. – Reduces the service life of the equipment – Causes environmental pollution and injuries	[34-37]
Scratch	– Contact with foreign objects, resulting in the removal of the material. – Electric shocks (e.g., spike blows) or impact from construction equipment (e.g., impact from bucket teeth)	**Changes in pipe shape:** Ovalization of the cross section near or at positions removed from the point of contact or area of most significant indentation. **Changes in wall thickness:** Thinning due to stretching, usually in a sharp dent or near a scrape, gouge, or similar anomaly.	[38]
Dents	– Ground settlement, landslip, frost heave, earthquake, land erosion, mud flow, washout,	**Changes in localized stresses and strains:** Residual stresses and strains. Stress and strain fields	[38,39]

	and heavy equipment operating over the buried pipe	have axial, circumferential, and radial components. The local stresses and strains are "path dependent," which means they are influenced by the order and magnitude of loads and deformations. **Changes of material properties**: Modification of mechanical (and magnetic) properties of the pipe material due to plastic strain. Strain hardening may increase yield strength, reduce ductility (i.e., tensile elongation),and/or affect toughness. These changes can range from modest, in areas where the local strains are the same order of magnitude as yield strains, to extreme, immediately under a sliding indenter.	
Combined damage (scratches + dents)	– Caused by external aggression (flooding) and a reduction in the thickness of the pipeline (scratches) which causes a local reduction in mechanical resistance. As a result, there is a local reduction in the mechanical resistance of the pipe.	Changes due to phase transformations resulting from rapid heating and cooling.	[39]

I.5 CORROSION PHENOMENON

Corrosion is the physical and chemical interaction between a metal and its surrounding environment, which will cause changes in the properties of the metal, and will usually result in the degradation of the metal itself, its environment or the technical system composed of these two factors. This definition recognizes that corrosion is a harmful phenomenon that can damage materials and reduce their performance [40].

Table I.2 summrizes the differents types of corrsion and their characterestics.

Table I.2: Type of corrosion and their characterestics.

Type of corrosion	Characterestics	Ref
Uniforme corrosion	– Characterized by a relatively uniform corrosion rate over the entire exposed surface. – Generally expected to sacrifice some of the structural components over time, but affects all base metals	[41,42]
Pitting and crevice corrosion	– The loss of metal is limited to the relative metal area. – Corrosion occurs due to local differences in the concentration of oxygen or aggressive ions (such as chloride ions) or ph differences – Related to scale and dirt deposits, which form a barrier between the main flow and the standing water remaining under the scale or dirt deposits	[43,44]
Filiform corrosion	– Starts at coating imperfections (transverse profile cutting, scratches, etc.) And spreads to the metal-paint interface, producing fine filaments. – Oxygen concentration cells induce attack on a metal surface beneath a coating.	[45]

I.6 STATISTICS OF ACCIDENT CAUSES

In the case of a delayed rupture mechanism, the average time from pipeline installation to rupture is 28 years [46]. There are many reasons for pipeline failures. They can be manifested by pipeline ruptures or leaks. Most of these failures are caused by pitting or stress corrosion cracking (SCC), but there are also defects. Ground movement (landslides, earthquakes, etc.) can also cause damage to underground pipelines [46]. Figure I.10 shows the contribution of each type to pipe accidents.

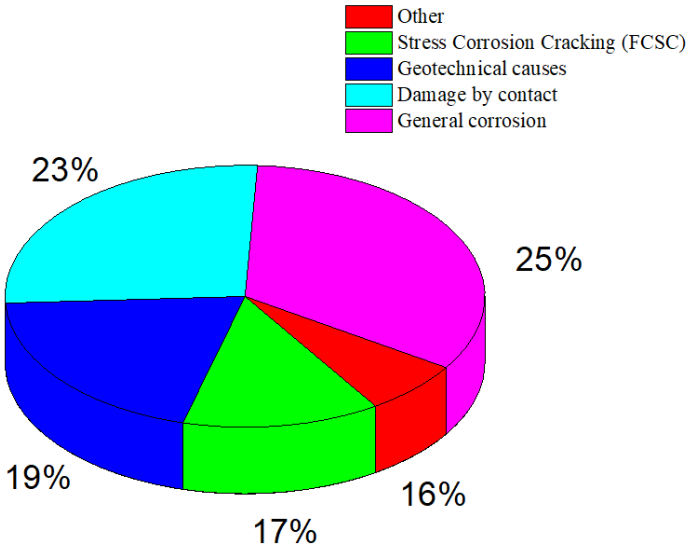

Figure I.10: Causes of in-service pipeline ruptures recorded by ACPRE members [46].

Pipeline operators have been studying these problems for a long time and know how to deal with them. However, we must not ignore external mechanical stresses. Indeed, during excavation work by construction equipment, the pipeline has been damaged or accidentally perforated.

I.7 PIPELINE FAULT DETECTION TECHNOLOGY

Fault detection includes the inspection of the pipe network in the pipeline. In fact, inspection is a set of theories and processes that can provide information about the health of parts or structures without causing failures [47]. The pipeline is subjected two types of forces: internal forces, which are exerted by the pump used to propel the product through the pipeline, and external forces, which result from the movement and pressure of the product being transported (such as gas or oil) inside the pipeline. Consequently, thorough inspection becomes imperative.

- Visual inspection,
- X-ray inspection,
- Ultrasonic testing,
- Intelligent tools detection.

I.8 METHODS OF REPAIR (REHABILITATION) OF PIPELINES

After the assessment of the damage, the choice of the type of repair will be made according to:

- The geometry of the pipe (diameter, bending, etc.)
- The grade of steel used in the manufacture of the steel.The location of the pipe.
- The operating conditions.
- The location of the defect.

- The nature and size of the defect.

A wide range of repair techniques are available. The main ones are composite lining repair, including composite fiber bonding and reinforcement, metal plate, and replacement (figure I.1).

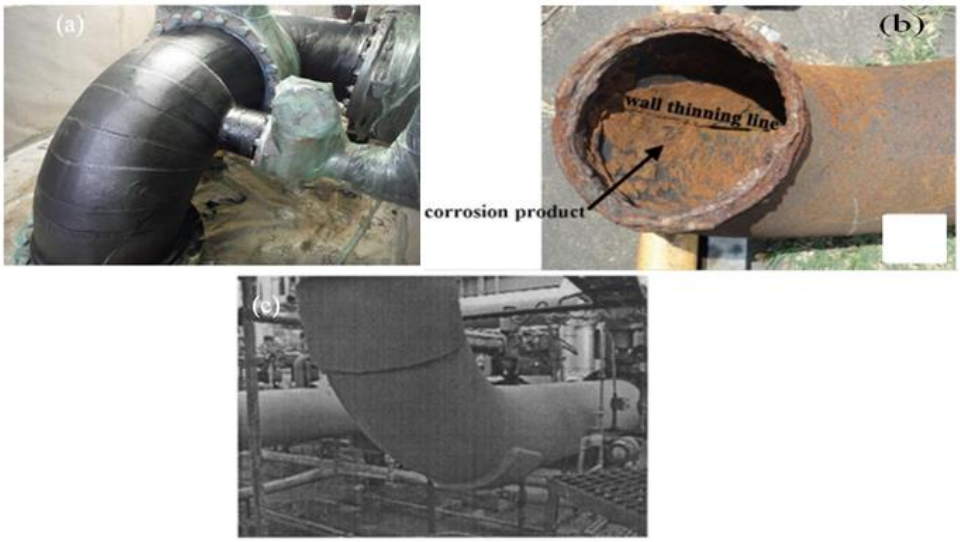

Figure I.11: Different methode of rehabilitation of pipe elbow: composite coating (a), metalic patch (b), and replacement (c) [48, 49].

Table I.3 summarizes the various pipe rehabilitation methods mentioned above.

However there are other repair techniques such as:

- The grinding method,
- The drilling method,
- Repair by half,
- Welded shell,
- Re-coating,
- Cutting and replacement after draining.

These techniques are beyond the scope of this thesis; they are mentioned here for information purposes only.

Table I.3: Methodes of rehabilitation of pipeline

Type of repairing	Characterestics	Ref
Repairing by composite patch	– High-performance materials composed of associations of several materials with complementary properties on a microscopic scale. – Reducing weight. – Orthotropic properties. – Enhancement of capacity of bearing of pipeline. – No fastener holes are required for patch application, no microcracks form, uniform stress transfer occurs, no drilling is required, and repair time and cost are significantly reduced. – Reduction of stress intensity factor.	[50-56]
Repairing by replacement	– The rehabilitation consists of a partial change of the pipeline. – Given the high cost. – Improve the capacity of bearing of pipe elbow based on the angle and bend radius of elbow.	[57-59]
Repairing by Metallic patch	– Allows the rapid repair of corroded steel members. – During tensile and bending situations, avoid brittle debonding of the patch plate. – Studs welded to the base plate near the ends of the connector plates transmit shear stress after the connector plates delaminate. – Cracked pipes did not manifest integrity issues and did not experience failure. – This method of restoration can be confidently applied to pipes with external flaws. – Reduce the stress intensity factor – Improve the capacity of resistence of pipeline.	[60-64]

I.8 CONCLUSION

This chapter examined the bend manufacturing process and the factors affecting pipeline integrity, such as internal pressure and bending moments. We analyzed stress distribution and deformation in different scenarios, highlighting the importance of regular maintenance and monitoring to prevent damage. The adverse effects of corrosion and the common causes of pipeline accidents were reviewed, with the emphasis on preventive measures. Advanced failure detection technologies and effective repair methods were also discussed, highlighting innovations in maintaining pipeline functionality. Overall, this chapter highlights the need for precision manufacturing, continuous monitoring and robust repair strategies to ensure the safe and efficient operation of pipeline systems.

REFERENCES

[1] Li H, Mackenzie D. Characterizing plastic collapse of pipe bends structures. International Journal of Pressure Vessels & Piping, 2006; 83 (2):85-95.

[2] Lanyun Li ,Yang Zhang,Jing Liu,Shuaishuai ,Xu Xiaoguang Fan, Geometric imperfections of large diameter and thick-walled pipe fabricated by push bending with induction heating. The International Journal of Advanced Manufacturing Technology .2021;114:2003–2018

[3] Srivastava A, Prabhakaran KM, Ghosh AK. Studies on the behavior of part-through circumferential crack at intrados in elbows under in-plane bending moment. Nuclear Engineering and Design. 2011; 241: 2386-2397.

[4] Natarajan R, Mirza S. Effect of thickness variation on stress analysis of piping elbows under internal pressure. Comp. Structures. 1984; 18:767-778.

[5] J.M. Duell a, J.M. Wilson a, M.R. Kessler b. Analysis of a carbon composite overwrap pipeline repair system Jr. International: Pressure Vessels and Piping2008 85:782–788.

[6] Mohitpour M, Golshan H, Murray A. Pipeline design and construction: a practical approach. 2nd ed. New York, NY: ASME Press; 2003: 499–518.

[7] Sherif H. EL-Gebaly.Ultra Deepwater Pipe Bend Design Guidelines, Department of Civil and Environmental Engineering. University of surrey 2015.

[8] Diana, Abdulhameed ,Roger Cheng ,Michael Martens ,Samer Adeeb.the influence of the internal pressure and in-plane bending on pipe elbows, resilient infrastructure,London 2016.

[9] Lee, G. H., Pouraria, H., Seo, J. K., & Paik, J. K. Burst strength behaviour of an aging subsea gas pipeline elbow in different external and internal corrosion-damaged positions. International Journal of Naval Architecture and Ocean Engineering, 2015; 7(3):435-451.

[10] Lee, G. H., Seo, J. K., & Paik, J. K. Condition assessment of damaged elbow in subsea pipelines. Ships and Offshore Structures, 2017; 12(1):135-151.

[11] Goodall IW. Lower bound limit analysis of curved tubes loaded by combined internal pressure and in-plane bending moment. Research Division Report RD/B/ N4360, Central Electricity Generating Board, UK.1978.

[12] Khalajestani, M. K., Bahaari, M. R., Salehi, A., & Shahbazi, S. Predicting the limit pressure capacity of pipe elbows containing single defects. Applied Ocean Research.2015;53:15-22.

[13] DNV. Corroded pipelines-recommended practice. RP-F101. Norway: DNV GL; 2015.

14] Shalaby, M. A. & Younan, M. Y.Nonlinear analysis and plastic deformation of pipe elbows subjected. International Journal of Pressure Vessels and Piping,1998.

[15] Shuai, Y., Wang, X. H., & Cheng, Y. F. Buckling resistance of an X80 steel pipeline at corrosion defect under bending moment. Journal of Natural Gas Science and Engineering,2021, 93: 104016.

[16] Abdulhameed, D., Martens, M., Cheng, J. R., & Adeeb, S. Investigation of Smooth Pipe Bends Under the Effect of In-Plane Bending. In Pressure Vessels and Piping Conference ,July 2017, (Vol. 57946, p. V03AT03A054). American Society of Mechanical Engineers.

[17] CSA Z662-15 Canadian code for oil and gas pipeline systems.

[18] Karamanos, S. A., Giakoumatos, E., and Gresnigt, A. M., "Nonlinear 768 Response and Failure of Steel Elbows Under In-Plane Bending and Pressure," 769 ASME J. Pressure Vessel Technol., 2003, 125(4): 393–402.

[19] Li H, Mackenzie D. Characterising plastic collapse of pipe bend structures. International Journal of Pressure Vessels & Piping, 2006;83(2):85-95.

[20] Guo CX. Plastic limit loads for surface defect pipes and bends under combined loads of tension, bending, torsion and internal pressure. Ph.D. thesis . Shanghai, China: East China University of Science and Technology; 1999.

[21] Liu B. Statement on research of limit load for bend. Process Equipment & Piping 2012; 49(5):64-66.

[22] Shalaby, M. A., & Younan, M. Y. A. Limit loads for pipe elbows with internal pressure under in-plane closing bending moments,1998.

[23] Chattopadhyay J. The Effect of Internal Pressure on In-Plane Collapse Moment of Elbows. Nuclear Engineering and Design, 2002:133-144.

[24] Chattopadhyay, J., Nathani, D. K., Dutta, B. K., & Kushwaha, H. S. Closed-form collapse moment equations of elbows under combined internal pressure and in-plane bending moment. J. Pressure Vessel Technol., 2000, 122(4):431-436.

[25] Li, J., Zhou, C. Y., Xue, J. L., & He, X. H. Limit loads for pipe bends under combined pressure and out-of-plane bending moment based on finite element analysis. International Journal of Mechanical Sciences, 2014, 88:100-109.

[26] Yun, S.H., et al., Collapse moment estimation for wall-thinned pipe bends and elbows using deep fuzzy neural networks. 2020. 52(11): 2678-2685.

[27] Hammadi, N., et al., Using XFEM to predict the damage with temperature of the steel pipe elbows under bending and pressure loading. 2021. 15(55): 345-359.

[28] Taieb, L.H., et al., Effect of integrating polymeric pipes on the pressure evolution and failure assessment in cast iron branched networks. 2020. 235: p. 107158.

[29] Oinonen, A. Water Hammer and Harmonic Excitation Response With Fluid-Structure Interaction in Elbow Piping. Journal of Pressure Vessel Technology, 2022,144(3).

[30] Essaidi, B., & Triki, A. On the transient flow behavior in pressurized plastic pipe-based water supply systems. Journal of Water Supply: Research and Technology-Aqua, 2021. 70(1): 67-76.

[31] Fitness-for-Service. API Recommended Practice 579, 1st ed. American Petroleum Institute, January 2000.

[32] M. E. Mayfield, W. A. Maxey, and G. M. Wilkowski, “Fracture Initiation Tolerance of Line Pipe“, Paper F, 6th Symposium on Line Pipe Research, American Gas Association,

[33] Habibi, H., Jarram, P., & Vo, C. Field Verification of Remote Magnetic Monitoring of Stress for Buried Unpiggable Pipelines. In Unpiggable Pipeline Solutions Forum, Houston, USA,2017.

[34] Lucas, B., Mathers, G., & Abson, D. Defects-Hydrogen Cracks in Steels– Identification. TWI, Cambridge, feb 2000.

[35] Du, G., Kong, Q., Zhou, H., & Gu, H. Multiple cracks detection in pipeline using damage index matrix based on piezoceramic transducer-enabled stress wave propagation. Sensors, 2017, 17(8):1812.

[36] Ginzel, R. K., & Kanters, W. A.Pipeline corrosion and cracking and the associated calibration considerations for same side sizing applications. NDT. net, 2002 ; 7(07) :1435-4934.

[37] M. ALLOUTI. Étude de la nocivité de défauts dans les canalisations de transport de gaz Telles les éraflures, les enfoncements ou leurs combinaisons, Thèse de Doctorat, Université Paul Verlaine de Metz, 2010.

[38] Cosham, A. and Hopkins, P. The pipeline defect assessment manual. Project IPC02-27067, International Pipeline Conference 2002, Alberta, Canada.

[39] Hopkins, P. and Leis, B.N. Mechanical damage gaps analysis. Final Report to Pipeline Research Council International, Battelle; March 2003.

[40] Scully. J. Corrosion protection. Principes fondamentaux Elservier Masson, 1997

[41] V.Q.kinth, Corrosion et protections des matériaux métalliques. callaquechimie, 2008.

[42] B. Schramm, A.D., A.Kuhlles, revêtement et lacorrosion. Technique compact 10e édition, décembre2004.

[43] Bakouri, H.E., Etude de l'inhibition de la corrosion de l'acier doux au carbone en milieu acide orthophosphorique par un antibiotique organique. Université Mohammed 1: Oujda

[44] Priya, V.S., A.A. Fathima Sabirneeza, and S. Subhashini, Synergistic Effect of Halides Ions on the Corrosion Inhibition of Abelmoschus esculentus Seed Extract on Mild Steel in H2SO4.Asian Journal of Chemistry, 2013. 25(13): p. 7083-7087.

[45] Khireche, S., Elaboration et étude de la corrosion des alliages Al-Zn et Al-Sn dans une solution à 3% en poids NaCl. Tizi ouzou.

[46] ACPRE. Risk Management Program Standard" (for use in the Pipeline Risk Management Demonstration Program), Produced by the Joint Risk Management Standard Team, The Office of Pipeline Safety, American Petroleum Institute, Interstate Natural Gas Association of America, National Association of Pipeline Safety Representatives, Gas Research Institute(1996).

[47] Marie- Pierre FOULC, José alcorta durabilite des assemblages par colles : etat de l'art. (Module Ma5), 2008.

[48] Pipe Repair Methods: How to Repair Leaks in Critical Water Lines, https://www.advancedfrpsystems.com/pipe-repair-methods/.

[49] Kim, Y. J., Lee, K. H., Oh, C. S., Yoo, B., & Park, C. Y. Effect of bend angle on plastic loads of pipe bends under internal pressure and in-plane bending. International journal of mechanical sciences, 2007. 49(12) :1413-1424.

[50] Ahmed Benhamouda, étude du comportement des fissures dans les tubes sous pression interne. Thèse de magistère en génie mécanique option : Mécanique des surfaces et Matériaux. Université MENTOURI Constantine, 2010.

[51] Yu Zhang , Ziyun Cheng & Zhike Jia .Failure loads analysis of corroded pipe repaired by composite material under tension and internal pressure, Journal of Marine Engineering & Technology, DOI: 10.1080/20464177.2020.1826675

[52] PRASSE .T .MICHEL F, MOOK. G, schulte. K, BAUHOFER. W. : A comparative investigation of electrical resistance acoustic emission during cyclic loading of CFRP laminates. Composites science and technology, 2000

[53] SOUTIS. C. SMITH. F. C , MATTHEWEUS. K. L. : predicting the compressive enginiring performance of carbon fiber renforced plastics composites. Composites part A : Applied science and manufacturing (Incorporating composites and composites Manufacturing), 1999, 31, PP 531-536.

[54] Tahar Nateche, Réhabilitation et Renforcement des Canalisations sous pression en présence des défauts de surfaces, thèse de doctorat en génie mécanique. Université des sciences et de la technologie Mohamed Boudiaf. Oran. Algérie.

55] Hossein Hosseini-Toudeshky, Ebrahim Fadaei, Effects of Composite Patch Geometry on Collapse Load of Pressurized Steel Pipes with Internal Longitudinal Flaws, Applied Mechanics and Materials 2012; (152-154), pp 381-386.

[56] Marioli-Riga, Z., & Gdoutos, E. E. Composite patch repair methodology for damaged aircrafts structural components. In 2004 SEM Annual Conference (pp. 7-10).

[57] M. Rameil« Handbook of Pipe Bursting Practice » http://www.nodig.de/doks/pdf/Read-Inside_Handbook_pipe-bursting-2007.pdf

[58] Chapter 11 « Pipeline Rehabilitation by Slipliningwith Polyethylene Pipe » https://plasticpipe.org/pdf/chapter11.pdf;

[59] Goland, M., & Reissner, E. The stresses in cemented joints. Journal of Applied Mechanics, 1944, 11:A17–A27.

[60] Hart-Smith, L. J. Adhesive-bonded double-lap joints. NASA contract report 1973, CR-112235.

[61] Ikeda, T., & Ishikawa, T. Shear strength of patch repair method combined adhesion and stud bolt. Proceedings of Constructional Steel JSSC, 2016, 24:74–79. (in Japanese).

[62] Ishikawa, T., Komoto, T., Hattori, A., & Kawano, H. Proposal of plate repair method combined adhesion and stud bolt for steel members. Journal of Structural Engineering, 2016,62A: 639–646.

[63] Shimizu, M., Ishikawa, T., Hattori, A., & Kawano, H.Failure criteria for debonding of patch plate bonded onto steel members subjected to bending. Journal of JSCE, 2014, 2:310–322.

[64] Smith, S. T., & Teng, J. G. Interfacial stresses in plated beams. Engineering Structures, 2001,23(7):857–871.

CHAPTER II

Methods of safety assessment of pipe elbow

II.1 INTRODUCTION

In the petrochemical, energy, and pharmaceutical sectors, pressure pipes are widely used. When a pressure pipe leaks or breaks, it can result in serious accidents such as explosions, fires, and toxic exposures. A significant majority of pipe explosion catastrophes are caused by elbows [1]. Elbows play a critical role in the pressure pipe transportation network. The stress conditions in elbows are more complex than in straight pipes, and they often become areas of stress concentration in the pipe system [2]. The quality of the pipes directly impacts the integrity and reliability of the entire piping system [3]. Therefore, it is crucial to study the bearing capacity of elbows to establish a solid foundation for evaluating their safety. This chapter discusses the assessment of pipelines with and without defects.

Mathematical formulas have been developed to describe the integrity of pipelines and to ensure their operational longevity. Several authors have evaluated the bearing capacity using various methods, including analytical, experimental, and numerical approaches. Graphical methods, in particular, are considered essential for determining the maximum moment value and accurately estimating the remaining lifespan of pipelines before they need to be replaced or repaired.

II.2 ANALYTICAL MODEL

II.2.1 Capacity of bearing of pipe elbow under only in plane bending moment

There has been a significant amount of debate surrounding the term "limit load", including how it should be calculated or measured, and how it should be applied in the design of pipe components. Analytical advancements in this area have been based on idealized limit analysis principles. The theoretical limit load, as defined by these theories, represents the maximum load that can be generated from an analytical model of the structure. In the case of pipe bends, all theoretical limit loads are derived from limit analysis theorems.

To simplify the process and obtain bounding solutions, both lower bound and upper-bound solutions have been developed to bracket the theoretical limit load [4]. Spence and Findlay [5] have further contributed to this field by obtaining approximate bounds on limit moments for in-plane bending. Their approach involved combining previously published studies with limit theorems of perfect plasticity. The results were presented in a non-dimensional format, covering a wide range of realistic pipe bend configurations and providing valuable design information.

In summary, their investigation yielded significant findings that can be effectively summarized as follows:

$$\begin{aligned} M_L &= 0.8h^{0.6}(D^2 t\sigma_y), \text{ for } h \le 1.45 \\ &= (D^2 t\sigma_y), \text{ for } h \ge 1.45 \end{aligned} \qquad \textbf{(II.1)}$$

Where M_L is the limit load, h bend factor, t thickness, D diameter, and σ_y yield stress.

Calladine [6] derived a relationship that determines the value of the pure bending moment at which the entire plastic bending of the bend occurs, based on classical limit analysis.

$$M_L = 1.19\pi h^{2/3} r^2 t\ \sigma_y\ ,\ for\ h \le 0.5 \quad \textbf{(II.2)}$$

Based on experimental research conducted at Atomic Energy and Alternative Energies Commission CEA, Department of Materials and Technologies Studies DEMT, Touboul et al. [7] presented the following equations for the collapse moments of elbows in the case of closing and opening bending moments, respectively:

$$M_L = 0.715 h^{2/3}(4 r_m^2 t \sigma_y) \quad \textbf{(II.3)}$$

$$M_L = 0.722 h^{1/3}(4 r_m^2 t \sigma_y) \quad \textbf{(II.4)}$$

Drubay et al [8] have suggested the closing mode collapse moment by:

$$M_L = 0.769 h^{2/3}(4 r_m^2 t \sigma_y) \quad \textbf{(II.5)}$$

Where r_m is the mean rayon of the elbow and t is thickness of elbow and h is the bend factor. All of the previous equations only apply to pure in-plane bending moments. The influence of internal pressure is not considered.

Goodall [9] conducted a comprehensive study on large displacements and obtained an approximate solution for the instability of elbows under in-plane closure bending forces. The maximum load-carrying capacity of the elbow with a factor (h = 0.5) can be determined by:

$$M_L = 1.04 h^{2/3}(D^2 t \sigma_y)/(1+\beta) \quad \textbf{(II.6)}$$

Where:

$$\beta = \left(2 + \frac{(3h)^{2/3}}{3}\right) \cdot 4 \sqrt{\frac{3(1-\nu^2)}{\pi}} \cdot \frac{\sigma_y}{E} \cdot \frac{r_m}{t}$$

II.2.2 Capacity of bearing of pipe elbow under combined internal pressure and bending moment

Through small displacement analysis, Goodall [10] was the first to propose a closed-form equation for the limit load of elbows under combined internal pressure and in-plane bending moment. The equation proposed is as follows:

$$M_L = 1.04 h^{2/3}\left(1 - \frac{P r_m}{2 t \sigma_y}\right)^{1/3}(D^2 t \sigma_y) \quad \textbf{(II.7)}$$

Because the stiffening effect of internal pressure is not considered in this small displacement approximation solution, the magnitude of the limit load is reduced by internal pressure.

Chattopadhyay et al [11] have provided two closed-form equations to evaluate the collapse moment based on previous findings of the normalized limit moments for various elbow Diameters subjected to different levels of constant internal pressure and closing/opening in-plane bending moments.

For closing case:

$$M_L = 1.122\,h^{2/3} + 0.175\,p/h - 0.508\,p^2 \quad \textbf{(II.8)}$$

For opening case:

$$M_L = 1.047h^{1/3} + 0.124\,p/h^{1.2} - 0.568\,p^2 \quad \textbf{(II.9)}$$

The condition of applicability of this equation is: $0.24 \le h \le 0.6\, and\, 0.0 \le p \le 1.0$

Based on Griffiths' experimental results [12], Miller [13] was the first to develop the closed-form PCM equation for elbows with through-wall cracks. Miller [13] provided the following equation to evaluate the collapse moment (ML) for elbows with through-wall circumferential fractures, ranging from the crown to the extrados, exposed to in-plane bending moments:

$$\frac{M_L}{M_0} = 1 - \frac{3\theta}{2\pi} \quad \textbf{(II.10)}$$

$$M_0 = 0.935(4R^2 t\,\sigma_f)h^{2/3} \quad \textbf{(II.11)}$$

Where 2θ represents the total crack angle, and 'σf' denotes the material flow stress, typically taken as the average of the yield and ultimate strength.

Based on Griffiths' experimental results [12], Zahoor [14] also proposed closed-form PCM equations for through-wall cracked elbows under in-plane bending moments. The equation suggested for the TCC (Through-Crack-Crown) elbow is as follows [14]:

$$M_L = M_0\left[1 - 0.2137\left(\frac{a}{D_m}\right) - 0.0485\left(\frac{a}{D_m}\right)^2 - 1.0559\left(\frac{a}{D_m}\right)^3\right] \quad \textbf{(II.12)}$$

Condition of applicability:

$$\begin{cases} \dfrac{a}{D_m} \le 0.8 \\ h \le 0.5 \\ \dfrac{D_m}{t} \ge 15 \end{cases}$$

Where M_0 is defined by Equation (II.11), a represents half of the crack depth, D_m is the mean diameter of the elbow cross-section, t denotes the elbow wall thickness, and h corresponds to the elbow factor or bends characteristics.

II.3 EXPERIMENTAL PROCEDURE

Xiaohui Chen [15] utilized the ratcheting behavior of steel pipe elbows in their experimental study, which involved the following steps:

- The straight pipe was welded to the ends of the elbow to allow pressurization of the specimens.
- Connection blocks were installed at the pipe ends of the elbow specimens and connected to the loading bar through pins.
- The top loading bar of the elbow was attached to the top clip head of the cyclic pull-push test machine, which controlled the opening and closing of the elbow.
- The bottom loading bar was linked to the bottom clip head of the test machine. A hydraulic accumulator was used to maintain a constant internal pressure during cycling.

The test machine software was configured with a triangular loading waveform. Finite element analysis was conducted to investigate three common loading waveforms. Figure II.1 illustrates the schematic drawing of the test setup.

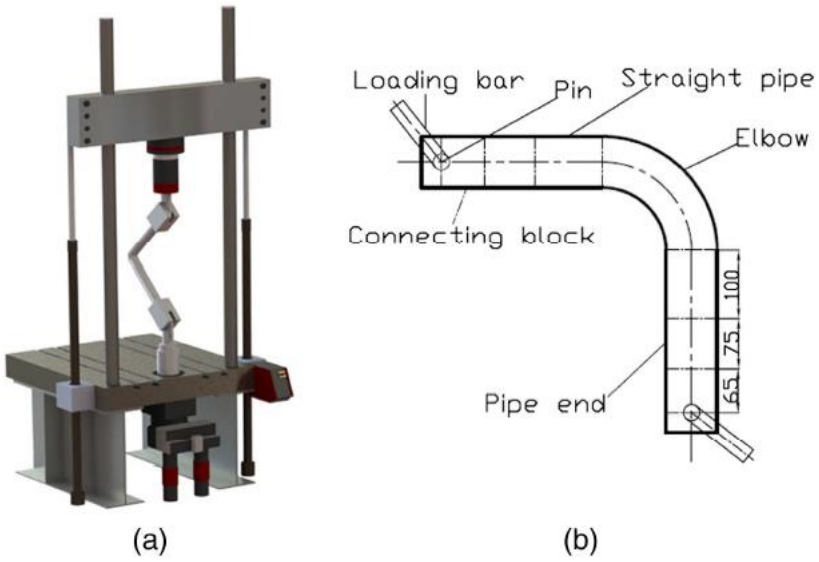

Figure II.1: schematic drawing of test set-up (a) Experimental apparatus; and (b) elbow specimen [15].

Chattopadhyay et al. [16] conducted a study on the limit load of cracked pipe elbows under in-plane bending moments (opening/closing). They performed fracture tests and analyzed the results using non-linear finite element analysis and the R6 method. A comparison of the obtained results was then carried out. Figure II.2 illustrates the description of the test setup.

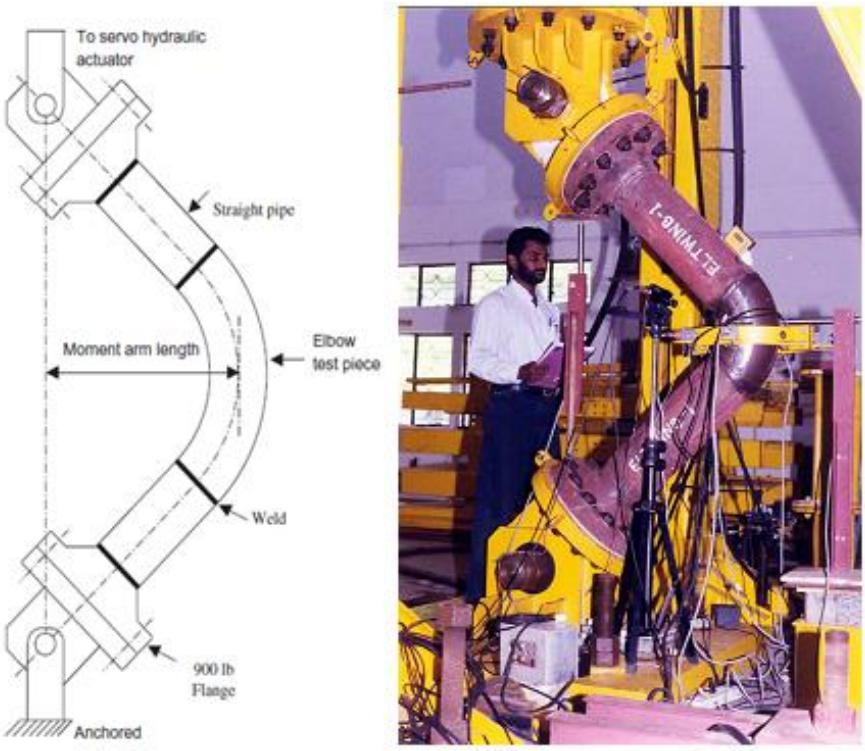

Figure II.2: Schematic drawing and Photograph of elbow test set-up [16].

The crack initiation loads obtained from the fracture experiments were compared to the predictions made by the Finite Element and Option 2 R6 techniques. It can be observed from Figure II.3 that there is a reasonable match between the experimental and predicted values.

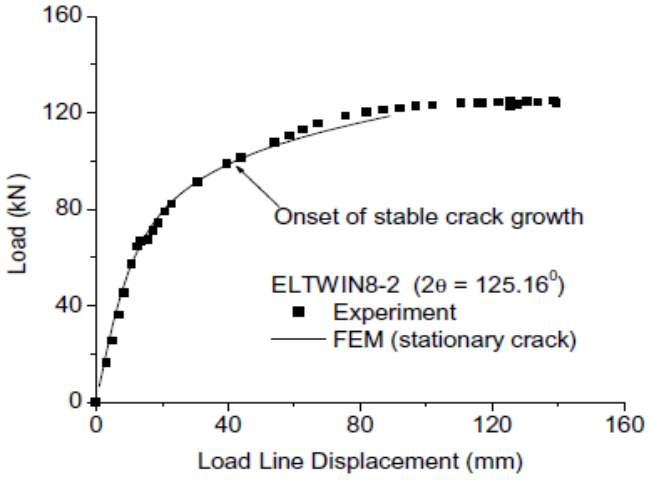

Figure II.3: Comparison of numerical and experimental results [16].

II.4 NUMERICAL METHODS

II.4.1 Extended Finite Element Method (XFEM)

The Extended Finite Element Method (X-FEM) has emerged as a powerful numerical technique for analyzing crack growth problems. The concept of X-FEM was introduced in

1974 by Benzley [17], who proposed the idea of using an asymptotic solution with enrichment near the crack tip to solve static failure problems. Subsequently, Attrulli et al. [18] and Nash Gifford et al. [19] further developed this method and achieved highly accurate results for static fracture analysis. Later, Melenek and Babuska [20] developed the basic unitary segmentation method of the Finite Element Method (PUFEM). Belytschkol and Black [21] made significant contributions in advancing the X-FEM approach. Sukumar et al. [22] extended the X-FEM method to model 3D fractures, while Stolarska et al. [23] combined the level set method with X-FEM to predict crack growth. Belytschko et al. [24] developed a new X-FEM formulation for arbitrary crack propagation in shells. Several researchers, including Moes [25], Chahine [26], Budyn [27], Gupta [28], Wang [29], and Hou [30], have utilized the X-FEM method to simulate fracture mechanics behavior in both static and dynamic cases.

According to Belytschko and Moes [31], the displacement field $U(x)^h$ can be expressed using the finite element approximation with the following equation:

$$U\left(x\right)^h = u^{FE} + u^{enr} \quad \textbf{(II.13)}$$

$$U(x)^h = \sum_{i \epsilon Ntot}^{n} N_i\left(x\right)u_i + \sum_{i \epsilon Nsaut} N_i\left(x\right)H\left(x\right)\mathrm{a}_i + \sum_{i \epsilon Nsing} N_i\left(x\right)(\sum_{j=1}^{4}\mathrm{F_j}\left(\mathrm{x}\right)\mathrm{b_{ji}}) \quad \textbf{(II.14)}$$

Where:

u^{FE}*:* Displacement field of finite element, u^{enr}*:* the enriched displacement, $N_i(x)$: Standard finite element interpolation functions. $H(x)$: The Heaviside enrichment function that represents the jump in displacement at the crack tip. a_i: Additional degrees of freedom associated with the Heaviside function. F_j (x): Singular enrichment functions located at the fracture front.b_{ji}: Additional degrees of freedom associated with the singular functions.These terms and functions are utilized within the Extended Finite Element Method (X-FEM) to incorporate the effects of cracks or fractures into the finite element analysis, allowing for accurate modeling of crack propagation and behavior.

The following equation represents the function $H(x)$:

$$H\left(x\right) = \begin{cases} -1 \quad pour \quad x < 0 \\ +1 \quad pour \quad x > 0 \end{cases} \quad \textbf{(II.15)}$$

The function $H(x)$ thus takes the values + 1 or -1 depending on which side of the crack one is located on. The enrichment function, shown as a schematic in Figure II.4, demonstrates the uniqueness of the crack front F_j nearby (x). The following equation may be used to represent it:

$$\left\{F_j\left(x\right)\right\} = \left\{\sqrt{r}\sin\frac{\theta}{2}, \sqrt{r}\cos\frac{\theta}{2}, \sqrt{r}\sin\frac{\theta}{2}\sin\theta, \sqrt{r}\cos\frac{\theta}{2}\sin\theta\right\} \quad \textbf{(II.16)}$$

Where (r, θ) is the polar coordinate system, with the fracture tip as its origin [32].

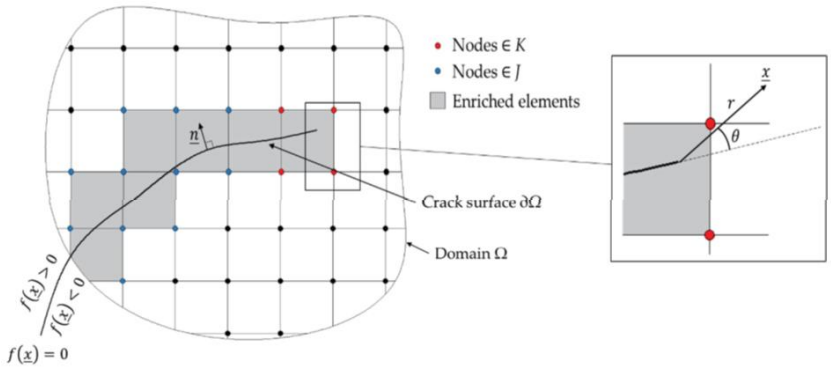

Figure II.4: Illustration of the extended finite element method (XFEM) approach [32].

II.4.2 Stress Intensity Factor (SIFs)

The stress intensity factor (SIF), denoted by *K*, and is dependent on the geometry, size, and stress distribution of the crack. According to Irwin's [33] failure criterion, the local stress field around the crack tip in a linear elastic material can be characterized by the stress intensity factor *K*. When the *K* factor exceeds the critical value K_c, which is a material property, the stress field near the crack tip exhibits crack-like behavior (as shown in Figure II.5).

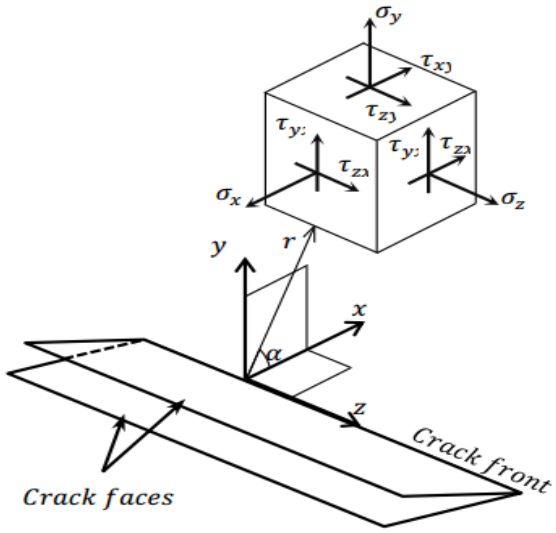

Figure II.5: Distribution of stresses at the crack tip [34].

Irwin [33] proposed three types of stress intensity factors (SIF) based on the force distribution on the crack surface and the propagation of energy along the crack. These three modes are illustrated in Figure II.6.

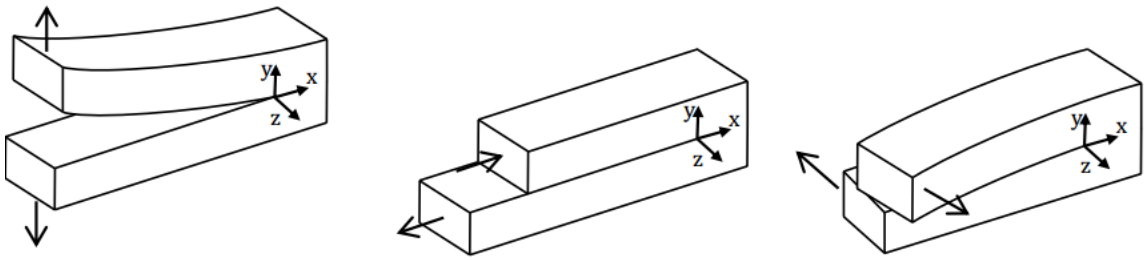

(a) (b) (c)

Figure II.6: Three standard loading modes of a crack, (a) Mode I: opening mode, (b) Mode II: in-plane shear mode, and (c) Mode III: tearing-antiplane shear mode [34].

It is worth noting that in the case of longitudinal cracks, the Mode I SIF (K_I) has a greater influence compared to the other modes, namely Mode II (K_{II}) and Mode III (K_{III}) [35-37].

The stresses in the vicinity of the crack tip are given by the following relations:

$$\sigma_x = \frac{K_I}{\sqrt{2\pi r}}\cos\frac{\theta}{2}\left(1-\sin\frac{\theta}{2}\sin\frac{3\theta}{2}\right)$$
$$\sigma_y = \frac{K_I}{\sqrt{2\pi r}}\cos\frac{\theta}{2}\left(1+\sin\frac{\theta}{2}\sin\frac{3\theta}{2}\right) \qquad \textbf{(II.17)}$$
$$\sigma_{xy} = \frac{K_I}{\sqrt{2\pi r}}\cos\frac{\theta}{2}\sin\frac{\theta}{2}\cos\frac{3\theta}{2}$$

In a general form:

$$\sigma_{ij} = \frac{K_I}{\sqrt{2\pi r}} f_{ij}(\theta) \qquad \textbf{(II.18)}$$

With: r and θ are polar coordinates of the considered point, and $K_I = \sigma_\infty\sqrt{\pi a}$ the Stress Intensity Factor in ($MPa\sqrt{m}$)

A correction coefficient "C" should be incorporated into the expression of K to account for the finite dimensions and geometry of the specimen. This coefficient is provided for each type of specimen in the form of a polynomial function of the ratio (a/w), where "w" represents the width of the specimen. :

$$K_I = C\sigma\sqrt{\pi a} \qquad \textbf{(II.19)}$$

In the case of a cyclic loading between σ_{max} and σ_{min}, the amplitude of the K factor is defined by:

$$\Delta K = C\left(\sigma_{max}-\sigma_{min}\right)\sqrt{\pi a} \qquad \textbf{(II.20)}$$

Let:

$$\Delta K = K_{\max} - K_{\min} = K_{\max}\left(1-R\right) \quad \textbf{(II.21)}$$

Irwin postulated that the condition $K \geq K_c$ represented a criterion of failure; K and K_c are given by the following relations:

$$K = C\sigma\sqrt{\pi a}$$
$$K_c = C\sigma_c\sqrt{\pi a} \quad \textbf{(II.22)}$$

Where σ_c is the value reached by the stress applied at failure.

In the pipe, stress is applied in two directions, as shown in Figure II.7: circumferential stress and longitudinal (or axial) stress. The different sources of circumferential and longitudinal stresses are as follows:

- Internal operating pressure is the most important pressure component,
- Pipe fabrication will generate residual stresses,
- Internal pressure on the oval pipe will produce bending stress,
- Settlement and landslides cause secondary stresses,
- Temperature changes along the pipeline axis.

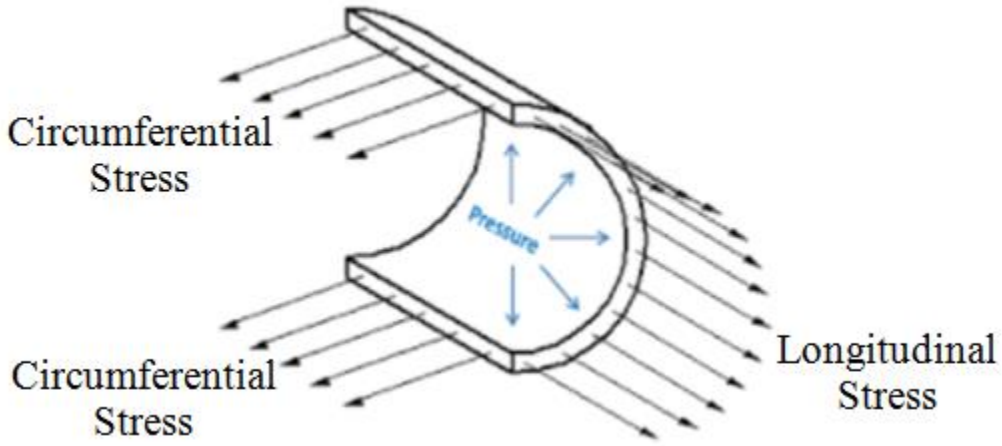

Figure II.7: Stresses on a pipeline [38].

$$\sigma_p = \frac{\mathrm{P\,R}_m}{2t} \quad \textbf{(II.23)}$$

In addition to longitudinal cracks, circumferential cracks (as shown in Figure II.8) can propagate through the entire thickness of the pipe under various stress conditions, potentially leading to sudden rupture. The stress intensity factor for a pipe subjected to uniaxial tension and bending moment can be calculated using the following formula [39]:

$$K_I = (F_t \sigma_t + F_b \sigma_{b)} \sqrt{\pi R_m \theta}) \quad \textbf{(II.24)}$$

With:

$$\begin{cases} \sigma_t = \dfrac{F}{2\pi R_m t} \\ \sigma_b = \dfrac{\mathrm{M}}{2\pi R_m{}^2 t} \end{cases} \quad \textbf{(II.25)}$$

F_t and F_b are geometric factors corresponding to σ_t and σ_b representing the normalized stress intensity factor

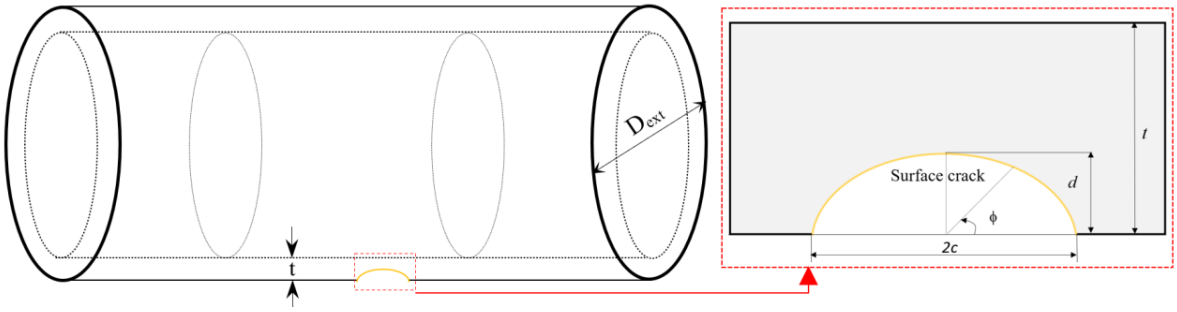

Figure II.8: Semi-elliptical crack in a piping system [39].

II.5 LIMIT LOAD DETERMINATION METHOD

Researchers [40–44] have presented various methodologies for limit load analysis. The concept of plastic limit load assumes the material to be perfectly plastic and only considers scenarios with minimal deformation. However, in reality, due to strain hardening and geometric effects, the occurrence of the plastic limit state using the ideal approach is quite rare. Therefore, it is crucial to consider engineering standards that define the plastic limit load for actual structural problems. Common criteria for determining the plastic limit load include the following [45]:

II.5.1 Double tangent criterion

As illustrated in Figure II.9, the tangents of the elastic and plastic flow sections of the load-strain or load-displacement curves are computed, and the limit load is defined as the load value at the intersection of the double tangents [46].

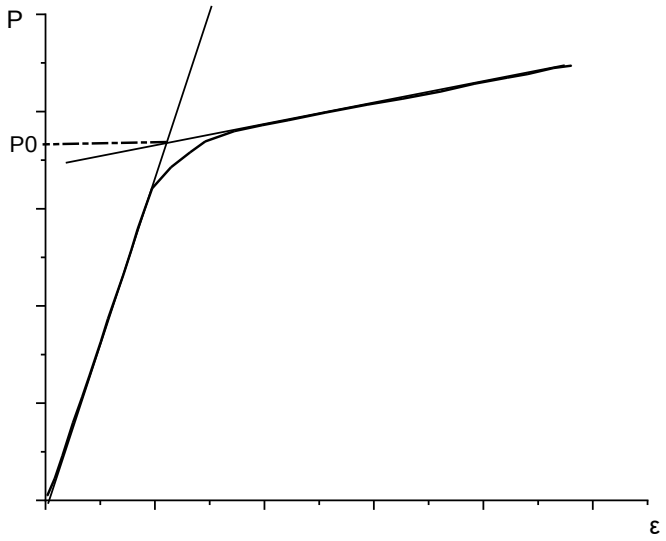

Figure II.9: Double tangent [46].

II.5.2 Double elastic deformation method

The limit load is defined as the load when the deformation reaches twice the elastic deformation at the initial yield load, as shown in Figure II.10 [46].

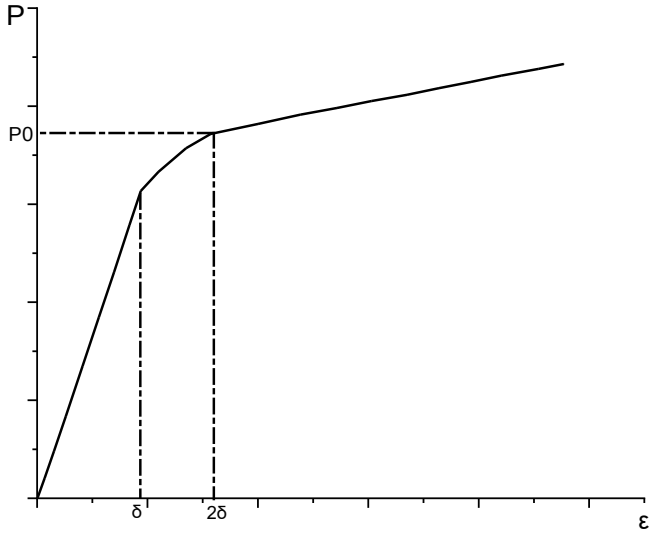

Figure II.10: Double elastic deformation [46].

II.5.3 Twice elastic slope criterion

As seen in Figure II.11, an elastic zone tangent line is drawn across the origin, with the slope being twice the slope of the elastic portion of the load deformation curve, and the load value corresponding to the intersection being the limit load [46]. In this thesis we used this method for calculate the limit load of pipe elbow, so that was calculated the collapse load (*M*) and correspond rotation (*r*) by using the Twice Elastic Slope (TES) and the instability

Moment (*M**) and correspond rotation *(r*)* by using the asymptot horizontal as shown in the figure III.11.

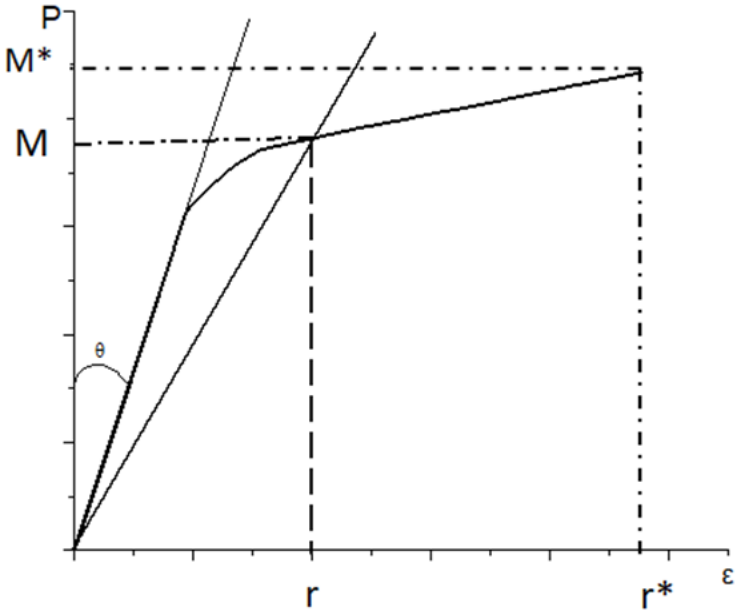

FigureII.11: Twice elastic slope [46].

II.6 CONCLUSION

This chapter examined in detail analytical, experimental, and numerical methods for assessing the structural performance of pipe bends under various loading conditions. The researchers developed an analytical model to determine the load-bearing capacity of pipe bends under combined in-plane bending moments, internal pressure, and bending moments, providing essential information on load limits and failure mechanisms. Experimental tests were also carried out to validate these analytical predictions, highlighting actual behavior and identifying discrepancies. Advanced numerical methods, such as the Extended Finite Element Method (XFEM) and Stress Intensity Factors (SIF), enabled precise stress distribution and crack propagation analysis. Finally, methods for determining limit loads, including the double tangent criterion and the double elastic deformation method, were examined to ensure the safety and reliability of pipeline networks.

REFERENCES

[1] W.P. Han, Large-scale Bending Pipe Hot Rolling System, Yanshan University, Qin Huang Dao, (2016).

[2] D.Z. Wei, X.B. Zheng, Discussion on failure method for oil and gas pipes with defects, Petro Plan and Design 2009, 20 (4):1–5.

[3] Y.M. Peng, C.Y. Zhou, Comparison of safety ass methods for bearing structures with cylindrical shells with volume defects, J. Nanjing Univ. Technol. (Nat. Sci. Ed.) 2014, 36 (5):64–69 .

[4] Shalaby, M. A., & Younan, M. Y. A. Limit loads for pipe elbows with internal pressure under in-plane closing bending moments 1998.

[5] Spence, J., and Findlay, G. E., ‘‘Limit Load for Pipe Bends Under In-Plane Bending,’’ Proceedings of the 2nd International Conference on Pressure Vessel Technology, San Antonio, 1973, pp. 393–399 .

[6] Calladine, C. R., ‘‘Limit Analysis of Curved Tubes,’’ J. Mech. Eng. Sci. Inst. Mech. Eng., 1974, 16(2):pp. 85–87.

[7] Touboul, F., M. Ben Djedidia, and D. Acker. "Design criteria for piping components against plastic collapse: application to pipe bend experiments." Design & Analysis. Pergamon, 1989: 73-84.

[8] Goodall, I. W., "Large Deformations in Plastically Deforming Curved T

ubes Subjected to In-Plane Bending," Research Division Report RD/B/N4312, Central Electricity Generating Board, England 1978a.

[9] Goodall, I. W,, "Lower Bound Limit Analysis of Curved Tubes Loaded by Combined Internal Pressure and In-Plane Bending Moment," Research Division Report RD/B/N4360, Central Electricity Generating Board, England 1978b.

[10] Drubay, B., Moulin, D. and Chapuliot, S. “A16: Guide for Defect Assessment and Leak before Break, Third Draft”. Commissariat a l'Energie Atomique (CEA), DMT 96.096, 1995

[11] Chattopadhyay, J., Nathani, D. K., Dutta, B. K., & Kushwaha, H. S. Closed-form collapse moment equations of elbows under combined internal pressure and in-plane bending moment. J. Pressure Vessel Technol., 2000, 122(4): 431-436.

[12] Griffiths JE. The effect of cracks on the limit load of pipe bends under in-plane bending: experimental study. Int J Mech Sci; 1979, 21(1):19–30.

[13] Miller AG. Review of limit loads of structures containing defects. Int J Press Ves Piping 1988,32:197–327

[14] Zahoor, Akram. "Ductile fracture handbook, vol. 3." Electric Power Research Institute, EPRI P-6301-D N 14 ,1991.

[15] Chen, X. Ratcheting effect of pressurized 90° elbow pipe under in-plane opening, closing, and reverse bending. Journal of Pipeline Systems Engineering and Practice, 2019, 10(2):04019004.

[16] Chattopadhyay, J., Pavankumar, T. V., Dutta, B. K., & Kushwaha, H. S. Fracture experiments on through wall cracked elbows under in-plane bending moment: Test results and theoretical/numerical analyses. Engineering fracture mechanics, 2005,72(10):1461-1497.

[17] Benzley, S.E.: Representation of singularities with isoperimetric finite elements. Int. J. Numer. Methods Eng. 1974, 8(3):537–545.

[18] Atluri, S.N., Kobayashi, A.S., Nakagaki, M.: An assumed displacement hybrid finite element model for linear fracture mechanics. Int. J. Fract. 1975, 11(2): 257–271.

[19] Gifford, L.N., Hilton, P.D.: Stress intensity factors by enriched finite elements. Eng. Fract. Mech. 1978, 10(3):485–496

[20] Melenk, J.M., Babuška, I.: The partition of unity finite element method: basic theory and applications. Comput. Methods Appl. Mech. Eng. 1996, 139(1–4): 289–314.

[21] Belytschko, T., Black, T.: Elastic crack growth in finite elements with minimal remeshing. Int. J. Numer. Methods Eng. 1999, 45 (5): 601–620.

[22] Sukumar, N., Moes, N., Moran, B., Belytschko, T.: Extended unite element method for three-dimensional crack modelling. Int. J. Numer. Methods Eng. 2000, 48: 1549–1570.

[23] Stolarska, M., Chopp, D.L., Moës, N., Beltyschko, T.: Modelling crack growth by level sets in the extended finite element method. Int. J. Numer. Meth. Eng. 2001, 51: 943–960.

[24] Beltyschko, T., Areias, P., Wang, H.W., Xu, J. X.: The extended finite element method for static and dynamic crack propagation 2005. https://www.researchgate.net/publication/239920441,The_extended_finite_element_method_for_static_and_dynamic_ crack propagation/references

[25] Nicolas Moës & Ted Belytschko: X-FEM, de nouvelles frontières pour les éléments finis. Rev. Eur. Elém. 2002,11(2–4):305–318.

[26] Chahine, Elie, Laborde, Patrick, Renard, Yves: Spider XFEM, an extended finite element variant for partially unknown crack-tip displacement. Eur. J. Comput. Mech. 2008, 17(5–7):625–636.

[27] Élisa Budyn & Thierry Hoc: Multiple scales modeling for cortical bone fracture in tension using X-FEM. Eur. J. Comput. Mech. 2007, 16(2):213–236.

[28] Gupta, P., Duarte, C.A., Dhankhar, A.: Accuracy and robustness of stress intensity factor extraction methods for the general ized/eXtended finite element method. Eng. Fract. Mech. 2017, 179:120–153

[29] Wang, Y., Waisman, H., Harari, I.: Direct evaluation of stress intensity factors for curved cracks using Irwin's integral and XFEM with high-order enrichment functions: stress intensity factors for curved cracks using Irwin's integral. Int. J. Numer. Methods Eng. 2017, 112(7):629–654.

[30] Hou, C., Wang, Z., Liang, W., Yu, H., Wang, Z.: Investigation of the effects of confining pressure on SIFs and T-stress for CCBD specimens using the XFEM and the interaction integral method. Eng. Fract. Mech. 2017, 178:279–300.

[31] Moës, N., Belytschko, T.: Extended finite element method for cohesive crack growth. Eng. Fract. Mech.2002, 69(7): 813–833

[32] De Cicco, D., & Taheri, F. Delamination buckling and crack propagation simulations in fiber-metal laminates using XFEM and cohesive elements. Applied Sciences, 2018, 8(12):2440.

[33] Irwin, G.R., Analysis of stresses and strains near the end of a crack traversing a plate, Transactions, ASME, Journal of applied mechanics, 1957, 24: 361-364.

[34] Levén, M. and Daniel, R., Stationary 3D crack analysis with Abaqus XFEM for integrity assessment of subsea equipment (Master's thesis), Chalmers University of Technology, 2012. https://publications.lib.chalmers.se/records/fulltext/164269.pdf;

[35] Ritchie, R.O. and Liu, D., Introduction to Fracture Mechanics. Elsevier, 2021.

[36] Erdogan, F.,Stress intensity factors. Journal of Applied Mechanics, 1983, 50(4b): pp.992–1002,

[37] Newman Jr, J.C. and Raju, I.S., An empirical stress-intensity factor equation for the surface crack. Engineering fracture mechanics, 1981, 15(1-2):pp.185-192.

[38] Trenchlesspedia™, Hoop Stress,en ligne, consulted on October 31, 2023,URL: https://www.trenchlesspedia.com/definition/2799/hoop-stress.

[39] Bassam Gamal Nasser Muthanna, numerical and experimental study of elliptical cracks in the critical positions of pipeline, PhD thesis in mechanical engineering, Chlef , Algeria 2021.

[40] Y.J. Kim, J. Kim, J. Ahn, Effects of local wall thinning on plastic limit loads of elbows using geometrically linear FE limit analyses, Eng. Fract. Mech. 2008, 75 (8): 2225–2245.

[41] X.H. Chen, Evaluation of Limit Load Analysis for Pressure Vessels. Part I: Linear and Nonlinear Methods. Steel and Composite Structures, 2016, pp. 1391–1415.

[42] F.Z. Ihab, R. Fanous, Seshadri, Limit load analysis using the reference volume concept, Int. J. Press. Vessel. Pip. 2009, 291–295.

[43] A. Reza, S. Seshadri, Variational method in limit load analysis—a review, J. Press. Vessel Technol. 2015, 433–439.

[44] X.H. Chen, B.J. Gao, Evaluation of limit load analysis for pressure vessels-Part II Robust methods, Steel Compos. Struct. 2017, 131–142.

[45] Z.X. Xu, Finite Element Analysis of Plastic Limit Load of Pressure Pipe Elbow, Shanghai: East China University of Science and Technology, 2003.

[46] Bao, S., Liu, Y., Mao, J., Ge, R., & Li, X. Numerical and experimental investigation on limit load of elbow with local thinning area. International Journal of Pressure Vessels and Piping, 2019, 172:414-422.

CHAPTER III

Damage predicting of pipe elbows containing single defects for different positions under combined bending and pressure loading

III.1 INTRODUCTION

In this chapter, we focus on two main sections that explain and calculate the resistance capacity of pipe elbows under the combined internal pressure of the fluid and in-plane opening and closing bending moments.The first section examines the bearing capacity of the elbow at different locations of defects in the internal wall of the extrados using the XFEM method. To implement this section, it is divided into three parts: The first part involves conducting a stress analysis to justify the choice of defect positions along the internal wall of the extrados.The second part entails calculating the elbow's bearing capacity at each defect position and for each mode of loading by plotting the moment-end rotation curve.The final section focuses on the elbow's safety check, where the weakening factor is one of the techniques used to analyze damage in piping systems. It demonstrates the reduction in the structural integrity or strength of a pipeline due to various factors such as defects, damage, or degradation. By determining the magnitude of the weakening factor, engineers and researchers can assess the remaining strength and durability of the pipeline, identifying potential failure points. This information is crucial for making informed decisions regarding the maintenance, repair, and replacement of pipelines to ensure their long-term performance and prevent catastrophic failures.

In the second section, we studied the effect of temperatures in various environments on the bearing capacity of a pipe elbow containing a corrosion defect under combined fluid pressure and opening bending moment, utilizing the XFEM method. This study involved conducting a comparison of the obtained results with the behavior of Steel X60 at this particular temperature degree. The temperature degree was selected based on the brittle-ductile curve of Steel API 5L X60.

III.2 FINITE ELEMENT METHOD

The finite element method is a technique used to solve differential equations. The system governed by the differential equation is represented as a set of algebraic equations with a finite number of variables. These methods are widely popular due to their ease of programming. Initially developed for structural problems, finite element technology has since been extended to numerous other fields. In this method, the entity is divided into simple geometric elements with shared edges, and its vertices or nodes are the points where multiple elements connect. These nodes serve as the points of application for internal or external forces. The process of dividing the entity is known as meshing.

In three-dimensional (3D) finite element analysis, commonly used solid elements include tetrahedral and hexagonal elements. Each node of the element possesses three translational degrees of freedom, allowing the element to deform in any of the three spatial directions [1]

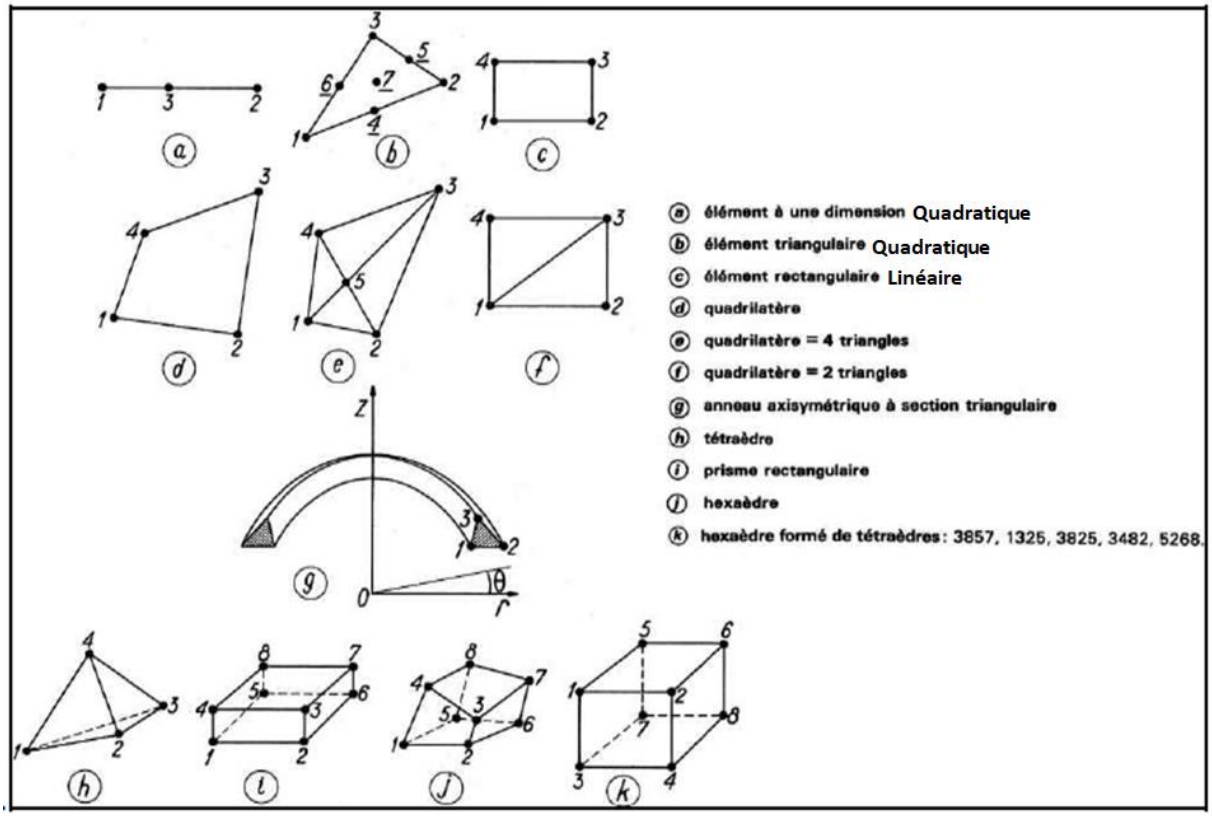

Figure III.1: The most frequently used elements [2].

III.3. PRESENTATION OF THE MATERIALS:

III.3.1 Steel API 5L X60

Steel is a metallic alloy primarily composed of iron and a small quantity of carbon. It is the presence of this chemical element, ranging from 0.02% to 2% by mass, that imparts distinctive properties to steel. The hardness of the metal increases with higher carbon content. Additionally, steel may incorporate other elements like copper or chromium to bestow specific usage characteristics, such as flexibility and resistance to temperature fluctuations.

III.3.2 The chemical composition of materials

Table III.1 shows the chemical composition of API 5L X60 steel, a carbon steel with several alloying elements.

Table III.1 : Chemical composition of X60 steel (mass content in %) [3,4]

C	Si	Mn	P	S	Cr	Ni	Al	Cu	Ti	Mo	Nb	Fe
0.018	0.036	1.400	0.017	0.013	0.028	0.017	0.049	0.032	0.005	0	0.095	Bal

III.3.3 Mechanical properties

The mechanical properties of X60 steel according to API 5L are defined in table III.2 and Figure III.2.

Table III.2: Mechanical properties of API5 L X60 steel[5].

Grade	E (MPa)	ῡ	σy(MPa)	UTS (MPa)
API 5L X60	210000	0.3	460	580

Where:

σy : yield strength [MPa].

UTS : ultimate strength [MPa]

The tensile curve illustrated in Figure III.3 offers valuable insights into the mechanical behavior of conventional steel X60 when subjected to tensile loading conditions. This curve typically represent the relationship between applied stress and resulting strain during a tensile test. The curve typically exhibits distinct regions, including the elastic region, where deformation is reversible, followed by the plastic region, where permanent deformation occurs. Additionally, features such as the yield point, ultimate tensile strength, and elongation at fracture can be determined from the curve, providing essential information about the material's strength, ductility, and overall mechanical performance.

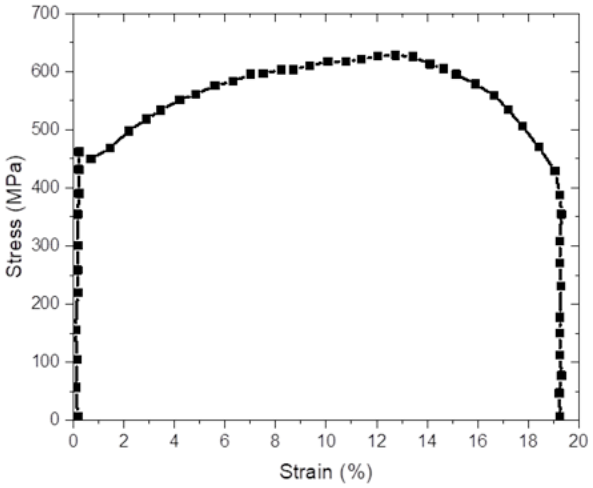

Figure III.2: Nominal stress-engineering strain curve for X60 steel [6].

III.4 STUDIED GEOMETRY

The geometries under investigation pertain to pipe elbows, which are critical components in pipeline systems. These structures include a semi-elliptical notch defect positioned at various

locations on the internal wall of the extrados. The choice of this shape was motivated by several factors. Firstly, these defects naturally occur during pipeline operation due to factors such as corrosion, fatigue, and manufacturing imperfections, making them realistic scenarios for study. Secondly, the simplified geometry of semi-elliptical defects aids in the development of analytical models and computational simulations, streamlining the analysis process and enhancing the efficiency and accuracy of the studies.

Additionally, semi-elliptical defects serve as common reference shapes in industry standards and regulations for evaluating pipeline integrity, ensuring consistency and compatibility with established practices. This standardization is crucial for maintaining uniformity in safety assessments and repair strategies across different pipeline systems. The defect is characterized by two dimensions: the depth of the defect (a), which is equal to half the thickness of the pipe elbow (a/t = 0.5), representing an unfavorable case scenario, and the length ($2c$), with a ratio of ($2c/a$ = 2). These dimensions provide a comprehensive understanding of the defect's impact on the pipe elbow's structural integrity.

The geometric properties of the pipe elbow and the defect are illustrated in Figure III.3. This figure provides a visual representation that complements the numerical and analytical data, offering a clear depiction of the defect's positioning and dimensions. By integrating these detailed descriptions and visual aids, the study ensures a thorough and precise examination of the defect's effects on pipeline performance, facilitating the development of effective maintenance and repair strategies..

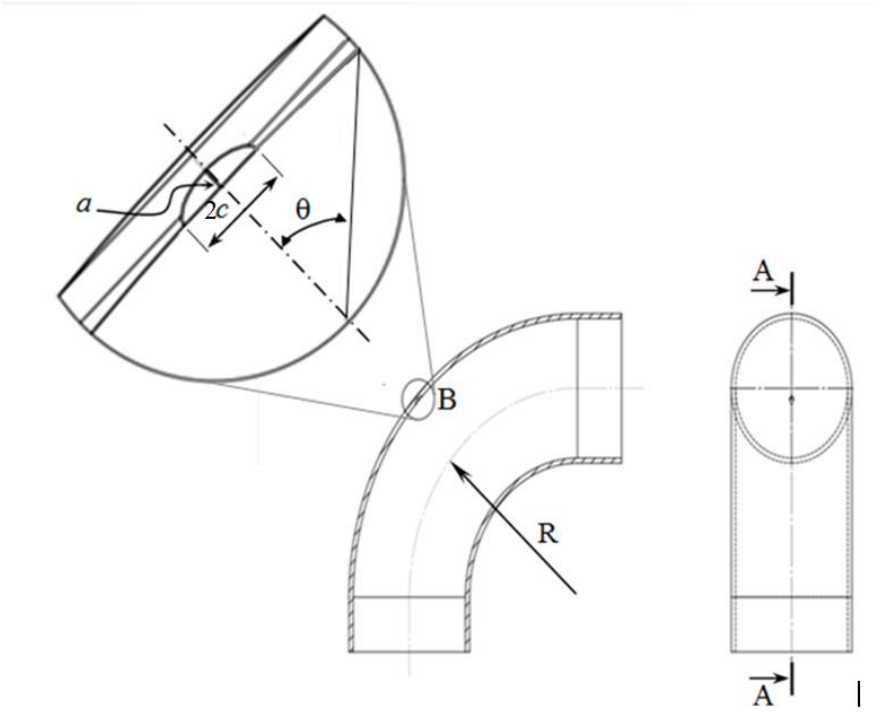

Figure III.3: Overview of studied geometry.

The steel tubular structure has the following dimensions: a diameter of 273 mm and a thickness of 9.27 mm. Only one crack-like elliptical defect is considered for each case. To evaluate the effects of damage, these elbows are uniformly subjected to an imposed rotational movement of 42 degrees. This value was chosen based on the studies by Kussmaul [7], Shalaby and Younan [8, 9], and Chattopadhyay et al. [10], which applied a 1 radian value as the angular displacement for applying the bending moment in either closing or opening mode. The load was extended far enough into the plastic regime to achieve plastic collapse or instability.

The two-mode in-plane bending moment (opening and closing) results in a significant difference in elbow deformation. The effect of the end pressure is considered as a load, which follows the direction of the cross-section and simulates the effect of the closed-end. In other words, the pressure effect at the end section is modeled as a force perpendicular to the section.

III.4.1 Loaded and Boundary conditions.

Throughout this study, the elbows are subjected to pressure P= 9MPa and in-plane closing or opening bending moments. Throughout this study, elbows are subjected to fluid pressure, generating in-plane closing or opening bending moments, as well as a thermal load due to the environment in which the pipe is operated. The same conditions apply to all structures: fixation at the linear part's edge and three displacements according to the *x*, *y*, and *z*-axis directions. In the other linear part at the tube's edge, depending on the case studied, a rotation is applied at a reference point according to the direction of opening or closing of the cross section of the tube. Figure III.4 represents the loaded and boundary conditions of the studied geometry.

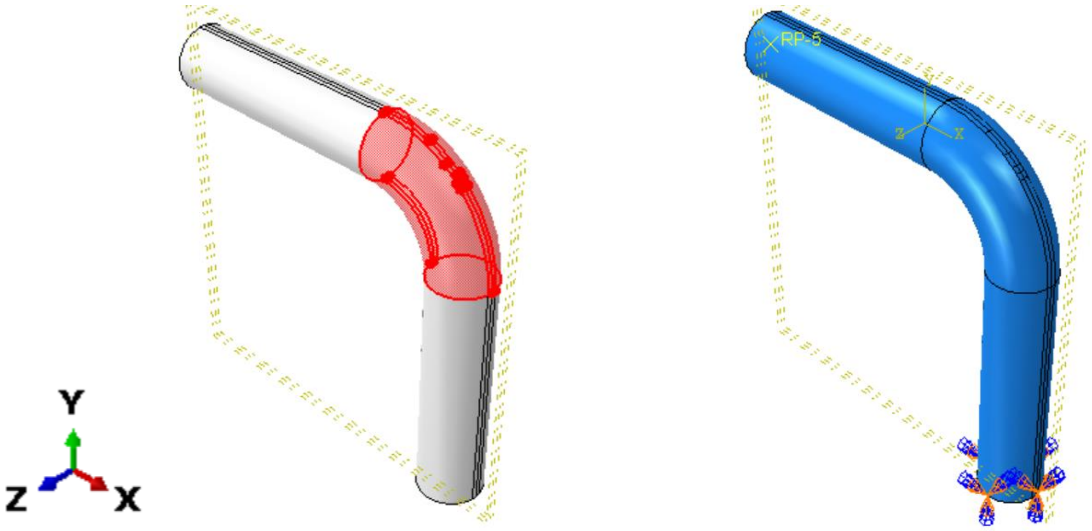

Figure III.4: Loaded and boundary condition of pipe elbow.

III.4.2 Effect of the mesh

III.4.2.1 Effect of the type of element used

Figure III.5 illustrates the adoption of a three-dimensional simulation approach in response to the unique shape and dimensions of the sample under investigation. This decision was made to

ensure a thorough analysis of the sample's behavior, necessitating the use of volume elements in the simulation model. This approach enables a more comprehensive representation of the sample's geometry and characteristics compared to a two-dimensional simulation.

In the numerical calculation of the element, the selection of the mesh is determined by the number of nodes and their arrangement. These nodes represent the element and its density in the mesh structure. To achieve computational convergence through the optimization of mesh density, a series of computational runs were initially selected. Two different types of meshes were used: C3D8R (linear brick with 8 nodes) and C3D10 (quadratic tetrahedron with 10 nodes). The stability of the results, such as the moment-displacement deflection, helps determine the best choice for the number and type of element.

(a)

(b)

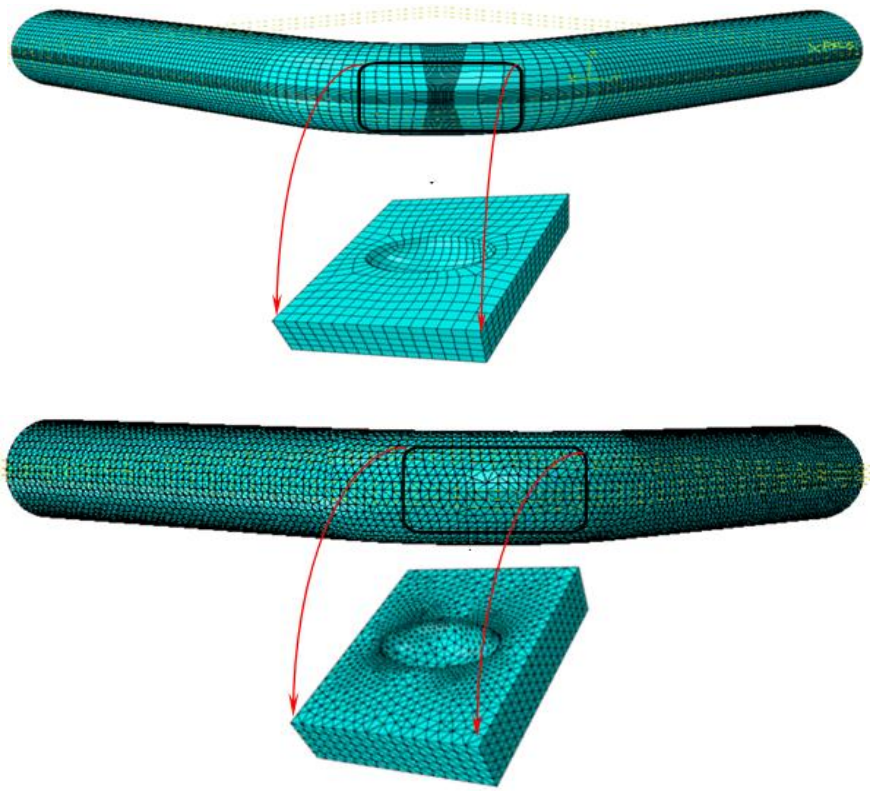

Figure III.5: Type of element used for the generation of the mesh
a) Hexahedron elements, b) Tetrahedron elements.

To better capture the value of the critical moment borne by the elbow, it is important to refine the mesh close to the cracks. The number of elements used in this structure is as follows: 33,284 hexahedron (C3D8R) elements and 33,498 tetrahedron (C3D10) elements in the pipe elbow mesh. Figure III.6 shows the results of the calculation by using two types of grid structure.

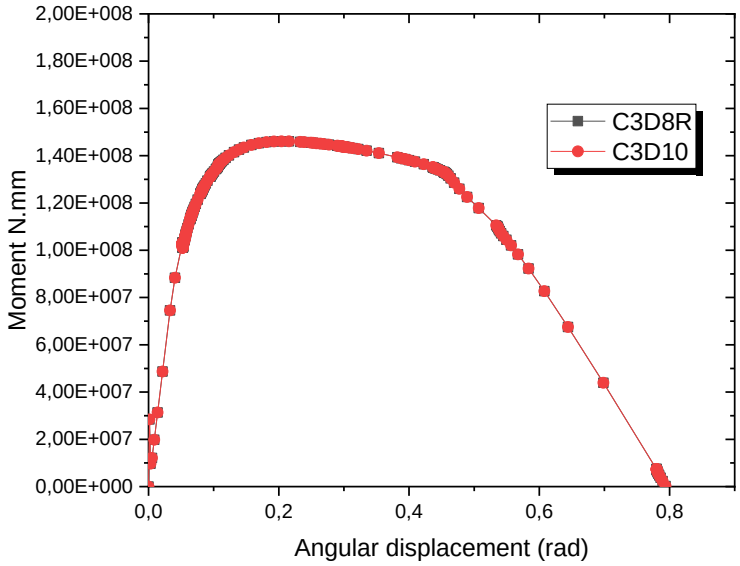

Figure III.6: Influence of mesh element type on the evolution of end-rotation-moment

The comparison between the two meshes is done by calculating the capacity of bearing of pipe elbow. We notice that the two techniques give the closed values along the numerique calculation.

III.4.2.2 Mesh and element size

A series of Mesh convergence tests were conducted for several situations to determine the appropriate mesh size and number of elements.Need to find the minimum number of hexahedron (C3D8R) elements that gives a converged solution . Figure III.7 shows the results of the mesh convergence test.

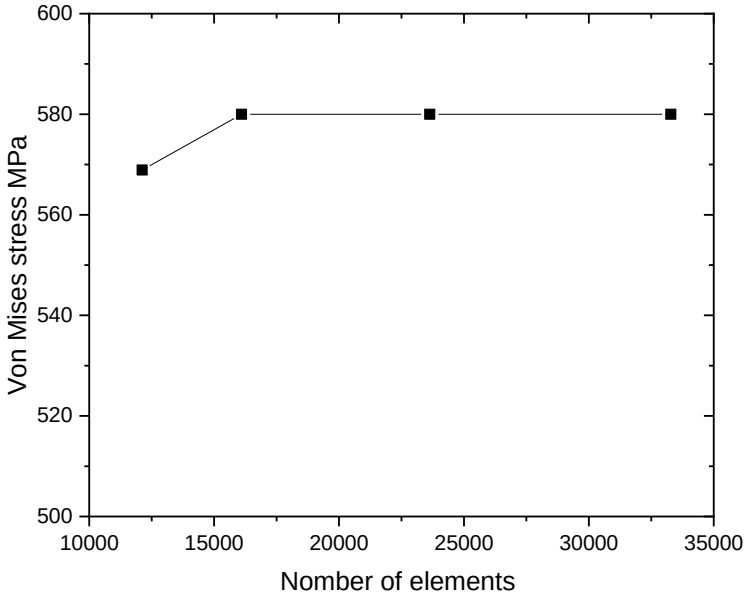

Figure III.7: Mesh convergence results.

III.5 NUMERICAL RESULTS AND DISCUSSION

III.5.1 Defect free elbow

In this section, we examine the response of the defect-free elbow under two loading modes: opening and closing. The load-deflection curve, depicted in Figure III.8, reveals distinct moment-rotation profiles for the elbow subjected to internal pressure and opening-closing bending moments. The shape of the curve in both scenarios is explained through the following annotations:

In the closing scenario, the application of pressure has dual effects of stiffening and strengthening. When internal pressure is applied at a smaller rotation angle, the moment initiating and progressing yielding over the net cross-section is higher. Prior to plastic instability, the net section can withstand a significantly higher moment with a corresponding large rotation before experiencing plastic instability due to pressure. Point A denotes the instability load or moment, determined using the method of horizontal asymptote (see chapter II), corresponding to the maximum load borne by the elbow. Conversely, point B signifies the collapse load, determined using the TES method.

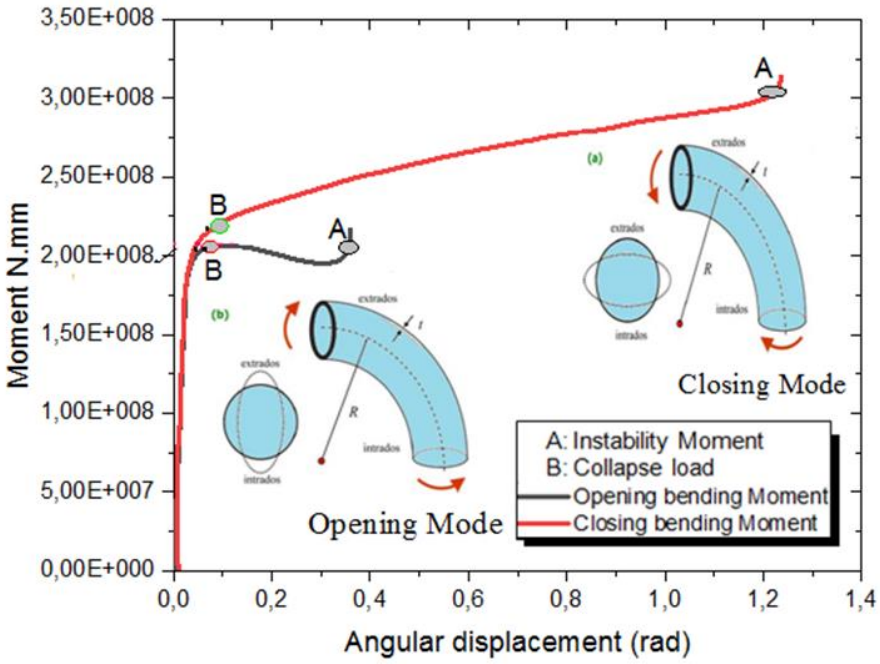

Figure III.8: Moment versus angular displacement for defect-free elbow with internal pressure P = 9MPa, temperature T = 80°C.

In the opening scenario, it is observed that the moment gradually increases with the application of internal pressure and bending moment. It reaches a peak and then declines with further increases in angular displacement until a critical damage rotation is reached. Ovalization of the elbow cross-section significantly contributes to its collapse. Application of uniform internal pressure counteracts the ovalization of the elbow cross-section and postpones the collapse. Here, the

pressure has a weakening effect and reduces the yielding moment. It slightly increases as yielding progresses across the entire section; however, the corresponding angle of rotation is typically reduced in this case. The moment leading to total plasticity of the section remains nearly the same, but pressure decreases the moment of plastic instability. Point A denotes the instability load or moment when using the method of horizontal asymptote, corresponding to the maximum load the elbow can bear, while Point B represents the collapse load when using the TES method.

Furthermore, the response of structures subjected to opening moments differs significantly from those subjected to closing bending moments. The response involves the flattening of the cross-section of the elbow, with failure occurring due to local tension at the central cross section [8]. From the figure III.8 the critical moment for the opening bending moment is 12% lower than that for the closing bending moment**.**

III.5.2 stress analysis

Steel elbows are an essential and frequently researched topic due to the multiple stresses they undergo, as well as their characteristic shape in tubular systems. Therefore, the concept of examining their behavior under various bending moments, in the presence of both internal pressure (90 bar), and at an operating temperature of 80°C, has gained significance. Figure III.9 depicts the influence of the opening bending mode on pressured elbows at different levels, as indicated by the Von Mises stresses measured along the internal wall of the elbow (extrados and intrados sides, from point A to B).

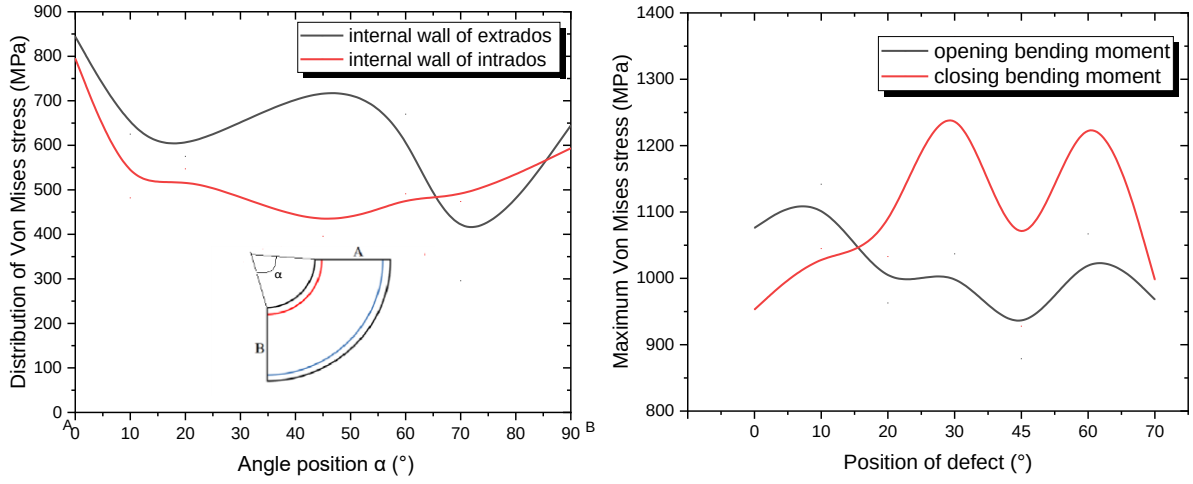

(a) (b)

Figure III.9: Distribution of Von Mises stress under opening-bending and pressure loading, a) along the defect-free elbow, b) along cracked elbow in different position of defect.

The highest value of Von Mises stress is prominently situated on the internal wall at the extrados section of the pipe elbow, as depicted in Figure III.9. This Figure illustrates the distribution of Maximum Von Mises stress at the internal wall's extrados at positions (α = 0°), (α = 45°), and (α

= 90°). Conversely, on the internal wall at intrados, the maximum Von Mises stress is concentrated at positions (α = 0°) and (α = 90°). These findings emphasize the significance of the internal wall at the extrados section of the pipe elbow. This stress distribution, influenced by the pressure effect, affects both the top and lower surfaces. In the open bending mode, compressive stresses accumulate on the top surfaces of the elbow, while tensile stresses concentrate on the lower surface of the pipe elbow.

Bending in tubular systems is a common occurrence, with elbows experiencing elevated stress levels compared to straight tubes when subjected to loads. This underscores the importance of investigating their behavior and the potential for damage when defects are present under compression loading and in-plane bending moments. The localization of these defects, in specific configurations, conditions, and loading modes, significantly impacts damage localization. The observed stress distribution arises due to the combined impact of pressure and in-plane bending moment, manifesting on both the upper and lower surfaces of the structure, including the defect site. S33, a critical stress component, plays a pivotal role in comprehending the interplay between the defect and the imposed loads, shaping the overall structural behavior. Particularly in scenarios involving axial defects on the inner wall, as in our study, this stress component significantly influences the stability and response of the defect area to the applied loads. This part examines the influence of defects in various scenarios, as detailed in Figure III.10.

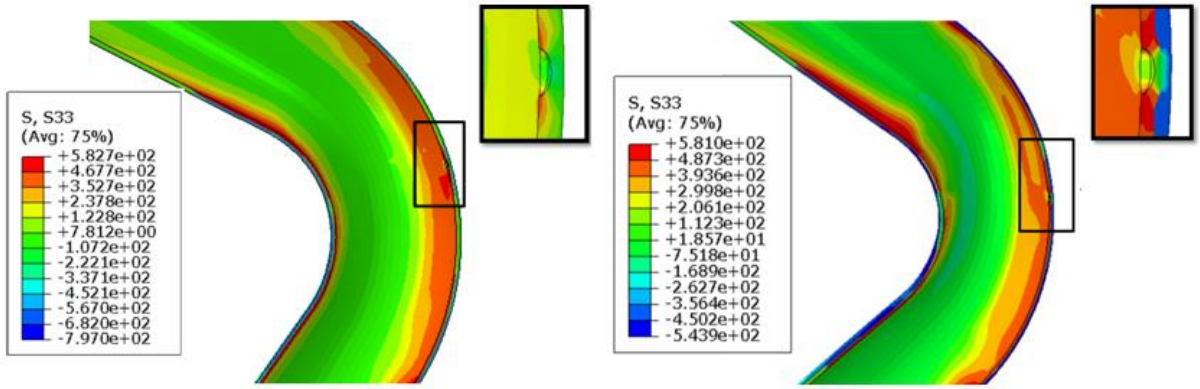

(a) (b)

Figure III.10: Example of the maximum Von Mises stress distribution in different defect positions (a) for Opening mode, (b) for closing mode.at internal pressure P = 9MPa and temperature T = 80°C.

III.5.3 Effect of position of the defect on the limit load of pipe elbow

The presence of a defect in the studied structure, when subjected to both internal pressure and bending moment, results in a combined effect on its integrity. The location of the defect becomes especially critical under in-plane bending moments. In thick elbows, where significant compression is experienced, the impact of the defect is heightened.

Figure III.11 (a) and (b) illustrate the collapse and instability moments in the pipe elbows without defects, reaching their peak values. However, upon the introduction of defects at various

positions, the collapse and instability moments decrease, reaching a minimum at positions (θ = 0° and θ = 45°), indicating an elevated risk of failure. The elbow undergoes increased compression due to angular displacements. Furthermore, variations in instability moments are observed with different defect positions, both in cases of opening and closing bending moments, with certain positions leading to an increase while others result in a decrease

Figure III.11 illustrates the evolution of the moment at instability and collapse concerning the position angle (θ) of the defect. The assessment of collapse moment (M) and instability moment (M*) is determined using the Twice Elastic Slope TES method (see § II.5) across different defect positions in the two modes studied. In this section, the defect's position on the elbow is considered, varying within the range of [10°-70°].

(a)

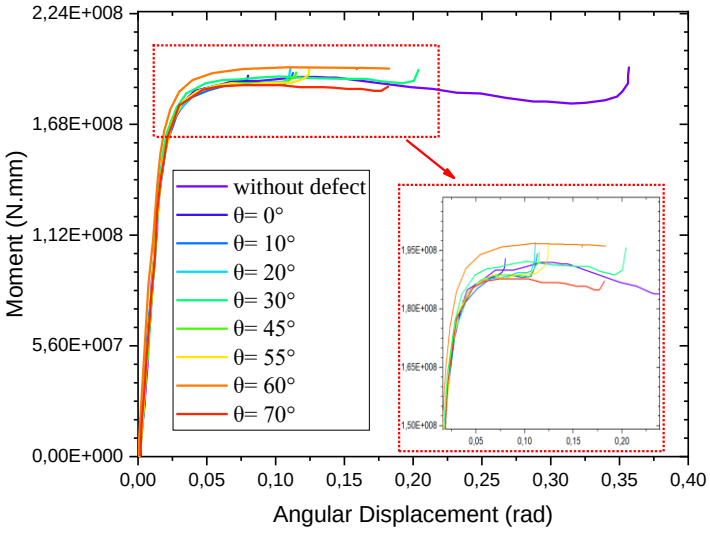

(b)

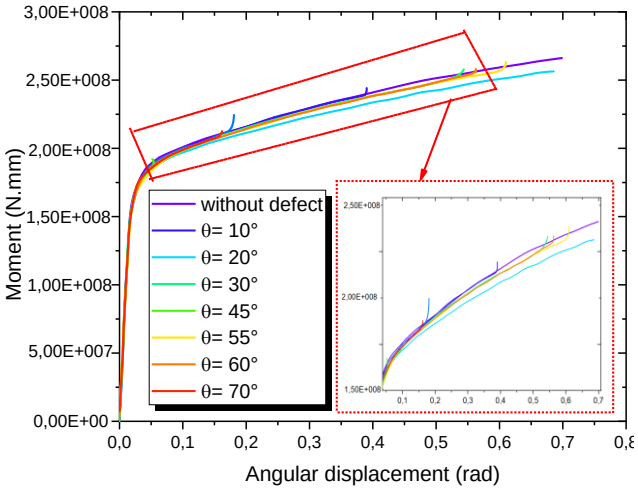

Figure III.11: Moment versus displacement angular
a) for opening bending moment, b) for closing bending moment.

Figure III.12 shows a notable pattern of instability and collapse moments which, both minimal at 0°, increase until reaching peaks at 20° for collapse and 30° for instability. They then decrease until reaching minima at 45°, before increasing again to reach maximum values at around 60°, then decreasing thereafter. A pseudo-symmetry or inflection is observed in relation to 45°.

The change in the curve indicates a fluctuation in instability and collapse behavior as the position of the defect varies. Initially, there is a gradual increase in both instability and collapse until reaching maximum values at specific angles. This is followed by a decrease until a point of minimum instability and collapse is reached at 45°, suggesting a stabilizing effect at this position. The subsequent rise and fall in the curve suggest further fluctuations in instability and collapse behavior, with a notable symmetry observed at the defect's position at 45°

(a)

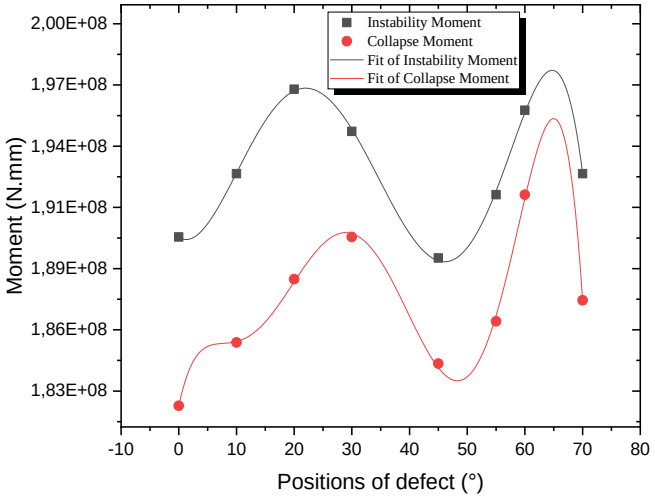

(b)

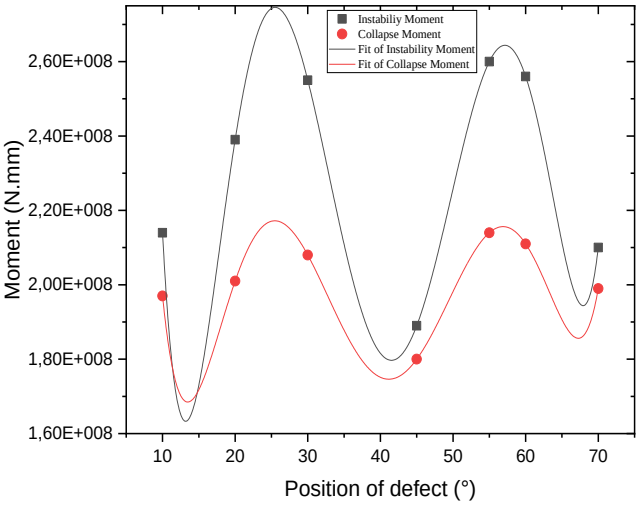

Figure III.12: Moment versus position of defect. a) For opening mode, b) For closing mode.

As shown in Figure III.12, the limit moment depends on the position of the defect. It is expressed in the following fifth-degree equation to obtain a better correlation. The equations are as follows:

Equation of limit moment in the case of opening mode

$$f(M) = 1{,}82\cdot10^{8} + 431539{,}68254\,\theta - 27775{,}92593\,\theta^{2} + 1949{,}41799\,\theta^{3} - 52{,}9709\,\theta^{4} + 0{,}42487\,\theta^{5} \quad \textbf{(III.1)}$$

$$f(M^{*}) = 1{,}9\cdot10^{8} - 384841{,}26984\,\theta + 117212{,}96296\,\theta^{2} - 5842{,}32804\,\theta^{3} + 102{,}94974\,\theta^{4} - 0{,}600\,\theta^{5} \quad \textbf{(III.2)}$$

Equation of limit moment in the case of closing mode

$$f(M) = 3{,}825\cdot10^{8} - 3{,}98814\cdot10^{7}\,\theta + 2{,}95715\cdot10^{6}\,\theta^{2} - 95399{,}20635\,\theta^{3} + 1371{,}86508\,\theta^{4} - 7{,}19841\,\theta^{5} \quad \textbf{(III.3)}$$

$$f(M^{*}) = 5{,}7936\cdot10^{8} - 8{,}18902\cdot10^{7}\,\theta + 6{,}34232\cdot10^{6}\,\theta^{2} - 209697{,}46032\,\theta^{3} + 3063{,}46825\,\theta^{4} + -16{,}26825\,\theta^{5} \quad \textbf{(III.4)}$$

Figure III.13 defines the evolution of the rotation at instability and collapse concerning the position angle θ of the defect. The evaluation of the collapse rotation (r) and instability rotation (r^{*}) is determined using the TES method across different defect positions in the two modes studied. In this section, the position of the defect on the elbow is considered and varies within the range [10°-70°].

As shown in Figure III.13, the rotation at the limit moment depends on the position of the defect. It is expressed in the following fifth-degree equation to obtain a better correlation. The equations are as follows:

(a)

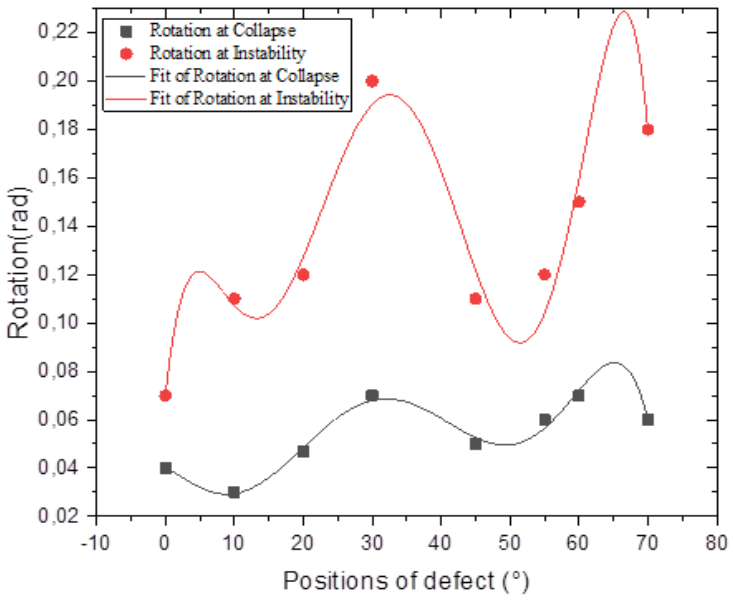

(b)

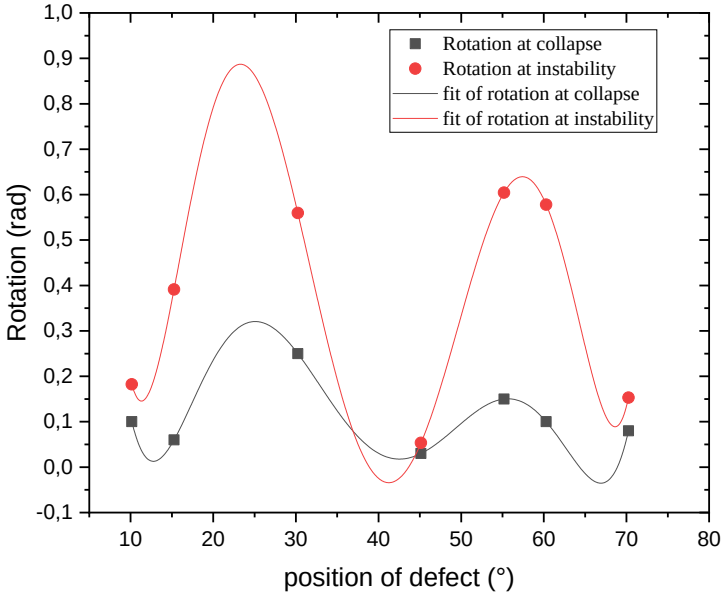

Figure III.13: Rotation versus position of defect.
a) for opening mode, b) for closing mode.

Equation of rotation at limit moment in the case of opening mode

$$f(r) = 0{,}04 - 0{,}00215\theta + 6{,}0445\cdot10^{-5}\theta^2 + 8{,}28011\cdot10^{-6}\ \theta^3 - 3{,}03434\cdot10^{-7}\ \theta^4 + 2{,}57037\cdot10^{-9}\theta^5 \quad \textbf{(III.5)}$$

$$f(r^*) = 0{,}07 + 0{,}02085\theta - 0{,}00299\theta^2 + 1{,}62665\cdot10^{-4}\theta^3 - 3{,}41037\cdot10^{-6}\theta^4 + 2{,}34497\cdot10^{-8}\theta^5 \quad \textbf{(III.6)}$$

Equation of rotation at limit moment in the case of closing mode

$$f(r) = 5{,}04714 - 1{,}17746\ \theta + 0{,}10284\ \theta^2 - 0{,}00425\ \theta^3 + 9{,}00525\cdot10^{-5}\ \theta^4 - 9{,}42959\cdot10^{-7}\ \theta^5 \quad \textbf{(III.7)}$$

$$f(r^*) = 8{,}80465 - 2{,}21061\theta + 0{,}20731\theta^2 - 0{,}009\theta^3 + 1{,}96034\cdot10^{-4}\theta^4 - 2{,}08415\cdot10^{-6}\theta^5 \quad \textbf{(III.8)}$$

III.5.4 Effect of position of defect on weakening factor

The equation (III.9) was developed by Chattopadhyay et al. [10], and it represents the weakening factor of the cracked elbow. This factor is defined as the ratio of the limit moments (M_L) of cracked elbows (collapse or instability) to the limit moments (M_0) of defect-free elbows (collapse or instability).

$$X = M_L / M_0 \quad \textbf{(III.9)}$$

All the necessary data have been collected from Figures (III.8) and (III.11) using the TES method and it is presented in the table. In the case of the opening bending moment, the value of M0 for the collapse moment was $2.05 \cdot 10^8$ N.mm, and for the instability moment, it was $2.10 \cdot 10^8$N.mm. However, for the closing bending moment, the collapse moment (M_0) was $2.20 \cdot 10^8$N.mm, and the instability moment was $3 \cdot 10^8$ N.mm.

Table III.3: The value of collapse and instability moment for cracked elbow and their weakening factors

Position of defect (°)	Opening Mode				Closing Mode			
	Collapse		Instability		Collapse		Instability	
	M (N.mm)	*X*	*M* (N.mm)	*X*	*M* (N.mm)	*X*	*M* (N.mm)	*X*
10	1.82×10^8	0.88	1.90×10^8	0.90	$1{,}97\times10^8$	0.89	$2{,}14\times10^8$	0.71
20	1.85×10^8	0.9	1.93×10^8	0.91	$2{,}01\times10^8$	0.91	$2{,}39\times10^8$	0.79
30	1.88×10^8	0.92	1.97×10^8	0.94	$2{,}08\times10^8$	0.94	$2{,}55\times10^8$	0.85
45	1.90×10^8	0.92	1.95×10^8	0.93	$1{,}80\times10^8$	0.81	$1{,}89\times10^8$	0.63
60	1.84×10^8	0.89	1.89×10^8	0.9	$2{,}11\times10^8$	0.95	$2{,}56\times10^8$	0.85
70	1.87×10^8	0.91	1.96×10^8	0.93	$1{,}99\times10^8$	0.90	$2{,}10\times10^8$	0.7

Figure III.14 depicts the influence of defects on the limit moment of cracked elbows under opening and closing bending moments. The weakening factor (M_L/M_0), influenced by the defect, and is plotted against the defect position on the elbow pipe wall. In the opening mode, a singular peak in the weakening factor occurs at the 30° defect position, with a minimum value observed at 60°. Conversely, in the closing mode, two peaks in the weakening factor are evident, occurring at the 30° and 60° defect positions. Additionally, two minimum values of the weakening factor are observed at the 45° and 70° defect positions, respectively. Notably, the weakening factor values associated with the collapse moment surpass those of the instability moment.

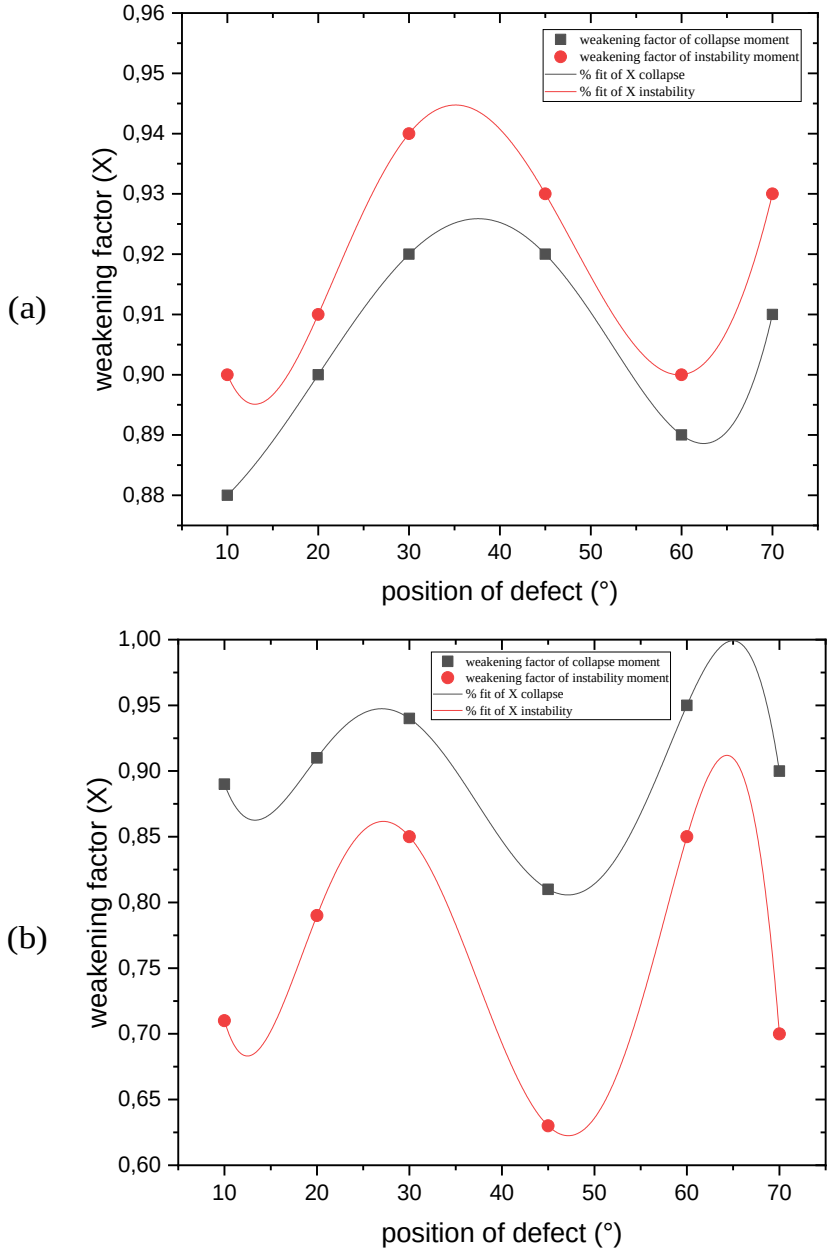

Figure III.14: Effect of position of defect on weakening factor: (a) opening bending moment. (b) Closing bending moment.

The correlation between the position of the defect on the elbow wall and the weakening factor of the collapse and instability moments is illustrated in Figure III.14. The weakening factor is determined by a fifth-degree equation, providing a more precise representation of the relationship.

For opening mode:

$$X(\text{collapse})= 0{,}8732 -1{,}64286\times10^{-4}\theta+7{,}96905\times10^{-5}\theta^2+1{,}35238\times10^{-6}\theta^3- 9{,}69048\times10^{-8}\theta^4+9{,}04762\times10^{-10}\theta^5 \quad \textbf{(III.10)}$$

$$X(\text{instability})=1{,}0368 -0{,}02767\theta+0{,}00182\theta^2-4{,}75746\times10^{-5}\theta^3+ 5{,}24683\times10^{-7}\theta^4-2{,}01587\times10^{-9}\theta^5 \quad \textbf{(III.11)}$$

For closing mode:

$$X(collapse) = 1{,}7184 -0{,}17864\theta + 0{,}01329\theta^2-4{,}29771\cdot10^{-4}\theta^3 + 6{,}18714\cdot10^{-6}\theta^4-3{,}24762\cdot10^{-8}\theta^5 \quad \textbf{(III.12)}$$

$$X(instability) = 1{,}9818 -0{,}28307\theta + 0{,}02175\theta^2-7{,}14916\cdot10^{-4}\theta^3 + 1{,}03977\cdot10^{-5}\theta^4-5{,}50317\cdot10^{-8}\theta^5 \quad \textbf{(III.13)}$$

III.5.5 The temperature effect

This section focuses on the effect of temperature on a 90-degree pipe elbow with an ellipsoidal corrosion defect on the internal wall of the extrados using the XFEM technique. Additionally, numerical results and their causes are compared with the results obtained in previous studies.

The obtained results enable the study of the elbow's behavior under various temperatures, which are determined by referencing the brittle-ductile curve of X60 steel. The selection of temperatures is based on the behavior of X60 steel according to this curve. First, we collected the mechanical properties of steel API 5L X60 at various temperatures and environmental conditions to serve as the basis for our numerical study. Subsequently, we compared these findings and inferred the factors influencing the behavior of the elbow at these specific temperature levels.

III.5.6 effect of temperatures on the yield and ultimate stress of steel API 5L X60

Figure III.15 depicts the variation in the yield and ultimate stress of API 5L X60 steel across different temperature degrees. These temperature values were selected to simulate the transition from high-temperature to low-temperature environments, reflecting the effects of climate change on the mechanical properties of the material. Despite its scattered behaviour, it can be observed that the stresses vary inversely with changes in temperature. In the range [-30°C to 50°C], the stresses show no significant variation. At temperatures of -30°C, 0°C, and 80°C, the yield stress values fall below the linear fit, while at -90°C, 20°C, and 30°C, the ultimate strength values exceed the linear fit, likely due to differences in the environments in which they were measured.

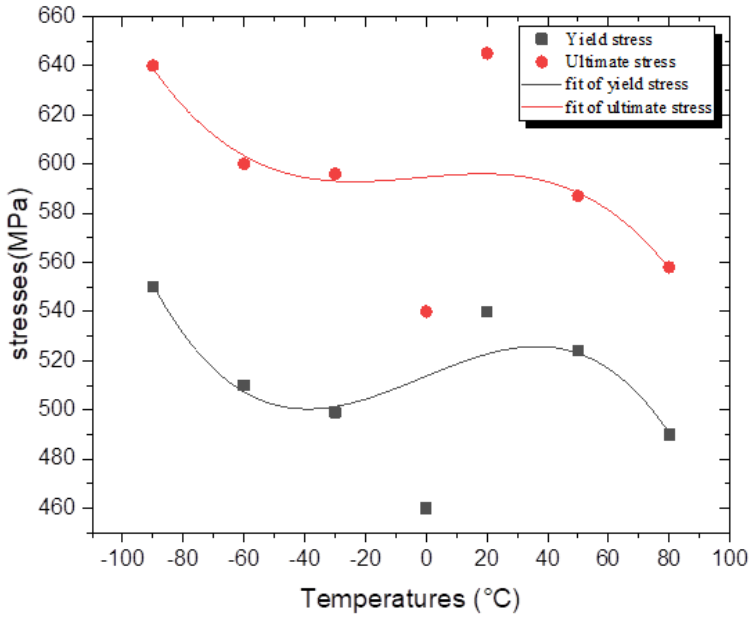

Figure III.15: Evolution of the yield and ultimate stresses of X60 steel with the influence of different temperatures [11-13].

III.5.7 Distribution of Von Mises stresses on the level of defect at different temperatures

Figure III.17 displays the distribution of Von Mises stress at the level of the defect in the critical position of the elbow when loaded by an opening bending moment at various temperatures. The stresses transit from compression to tension along the circumference of the elbow. It should be noted that when subjected to opening bending, the areas closest to the sides of the elbow experience significant tensile stresses, while compressive stresses occur in the upper regions. Figure III.16 displays the distribution of Von Mises stress at the defect's critical position on the elbow when subjected to an opening bending moment at various temperatures. The stresses transition from compression to tension along the elbow's circumference. It should be noted that when subjected to opening bending, the areas closest to the sides of the elbow experience significant tensile stresses, while compressive stresses occur in the upper regions. This distribution highlights the complex nature of stress responses in the elbow, with the tensile stresses potentially exacerbating crack propagation or defect enlargement at lower temperatures. Conversely, the compressive stresses might mitigate some of the damaging effects in the upper regions. The variation in temperature further influences these stress distributions, underlining the need for precise temperature management and stress analysis in maintaining the integrity of the elbow under operational conditions.

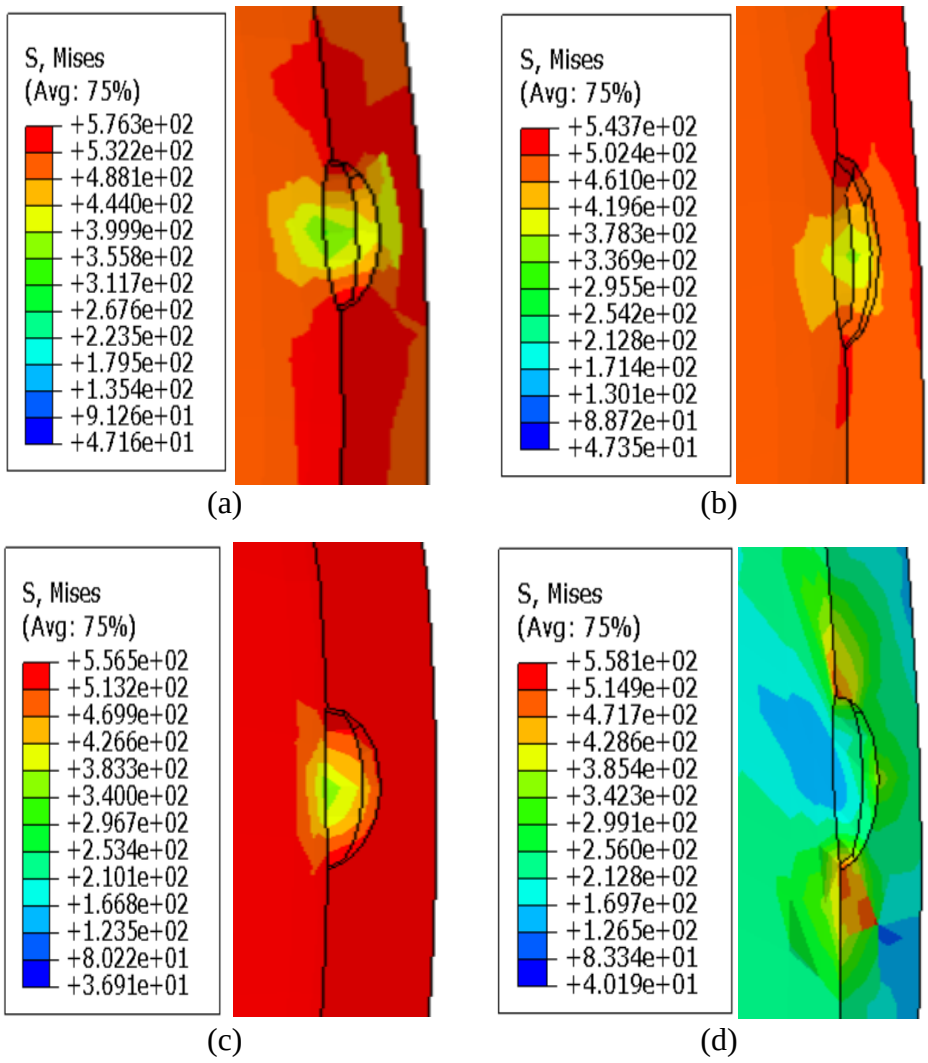

Figure III.16: Von Mises stresses at the level of defect in elbows of angular 90° for different temperature degree under opening bending moments: a)-30°C, b) 20°C, c) 50°C, d) 80°C.

Figure III.18 depicts the most stressed area of the elbow, along with the location of damage initiation. It also illustrates the additive effect of temperature, which directly influences the stress distribution under an opening bending moment. For all values of temperatures (-30°C, 20°C, 50°C, 80°C), the Von Mises stress at the level of the defect varies with temperature, and the maximum value of Von Mises stress is concentrated at the sides and depth of the defect.

The analysis also considered the influence of temperature on the peak values of Von-Mises stress, as illustrated in Figure III.17. The evolution of Von-Mises stress delineates three distinct zones: The Security Zone, identified by Von-Mises stress values below the fracture safety factor (*Fs* = 2). The Safety Zone extends between the maximum Von-Mises stress value and the fracture safety factor. The Failure Zone is situated above the maximum Von-Mises stress value.

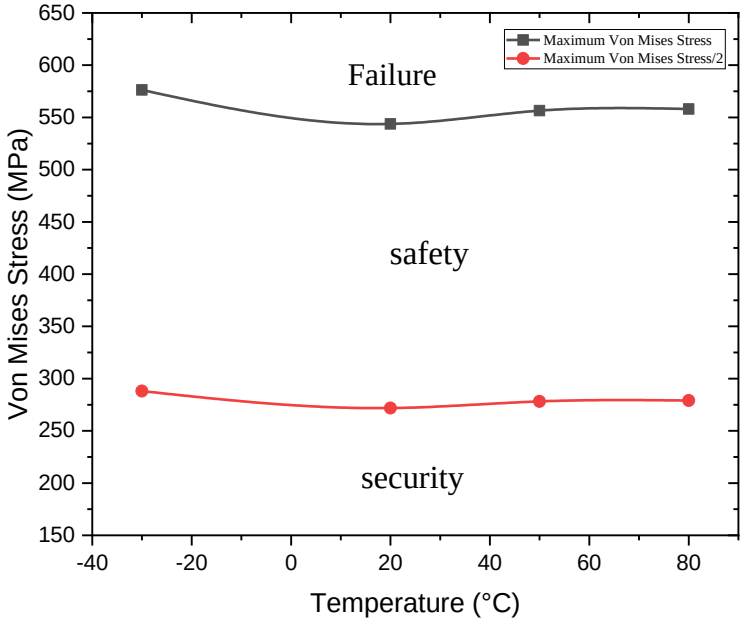

Figure III.17: Effect of Temperature on maximum Von Mises Stress.

III.5.8 The effect of temperature on the failure of structure

The bending of the straight pipe-elbow-straight pipe system determines the structure's response to the load and its level of resistance. In this part of the study, the structure was subjected to an opening bending moment under varying temperatures until damage occurred. This analysis provides critical insights into how temperature variations affect the structural integrity and load-bearing capacity of the system..

Figure III.18 illustrates the nonlinear response of the elbow to the opening bending moment, displaying distinct levels that vary significantly based on temperature changes. The findings reveal that X60 pipeline steel undergoes brittle fracture at both 20°C and 50°C, as confirmed by Velazquez et al. [11]. Conversely, at 80°C, the temperature's impact on the elbow's resistance capacity leads to a ductile fracture, consistent with the observations of Sung et al. [13]. With higher temperatures, both yield and ultimate stresses decrease, resulting in a lower threshold for damaging the elbow. Notably, the steel's maximum bearing capacity is observed at -30°C, possibly due to the elevated stress required to cause damage to the elbow as documented in [14, 15].

This comprehensive analysis underscores the critical role of temperature in determining the fracture behaviour of the elbow. It highlights that at lower temperatures, the material exhibits higher resistance to deformation and fracture, leading to increased bearing capacity. In contrast, at elevated temperatures, the material's reduced yield and ultimate stresses make it more susceptible to ductile failure, which is less abrupt but still detrimental.

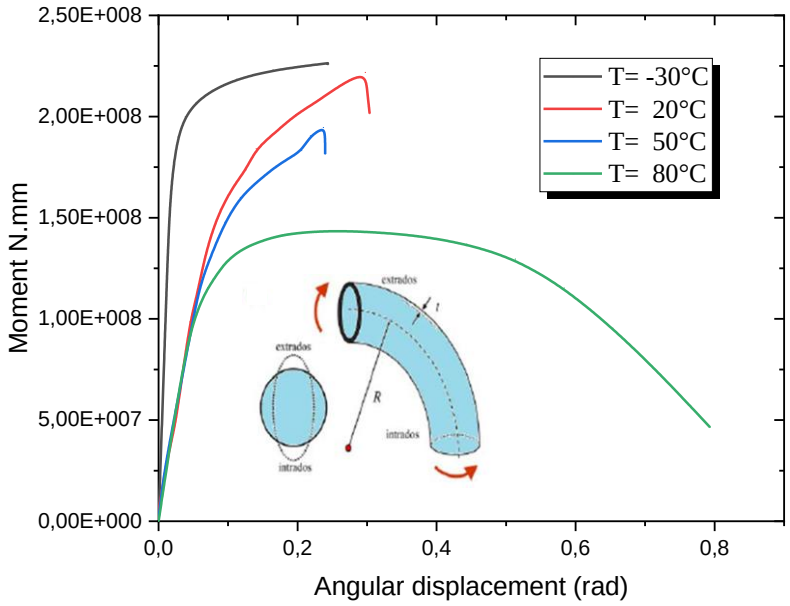

Figure III.18: Damage moment–rotation curve with effect of temperature values in the case of angular elbows 90° and pressure of 9 MPa under opening bending moment.

Figure III.19 depicts the evolution of the instability moment and the corresponding rotation as functions of temperature within the considered range. As shown in this figure, there is a slight decrease in the moment value followed by an increase in rotation. The same trend can be observed in the change of collapse load concerning temperature. Notably, there is a significant decrease in both the instability and collapse moments when transitioning from lower to higher temperatures, with reductions of 45% and 48%, respectively.

Additionally, we observe that the variation in limit load across different temperatures is relatively minimal; indicating that the material's capacity to bear the limit load remains fairly consistent despite temperature changes. However, there is a significant disparity in the rotation associated with the limit load between the two temperature ranges. This suggests that while the structure maintains its load-bearing capacity, it undergoes greater deformation at higher temperatures. The increased rotation at higher temperatures indicates a reduction in the material's stiffness, highlighting the importance of considering thermal effects in the design and analysis of structural components.

This plot can be expressed in the following three-step analytical form to achieve a better correlation:

$$f(M) = -94,25T^3 - 2912,5T^2 - 319550T + 2,01\cdot 10^8 \quad \textbf{(III.14)}$$

$$f(M^*) = -144,5T^3 - 3625T^2 - 73700T + 2,20\cdot 10^8 \quad \textbf{(III.15)}$$

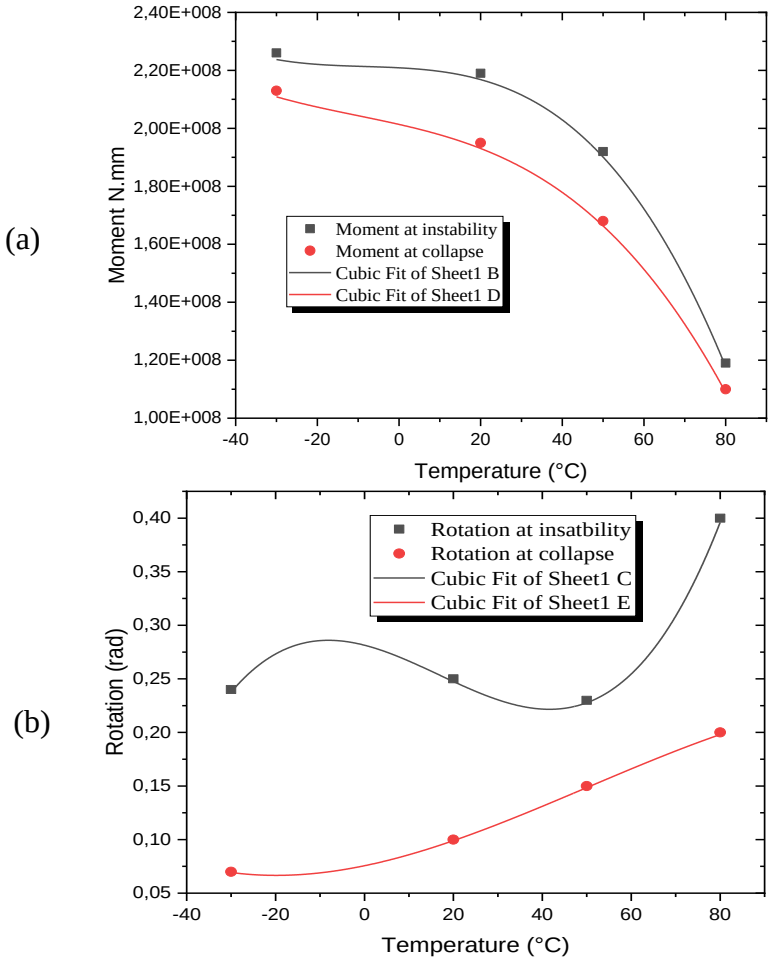

Figure III.19: Rotation vs. moment for different temperatures value.

Regarding the rotation at instability and collapse, we observe an inverse relationship with moment changes. Specifically, we note an increase in the rotation's value between lower and higher temperatures, with a 42.5% increase for the instability moment and a 65% increase for the collapse moment.

This plot can be translated into the following three-step analytical form to achieve a better correlation:

$$f(r) = -1,2.10^{-7}T^3 - 1,8.10^{-5}T^2 - 8,58\cdot10^{-4}T + 0,07 \quad \textbf{(III.16)}$$

$$f(r^*) = 1,14.10^{-6}T^3 - 5,66.10^{-5}T^2 - 0,0011T + 0,2844 \quad \textbf{(III.17)}$$

III.5.9 Damaged area at different temperatures

One of the objectives of our study is to observe the initiation and propagation of defects in the structure under the influence of opening bending moments at different temperatures.

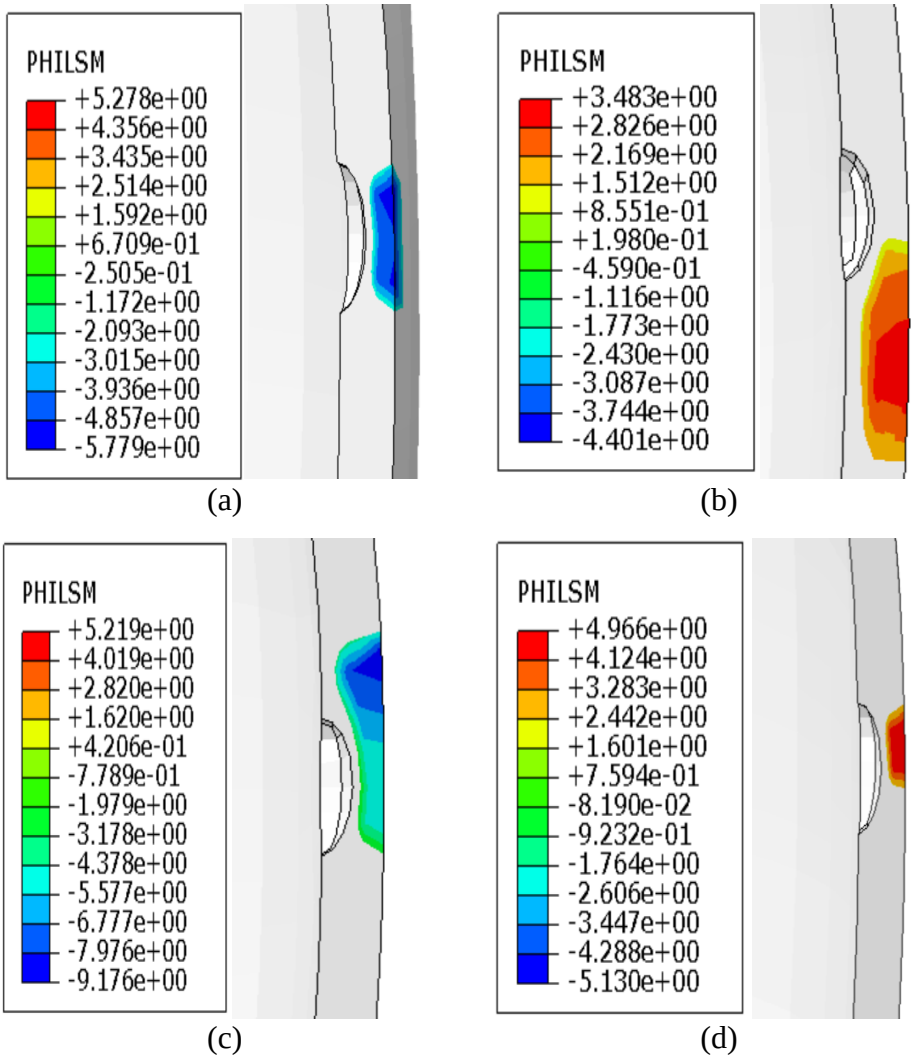

Figure III.20: Damage area of defect elbows under different temperature degrees in opening bending moments: a) the damaged area at level of defect, b)-30°C, c) 20°C, d) 50°C, e) 80°C.

Figure III.20 represents the areas of damage caused by opening bending modes at different temperatures with a deflected bend angle of 90°. These zones are consistently influenced by the bending mode and temperature degrees. In all cases, the areas of stress concentration are the points of damage initiation. Their magnitude varies with different temperatures, ranging from the smallest value at the internal defect level to the highest value at the external surface above the defect. The damage is primarily concentrated at the position of the defect during opening and high tensions, accelerating structural damage at various levels. The propagation of damage is determined by its location within the structure. For instance, it propagates towards the exterior of the structure if the defect is internal, as demonstrated in Figure III.20, which corroborates the findings of Bensoltane et al. [16].

III.6 CONCLUSION

In this chapter, the numerical study explores the behavior of defected pipe elbows at various positions on the internal wall of the extrados using the XFEM method. The chapter is divided into two sections: the first examines the bearing capacity of elbows with defects at different positions, while the second investigates the impact of temperature levels on an elbow with a defect at a critical position (45°). The results show that defects reduce the limit load of the elbow, with the relationship between defect positions and limit load displaying a nonlinear pattern. Temperature variations also affect the bearing capacity, and both defect initiation and propagation are influenced by defect positions, temperature levels, and high tensile stress.

REFERENCES

[1] David Lebaillif, Naman Recho, « Prevision de la rupture en milieu élastique par Remaillage », 9ème Colloque National AIP PRIMECA, La Plagne - 5-8 avril 2005.

[2] BATHE. «Finite Element Procedure », Prentice All, 1996. 24: 92-101

[3] Zienkiewicz et Taylor. « The Finite Element Method », Vol 1, 2, 3. McGraw-Hill, London, 1991. 24, 45.

[4] AMARA ZENATI Abdeljalil. Étude du comportement des aciers API 5L X60 sollicités par contraintes mécaniques et milieu de sol Algérien Simulé. Thèse de doctorat, université de Tlemcen, Algérie 2014.

[5] API specification 5L (SPEC 5L), specification for line pipe, 14th edition, November 1,

[6] Araújo, B. A., Travassos, G. D., Silva, A. A., Vilar, E. O., Carrasco, J. P., & de Araújo, C. J. Experimental characterization of hydrogen embrittlement in API 5L X60 and API 5L X80 steels. In Key Engineering Materials 478, pp. 34-39, (2011). Trans Tech Publications Ltd. https://doi.org/10.4028/www.scientific.net/KEM.478.34

[7] Kussmaul, K., Diem, H. K., Uhlmann, D., and Kobes, H.,‘‘Pipe Bend Behavior at Load Levels Beyond Design,’’Proceedings of 13th InternationalConference on Structural Mechanics in Reactor Technology, SMiRT, Brazil.Vol. G., 1995, 187–198.

[8] Shalaby MA, Younan MYA. Limit loads for pipe elbows with internal pressure under in-plane closing bending moment. J Press VesTechnol ASME Trans. 1998, 120(1):35–42.

[9] Shalaby MA, Younan, MYA Effect of Internal Pressure on Elastic-Plastic Behavior of Pipe Elbows under In-Plane Bending Moments. J Press VesTechnol ASME Trans NOVEMBER 1999, Vol.121/401.

[10] Chattopadhyay, J., Kushwaha, H. S., & Roos, E. Some recent developments on integrity assessment of pipes and elbows. Part I: Theoretical investigations. International journal of

solids and structures, (2006) 43(10), 2904-2931, https://doi.org/10.1016/j.ijsolstr.2005.06.054

[11] Velazquez, Z., E. Guzman, and A. Contreras, Stress corrosion cracking behavior of X60 pipe steel in soil environment. %J MRS Online Proceedings Library, 2009. 1242

[12] Ren, X., et al. Tensile properties of 420 MPa steel at low temperature. in The Twenty-fifth International Ocean and Polar Engineering Conference. 2015. OnePetro.

[13] Sung, H.K., et al., Effects of finish cooling temperature on tensile properties after thermal aging of strain-based API X60 linepipe steels. %J Metallurgical Materials Transactions A, 2015. 46(9): p. 3989-3998.

[14] Akselsen, O.M., E. Østby, and B. Nyhus. Low temperature fracture toughness of X80 girth welds. in The Twenty-second International Offshore and Polar Engineering Conference. 2012. OnePetro.

[15] Tubex, H., K. Van Minnebruggen, and W. De Waele, Low temperature tensile properties of line pipe steels. SUSTAINABLE CONSTRUCTION DESIGN, 2015. 6(3).

[16] Ahmed-Bensoltane, A., et al., Using XFEM Technique to Predict the Effect of Default on the Damage of Steel Pipe Reduced-Connection Under Bending and Pressure Loading. International Journal of Steel Structures, 2022: p. 1-15.

CHAPTER IV

Proposal Engineering Methods to Repair Bend Elbow Pipe Contain Internal Corrosion Defect

IV.1 INTRODUCTION

In this chapter, our objective is to numerically assess the impact of bending loads on the failure moment and correspond rotation (M^* and r^*) of locally wall-thinned elbows subjected to load-controlled in-plane bending loads and internal pressure. To represent wall thinning, we modelled semi-elliptical cracks with a depth (a/t) of 0.5 and a length (c/a) of 2. These cracks were positioned at various locations on the inner and outer surfaces of the elbow pipe, based on the weaknesses identified in Chapter III. These locations required reinforcement due to their limited resistance capabilities. The Twice Elastic Slope (TES) method described in chapter II was used to extract the values of these limit resistances.

To accomplish this, we conducted multiple numerical tests on the elbow pipes, each featuring distinct local wall-thinning defects. These tests involved applying combined internal pressure and constant in-plane bending loads in both opening and closing modes. However, our focus in this chapter is solely on the opening mode. We propose engineering solutions to evaluate the impact of load-controlled bending loads on the failure moment while repairing the elbows, using either a rolling composite or a local metallic patch.

Additionally, we examined how load-controlled in-plane bending influences the safety margin against burst failure of wall-thinned elbows. This was done by comparing the numerical failure moments with the original design proposal, allowing us to investigate any variations in safety margins.

IV.2 GEOMETRICAL AND MATERIALS MODELS

In this section, we employed two repair methods. Initially, the damaged elbow was repaired by attaching a composite patch using adhesive. Subsequently, a metallic patch was utilized for the repair. Figure IV.1 illustrates the geometrical model implemented for the repair procedure.

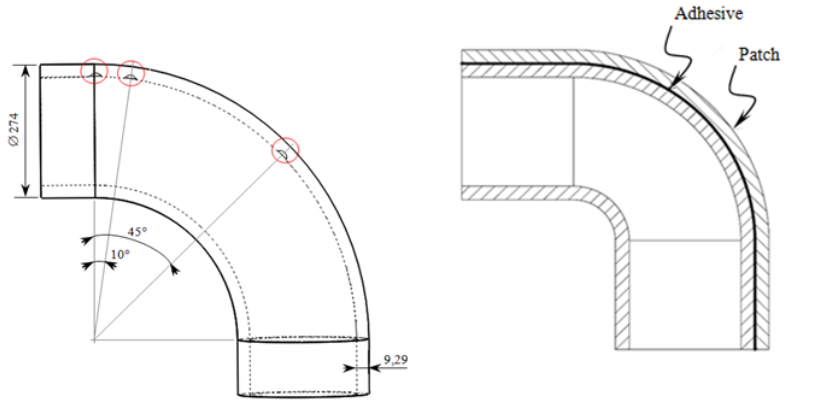

(a) (b)

Figure IV.1: Geometry of corroded elbow, a) the critical positions of defect at elbow, b) pipe elbow repair by patch.

The elastoplastic behavior and strength characteristics are presented in Figure III.3 and table III.3. The bent element is connected to two straight pipes with a length of 960 mm. This Length ensures that the bend area is not subjected to stress interference from the load applied to the end of the linear member. The straight tubes are employed solely to evenly transmit the bending moment to the bend. In numerical analysis, the bending moment load on the bend is obtained by rotating around the axis of the bend.

Table IV.1: Mechanical properties of composite patch.

Composite patch								
Young's modulus, (GPa)			Shear modulus, (GPa)			Poisson's ratio		
E_{px}	E_{py}	E_{pz}	G_{pxy}	G_{pxz}	G_{pyz}	υ_{pxy}	υ_{pxz}	υ_{pyz}
200	19.6	19.6	7.2	5.5	5.5	0.3	0.28	0.28

TableIV.2: Mechanical properties of adhesives FM73 and Adhesive DC-80 for metallic patch.

Adhesive (FM73)					Adhesive (DC-80 for metallic patch)	
Young's modulus E_a (GPa)	Poisson's ratio υ_a	Thermal expansion (10^{-6} °C)			Young's modulus E_a (MPa)	Poisson's ratio υ_a
		α_{12}	α_{12}	α_{12}		
0.42	0.3	4.5	23	23	2383	0.336

The tubular structure has specific measurements: a diameter of 274 mm and a thickness of 9.27 mm. Within the elbow, there are three critical positions where defects are present. These positions were chosen based on the elbow's maximum moment capacity at those locations, considering the combined influence of internal pressure and opening bending moment. Chapter III provides a description of these positions, and Figure III.13 illustrates their locations. To compare them with the unpatched elbow, these bends undergo a consistent rotational displacement of 42°.

IV.3 FINITE ELEMENT MODEL

In this study, the ABAQUS finite element (FE) code was employed to calculate the bearing capacity of the pipe elbow in response to end rotation. The pipeline ends (*Ux, Uy*, and *Uz = 0*) were fixed at a specific linear section of the tube edge, and rotation was applied to induce structural damage. The Finite Element Method (FEM) was utilized to model various components, including the cracked pipe elbow, composite patch, and adhesive. To account for symmetry, only one half of the pipe elbow was considered during the modeling process. In all analyzed cases, the

tubular structure experienced pressure and temperature, resulting in a maximum principal stress equal to the nominal strength value of 580 MPa. The damage assessment criterion was based on the maximum tensile strength; with a critical crack opening displacement set at 1 mm. Meshing of the pipe elbow involved the use of three-dimensional hex-dominated quadratic elements. Due to ovalization and force concentration that lead to damage in specific zones, mesh refinement became necessary. This refinement allowed for a more precise recording of maximum stresses and the initiation load for fracture. The pipe elbow's symmetry, considering only one half, was taken into account. Figure IV.3 illustrates the mesh of the specimen, demonstrating the internal defect repair using an alternative method.

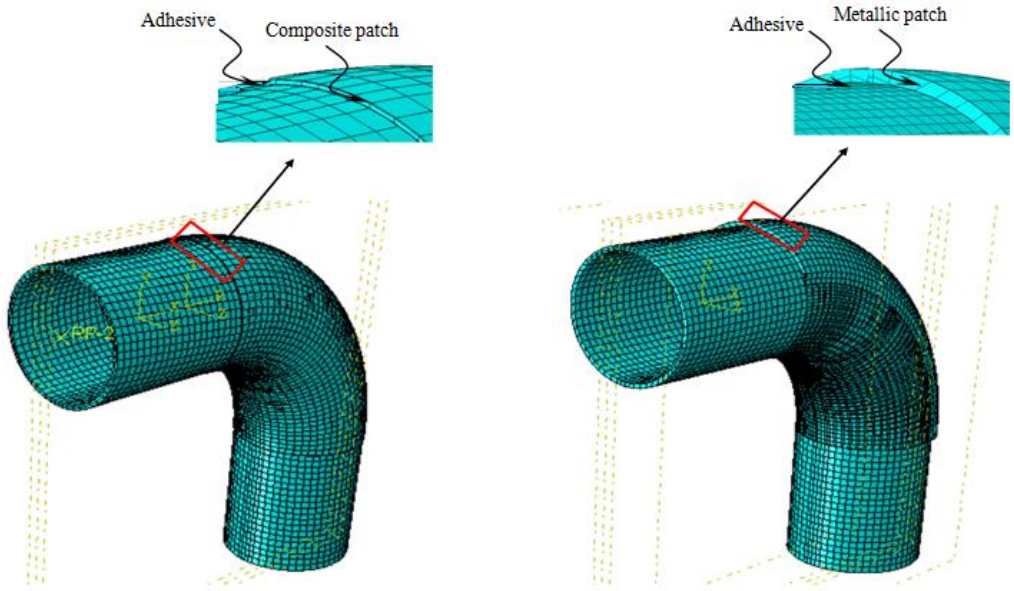

(a) (b)

Figure IV.2: Mesh of elbow with internal defect repair by different method: (a) Composite patch, (b) Metallic patch.

IV.4 RESULTS AND DISCUSSION

Various methods of repairing cracked pipe elbows at 0°, 10°, and 45° angles are examined. These methods involve the application of two types of patches to the damaged pipe elbow, one using composite bonding and the other using a metallic patch. The analysis primarily centers on calculating the critical moment supported by the damaged pipe elbow, employing the finite element approach. This assessment aims to predict the behavior of the pipe elbow and assess the impact of these repair methods on enhancing its critical load-bearing capacity.

IV.4.1 bonding composite rolling

The standards ISO/TS 24817 [1] and ASME PCC-2 [2] do not specifically address defects that resemble cracks. However, suppose it can be demonstrated through a defect assessment procedure that such a defect will not propagate further. In such instances, a composite repair can

fortify and bolster the affected region. Composite repairs are frequently employed to remedy surface cracks and prevent leakage. In numerous scenarios, employing composite repairs for crack-like defects may not impede further crack propagation [1, 2]. There are no restrictions on the materials or fiber-resin configurations utilized. Generally, composite repair systems employ one of the following combinations: (Fibers—Aramid, Carbon, Glass) and (resin—Epoxy, Polyurethane). Both ISO/TS 24817 and ASME PCC-2 standards encompass these material combinations [1, 2].

The standards refrain from using the terms "temporary" or "permanent" due to their potential ambiguity. Instead, the duration of the repair's effectiveness is determined by the end user, forming the basis for the repair design. Both standards specify a maximum lifetime of 20 years [1, 2]. The repair is engineered to endure this designated period, implying that, upon reaching the end of its service life, the end user must either replace the repaired section or evaluate the condition of the repair for potential extension.

The core components for design consideration include the composite structure, surface preparation procedure, and substrate. When addressing internal defects and through-wall defects, applying a composite repair won't impede internal corrosion. Therefore, it's prudent to anticipate continued internal defect propagation throughout the design lifespan. Conversely, for external defects, a composite repair application can effectively halt further corrosion. The incorporation of qualification test data is vital for informing the repair design process.

IV.4.1.2 Proposal solution

For structural repairs in areas containing internal defects or impacted regions, bonded composite patches are suggested to inhibit their propagation. These areas typically fall within the 0° to 45° range. The present investigation aims to bolster elbow strength by employing composite patches to delay damage initiation. Detailed discussions are provided on the ideal patch features, such as geometry, ply count, ply orientations, and structural positioning, aiming to mitigate stress concentration within specific regions. Figure IV.3 shows a composite repair system being applied on the pipeline. 1 and 2 show the fiber reinforcement sleeve polymer and interlayer adhesive respectively. 3 show the infill (resin) that binds the composite to the pipeline. While 4 shows the defect.

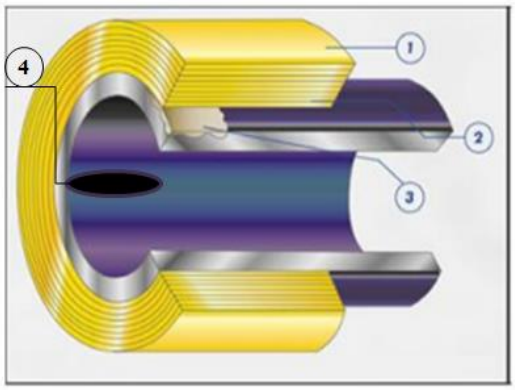

Figure IV.3: Composite wrap process [3].

IV.4.1.2.1 Effect the number of plies

The composite patch significantly extends the structure's lifespan by increasing the critical moment (refer to Figure IV.4). When the defect is positioned at 0°, the composite patch boosts the critical moment by 14%, 30%, and 50% with 2, 4, or 8 composite bondings, respectively. Similarly, at a 10° defect angle, critical moment enhancement is 10%, 17%, and 64% with 2, 4, and 8 composite bondings, respectively. Notably, no failures occur in the elbow with an 8-composite bonding patch at a 45° defect angle.

Moreover, Figure IV.4 indicates that the critical moment is consistently lowest with two composite bondings across all defect positions. When the defect is at 0°, four composite bondings outperform other configurations in enhancing the critical moment. However, across all specimens analyzed, employing eight composite bondings emerges as the most effective method for increasing the critical moment of the pipe elbow.

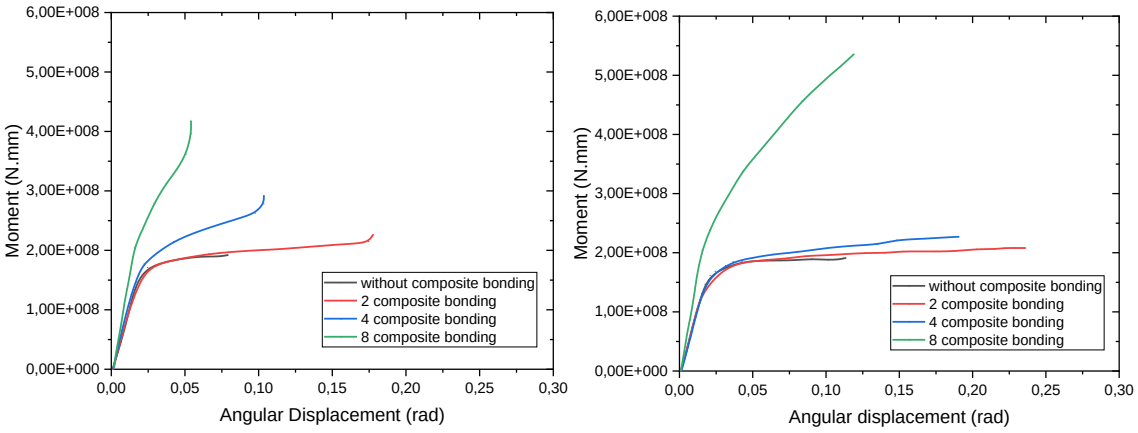

(a) (b)

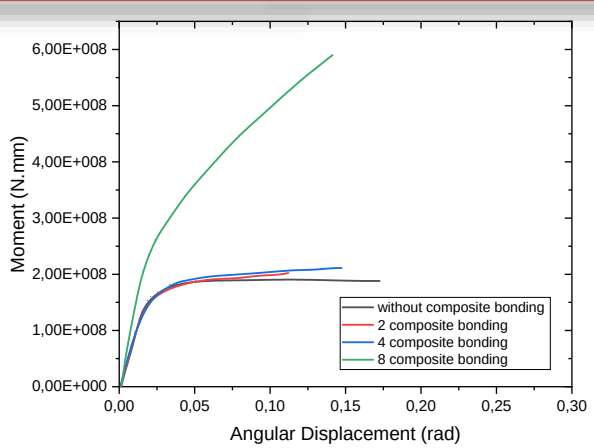

(c)

Figure IV.4 : Bending moment versus angular displacement of elbow repaired by composite patch (a) position 1 with default of 0°, (b) position 2 with default of 10° and(c) position 3 with default of 45°.

Within this section, we examine the pivotal defect positions on the elbow, which span the range of [0°, 10°, 45°]. Illustrated in Figure IV.5, both the critical moment and the associated rotation are contingent on the number of layers (*N*). To establish a more precise correlation, this connection is articulated through the subsequent three-degree equation. The equations are outlined as follows:

Position θ = 0°

$$f(M^*) = 8\cdot10^6 N^3 - 4\cdot10^7 N^2 + 8\cdot10^7 N + 1\cdot10^8 \quad \textbf{(IV.1)}$$

$$f(r^*) = 0,0317N^3 - 0,275N^2 + 0,7033N - 0,39 \quad \textbf{(IV.2)}$$

Position θ= 10°

$$f(M^*) = 5\cdot10^7 N^3 - 3\cdot10^8 N^2 + 5\cdot10^8 N - 1\cdot10^8 \quad \textbf{(IV.3)}$$

$$f(r^*) = 0,02N^3 - 0,2N^2 + 0,58N - 0,29 \quad \textbf{(IV.4)}$$

Position θ= 45°

$$f(M^*) = 6\cdot10^7 N^3 - 4\cdot10^8 N^2 + 7\cdot10^8 N - 2\cdot10^8 \quad \textbf{(IV.5)}$$

$$f(r^*) = -0,0217N^3 + 0,18N^2 - 0,4583N + 0,48 \quad \textbf{(IV.6)}$$

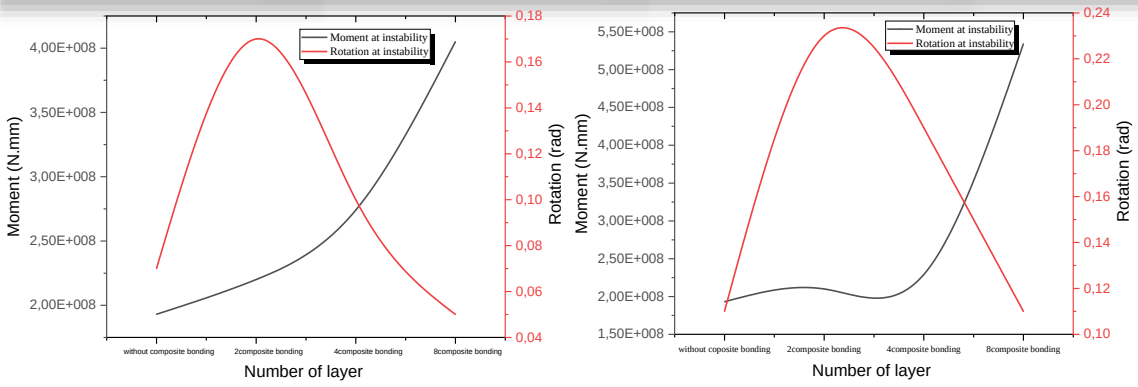

(a) (b)

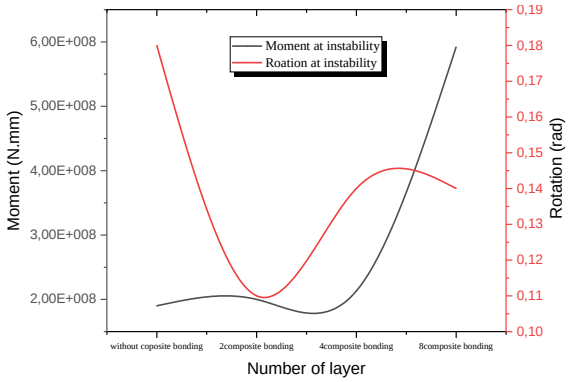

(c)

Figure IV.5: Rotation-moment versus Number of layer for different critical position of defect a) 0° b) 10° c) 45°.

IV.4.1.2.2 Effect of the patch type

The choice of composite reinforcement is a sensitive issue. Various types of reinforcement exist, with the primary ones being carbon/epoxy and boron/epoxy.

Table IV.3: Mechanical properties of composite patches .

	Young's modulus (GPa)			Shear modulus (GPa)			Poisson's ratio			Thermal expansion		
	E_1	E_2	E_3	G_{12}	G_{13}	G_{23}	υ_{12}	υ_{13}	υ_{23}	α_{12} (10^{-6})	α_{12} (10^{-6})	α_{12} (10^{-6})
Bore/Epoxy	200	25	25	7.20	5.5	5.5	0.21	0.21	0.21	4.5	23	23
Carbon/Epoxy	112	8.20	8.20	4.5	4.5	4.5	0.3	0.3	0.4	-1.2	34	34
Glasse/Epoxy	50	14.5	14.5	2.56	2.56	2.24	0.33	0.33	0.33	5.5	15	15

Figure IV.6 depicts the progression of bearing capacity or ultimate load for cracked elbows post-repair using three distinct configurations of composite patches. It's apparent that the choice of composite patch significantly impacts moment values. Boron/epoxy displays superior crack repair efficacy compared to carbon/epoxy and graphite/epoxy. The limit moment sees an increase of approximately 59% when the defect is situated at 0°, while it rises by about 62% and 32% with defects at 10° and 45°, respectively. Considering these advantages, boron/epoxy will be utilized for the remainder of the numerical investigation.

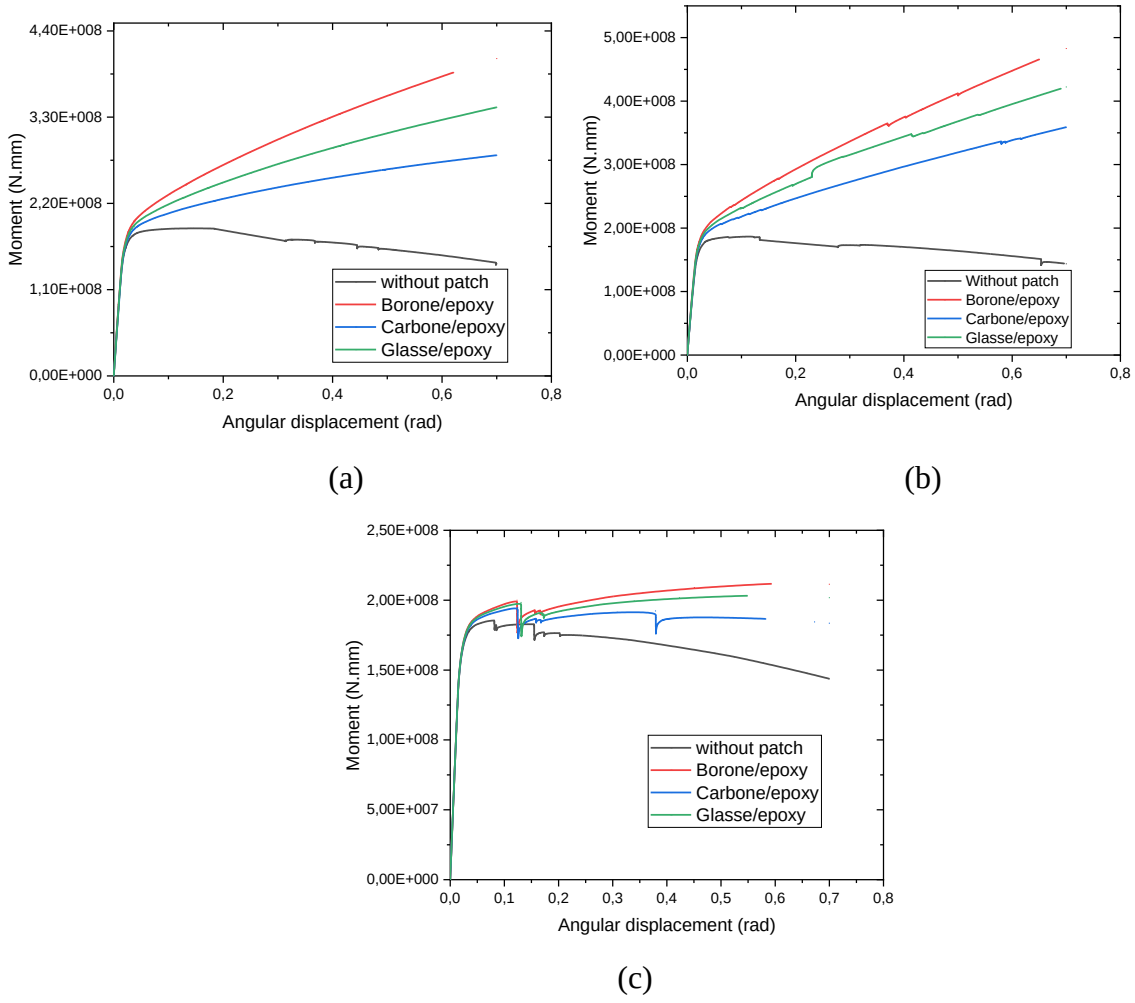

Figure IV.6: Moment vs. end angular rotation with different patch material (a) position 1 with defect at 10°, (b) position 2 with defect at 10° and(c) position 3 with defect at 45°.

IV.4.1.2.3 Effect of the patch thickness on the elbow failure

Figure IV.7 presents a summary of the impact of composite bonding thickness on bearing capacity. The findings highlight the substantial influence of composite bonding thickness on the limit moment. A greater thickness of composite bonding correlates with an increased bearing capacity. Notably, the difference in the limit moment is approximately 10% when the defect is situated at 0°, and this discrepancy rises to about 50% and 14% with defects at 10° and 45°,

respectively. Examining this Figure indicates that enhancing the wrap thickness results in a corresponding augmentation of the limit moment.

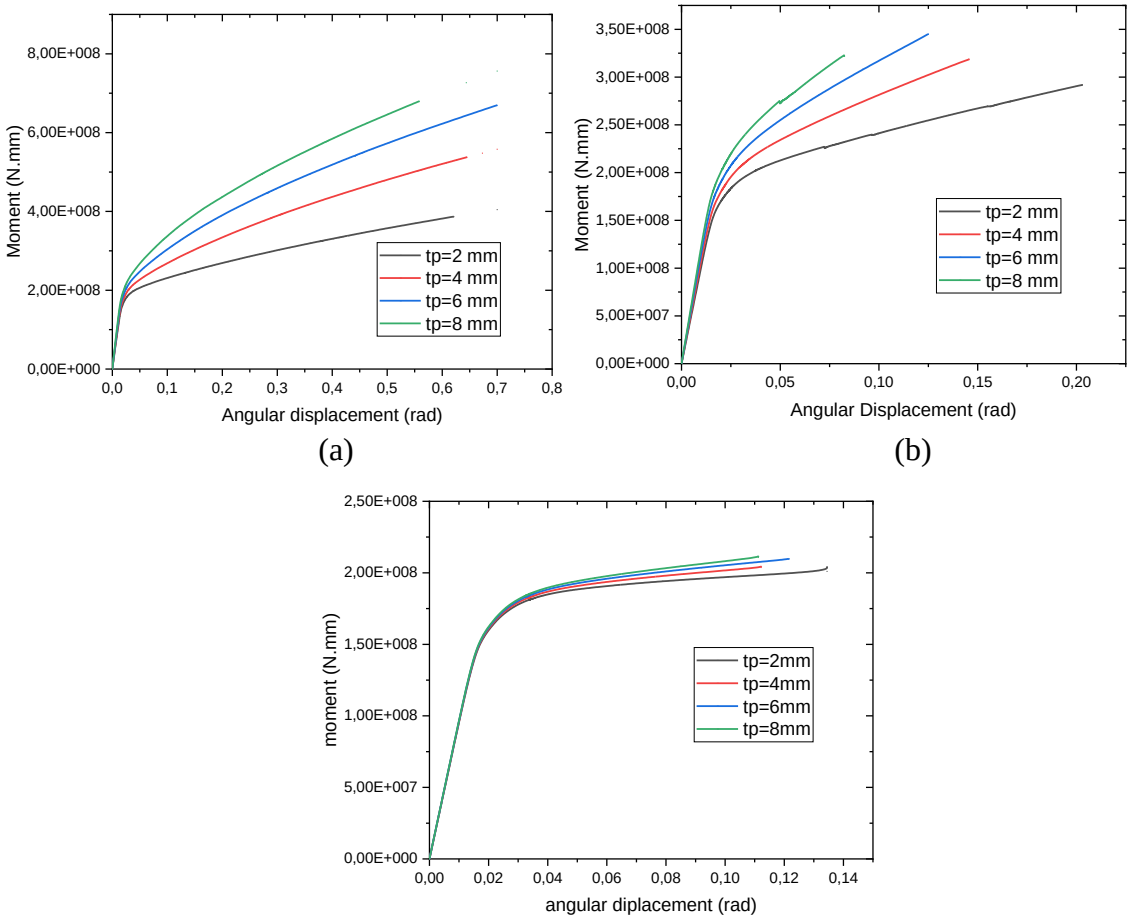

Figure IV.7: Moment vs. end rotation angle with different patch thickness.(a) position 1 with defect at 10°, (b) position 2 with defect at 10° and(c) position 3 with defect at 45°.

This section focuses on investigating the critical defect location within the elbow, which varies from [0°, 10°, 45°]. As depicted in Figure IV.8, the limit moment and corresponding rotation are influenced by the thickness of the composite patch(t_p). To establish a more accurate correlation, a three-degree equation is employed:

Position θ = 0°

$$f(M^*) = -2\cdot10^6 t_p^3 + 2\cdot10^7 t_p^2 - 2\cdot10^6 t_p + 3\cdot10^8 \quad \textbf{(IV.7)}$$

$$f(r^*) = -0,0046 t_p^3 + 0,0587 t_p^2 - 0,2142 t_p + 0,85 \quad \textbf{(IV.8)}$$

Position θ= 10°

$$f(M^*) = -1\cdot10^6 t_p^3 + 1\cdot10^7 t_p^2 - 3\cdot10^7 t_p + 3\cdot10^8 \quad \textbf{(IV.9)}$$

$$f(r^*) = -0,0012t_p^3 + 0,02t_p^2 - 0,115t_p + 0,36 \quad \textbf{(IV.10)}$$

Position θ= 45°

$$f(M^*) = -145833t_p^3 + 2\cdot10^6 t_p^2 - 9\cdot10^6 t_p + 2\cdot10^8 \quad \textbf{(IV.11)}$$

$$f(r^*) = -145833t_p^3 + 2\cdot10^6 t_p^2 - 9\cdot10^6 t_p + 2\cdot10^8 \quad \textbf{(IV.12)}$$

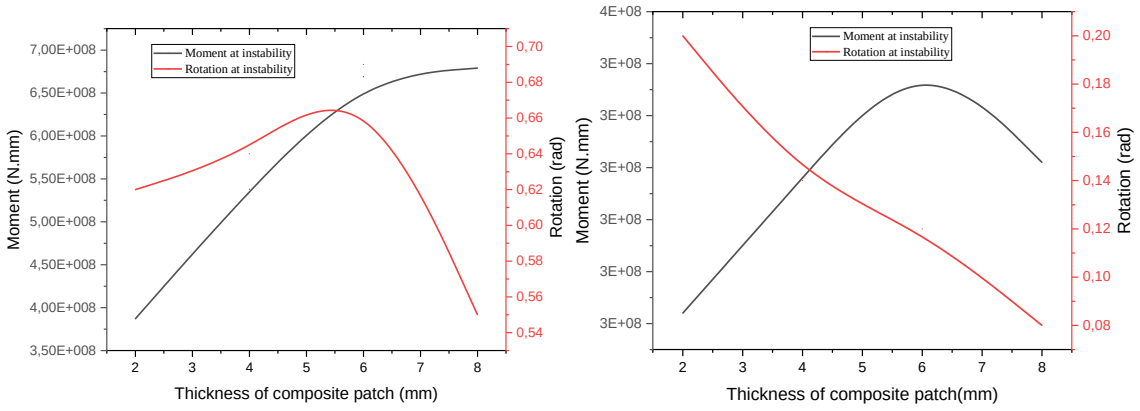

(a) (b)

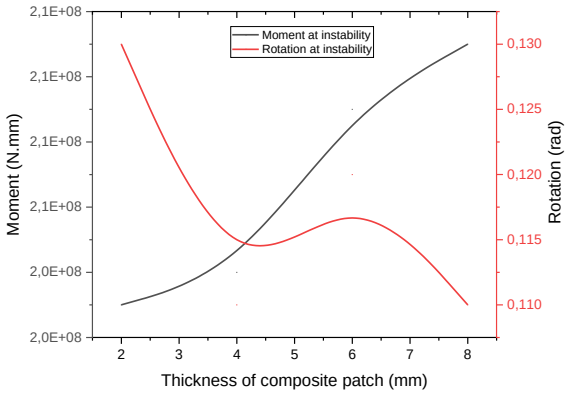

(c)

Figure IV.8: Rotation-moment versus thickness of composite patch for different critical position of defect. a) 0°, b) 10°, c) 45°.

IV.4.1.2.4 Effect thickness of adhesive

The adhesive layer holds significant importance in the repair method for cracked elbows as its effectiveness relies on both its geometry and material characteristics. Its primary role involves transferring the load from the crack to the composite materials (patch). Figure IV.9 demonstrates the impact of adhesive thickness on the bearing capacity variation of pipe elbows with defects positioned at 0°, 10°, and 45°. The considered adhesive thicknesses are 0.2 mm, 0.4 mm, 0.6 mm, and 0.8 mm, respectively.

Observing Figure IV.9 reveals that reducing the adhesive thickness leads to a decrease in the bearing capacity of the pipe elbow. This indicates that thinner adhesives improve the load transfer to the composite patch. Consequently, this study suggests that employing thin adhesives is advisable for reinforcing damaged specimens.

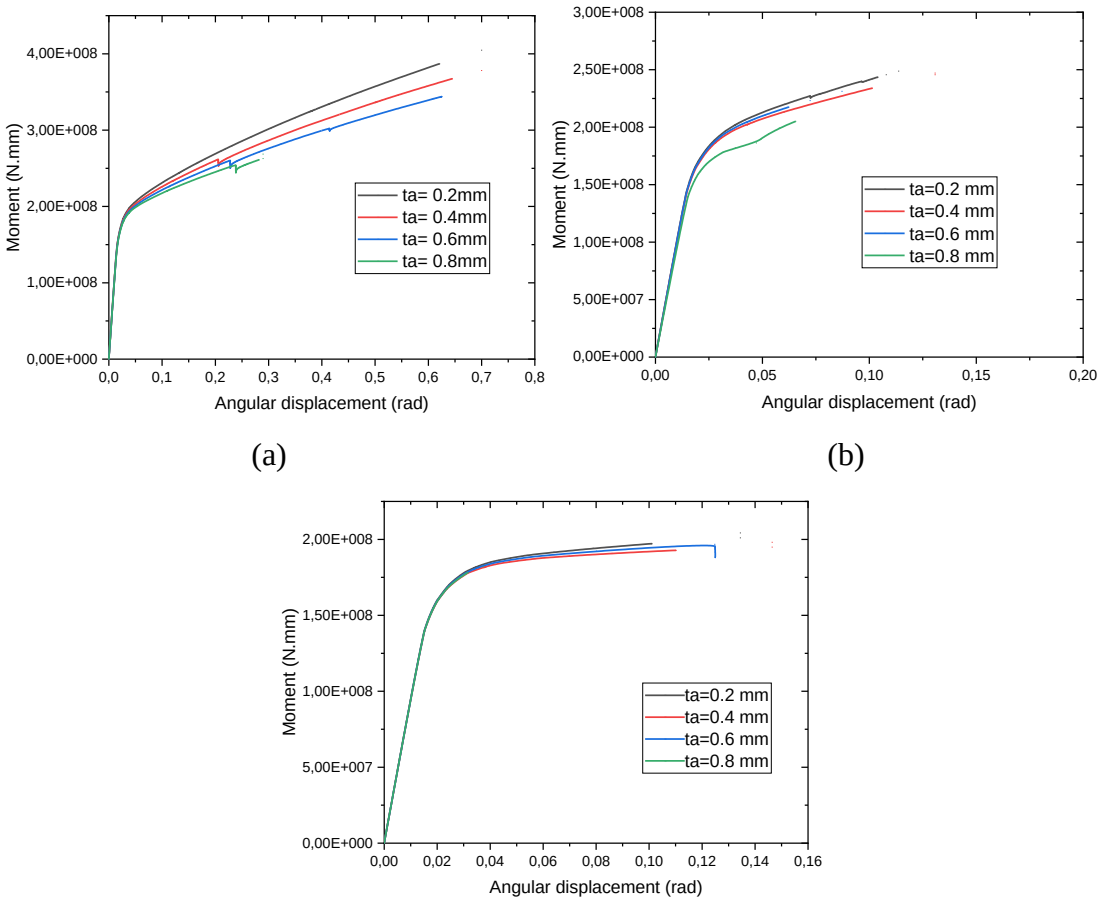

Figure IV.9: Moment vs. end rotation angle with different thickness of adhesive.(a) position 1 with defect at 10°, (b) position 2 defect at 10° and (c) position 3 with defect at 45°.

This section discusses the critical positioning of defects on the elbow, which varies between 0°, 10°, and 45°. As depicted in Figure IV.10, the critical moment and the corresponding rotation are influenced by the adhesive thickness (t_a). To achieve a more accurate correlation, the following three-degree equation is defined. The equations are as follows:

Position θ = 0°

$$f(M^*) = 1\cdot10^9 t_a^3 - 2\cdot10^9 t_a^2 + 1\cdot10^9 t_a + 7\cdot10^7 \quad \textbf{(IV.13)}$$

$$f(r^*) = 5{,}8333 t_a^3 - 11 t_a^2 + 6{,}6667 t_a - 0{,}66 \quad \textbf{(IV.14)}$$

Position θ= 10°

$$f(M^*) = 2\cdot10^9 t_a^3 - 3\cdot10^9 t_a^2 + 1\cdot10^9 t_a + 4\cdot10^7 \quad \textbf{(IV.15)}$$

$$f(r^*) = 3,3333 t_a^3 - 5 t_a^2 + 2,2667 t_a - 0,22 \quad \textbf{(IV.16)}$$

Position θ= 45°

$$f(M^*) = -6\cdot10^8 t_a^3 + 8\cdot10^8 t_a^2 - 3\cdot10^8 t_a + 2\cdot10^8 \quad \textbf{(IV.17)}$$

$$f(r^*) = -2,0833 t_a^3 + 2,5 t_a^2 - 0,8667 t_a + 0,19 \quad \textbf{(IV.18)}$$

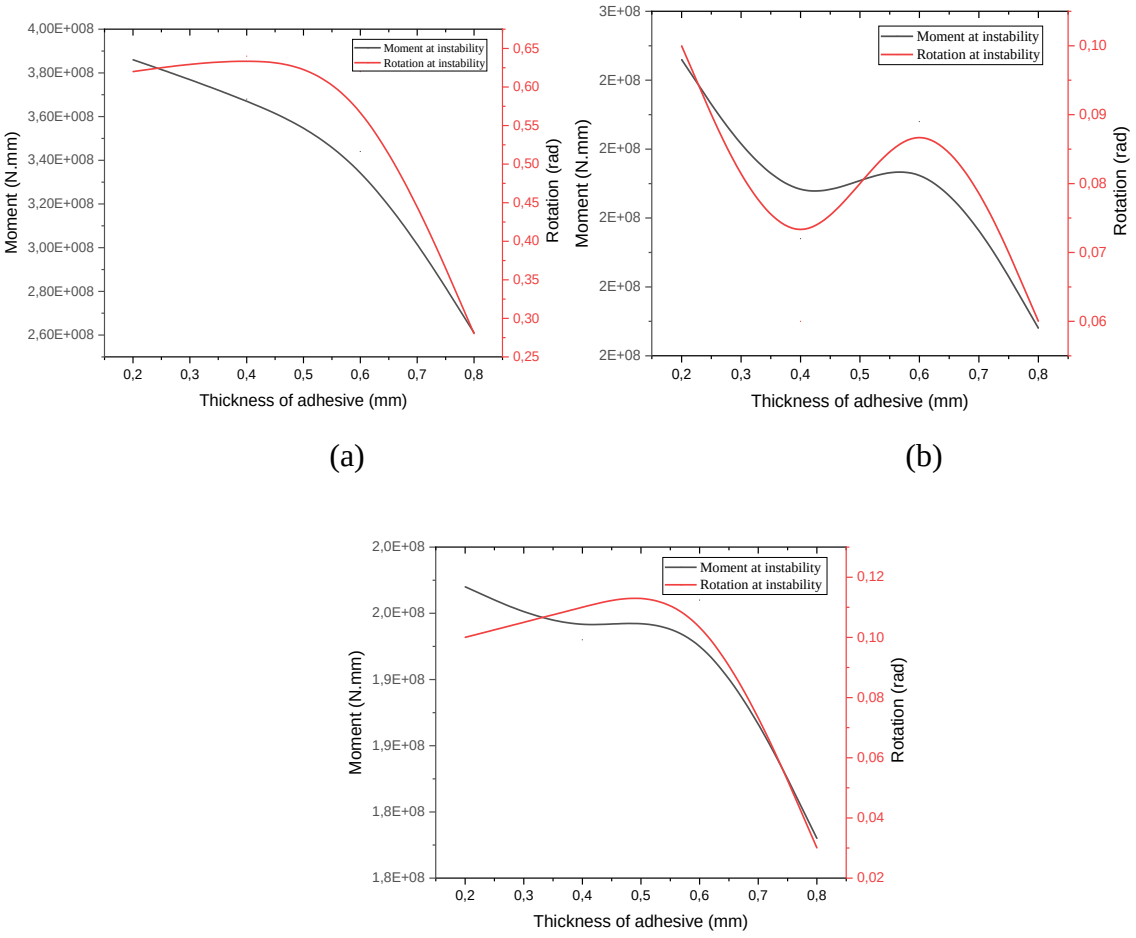

Figure IV.10: Rotation-moment versus thickness of adhesive for different critical position of defect .a) 0° b) 10°, c) 45°.

IV.4.2 Metallic patch

More accidents, such as pipeline leakage, are frequently encountered and require online repairs during service. Pipe leaks are typically addressed by welding a sleeve-like patch on-site.

IV.4.2.1 The effect of metallic patch on the limit load of cracked pipe elbow

In order to examine the impact of a metallic patch on the critical moment of a pipe elbow containing a single defect positioned at three distinct angles (θ = 0°, 10°, 45°), Figure IV.11 illustrates the relationship between reaction moment and angular displacement across various elbows with defects at θ = 0°, 10°, 45°. This visual representation reveals notable alterations in the critical moment of the pipe elbow subsequent to the application of a metallic patch. Specifically, the introduction of a metallic patch results in a 24% augmentation in the critical moment when the defect is situated at 0°, a 30% increase when the defect is at 10°, and a 36% rise when the defect is located at 45°.

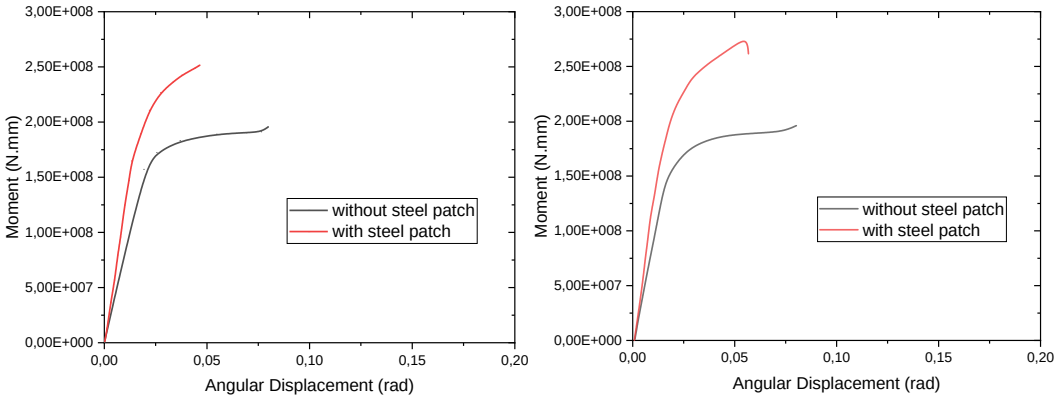

(a) (b)

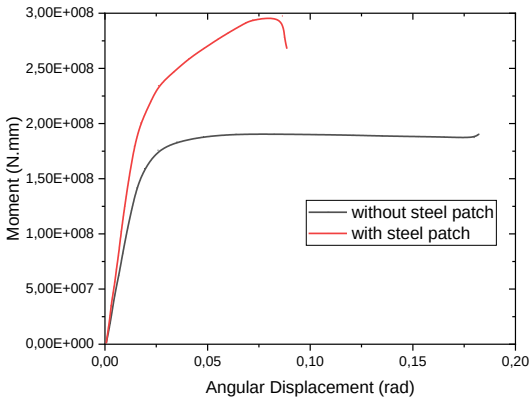

(c)

Figure IV.11. bending moment versus angular displacement of elbow repaired by metallic patch (a) position 1 with defect at 10°, (b) position 2 defect at 20° and(c) position 3 with defect at 45°.

IV.4.2.2 Effect the thickness metallic patch

Figure IV.12 depicts the influence of patch thickness on the bearing capacity of a pipe elbow exhibiting defects at three distinct positions (0°, 10°, and 45°). It is evident that augmenting the patch thickness leads to an increase in the critical moment for the pipe elbow. Specifically, notable enhancements in the critical moment are observed: approximately 7% when the defect is situated at 0°, and 22% and 8% when the defect is positioned at 10° and 45°, respectively. The degree of critical moment enhancement is not solely determined by the patch thickness but also by its material composition. This underscores the significance of selecting an appropriate thick patch to optimize performance.

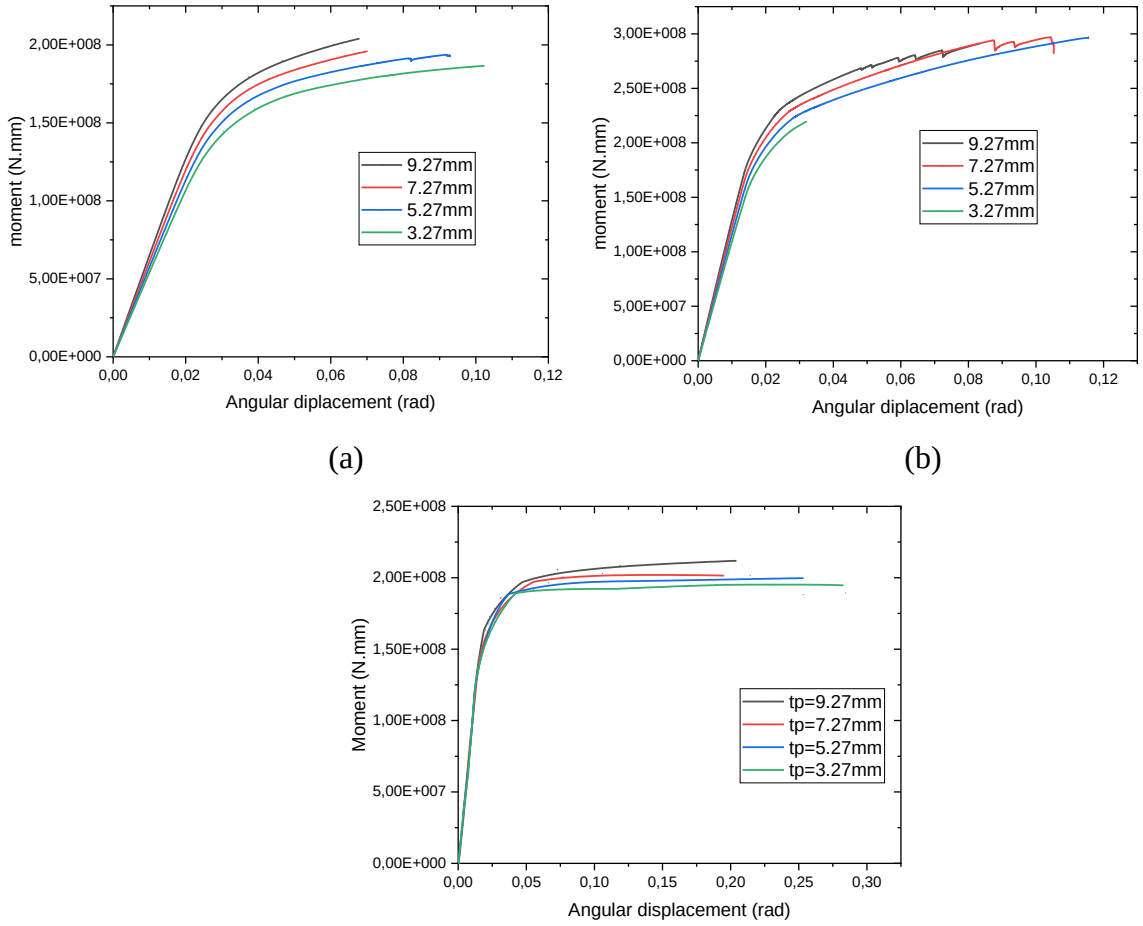

Figure IV.12: Moment vs. end rotation angle with different thickness of adhesive.(a) position 1 with defect at 10°, (b) position 2 with defect at 10° and(c) position 3 with defect at of 45°.

According to Celso Cruz et al. [4], the utilization of metallic patch repairs has demonstrated the continued effectiveness of steel patch adhesion, effectively stalling crack propagation while maintaining structural integrity. This method prolongs the operational lifespan of rehabilitated pipelines. By accounting for variables such as crack dimensions, internal pressure, stress distribution, and strain analysis, adhesive technology emerges as a viable recommendation for the

efficient and secure repair of API pipelines afflicted with diverse defects, including surface cracks or minor external corrosion. This approach presents a cost-effective solution within the realm of API pipeline maintenance, ensuring the structural integrity of pipelines under internal pressure.

This section delves into the critical defect positions along the elbow, spanning from 0° to 45°. As illustrated in Figure IV.13, both the limit moment and corresponding rotation are influenced by the thickness of the metallic patch (t_p). To establish a more precise correlation, the following three-degree equation is defined:

Position θ = 0°

$$f(M^*) = 250000t_p^3 - 5\cdot10^6 t_p^2 + 3\cdot10^7 t_p + 1\cdot10^8 \quad \textbf{(IV.19)}$$

$$f(r^*) = 0,0004t_p^3 - 0,0078t_p^2 + 0,0387t_p + 0,0426 \quad \textbf{(IV.20)}$$

Position θ = 10°

$$f(M^*) = 1\cdot10^6 t_p^3 - 3\cdot10^7 t_p^2 + 2\cdot10^8 t_p - 2\cdot10^8 \quad \textbf{(IV.21)}$$

$$f(r^*) = 0,0015t_p^3 - 0,0343t_p^2 + 0,2517t_p - 0,4774 \quad \textbf{(IV.22)}$$

Position θ= 45°

$$f(M^*) = 208333t_p^3 - 4\cdot10^6 t_p^2 + 2\cdot10^7 t_p + 2\cdot10^8 \quad \textbf{(IV.23)}$$

$$f(r^*) = 0,0021t_p^3 - 0,0367t_p^2 + 0,1823t_p + 0,0034 \quad \textbf{(IV.24)}$$

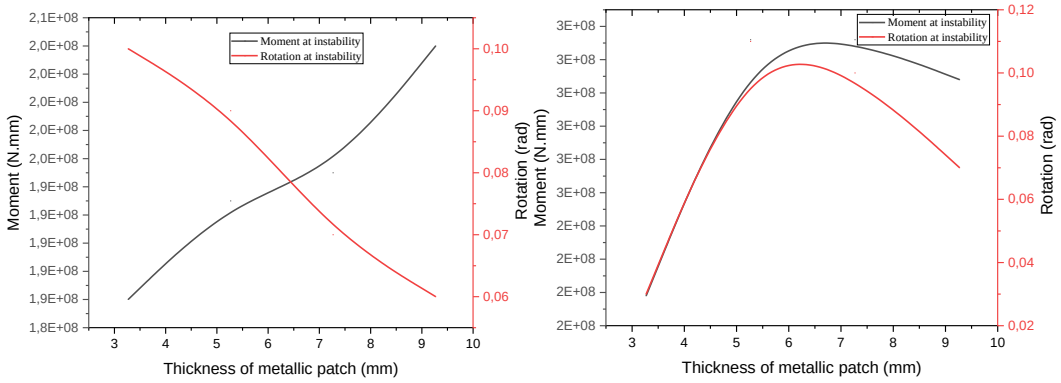

(a) (b)

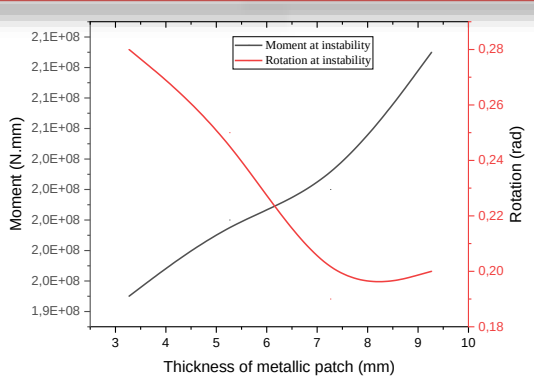

(c)

Figure IV.13: Rotation-moment versus thickness of metallic patch for different critical position of defect .a) 0°, b) 10°, c) 45°.

IV.4.3 Comparison between composite patch and metallic patch

In this section of the investigation, we conducted a comparative analysis between two techniques for repairing damaged elbows, with the aim of evaluating the disparity in the enhancement of the limit load for each scenario. The objective was to ascertain the superior method among composite patch and metallic patch repairs.

Figure IV.14 demonstrates that, across all defect positions, repairing with a composite patch surpasses the effectiveness of the metallic patch approach. The improvement in the limit load between these two repair methods varies by 49.6%, 39.8%, and 0.4% for the three critical defect positions of 0°, 10°, and 45°, respectively. Additionally, the composite repair displays considerably greater displacement values compared to the metallic method, attributed to the superior mechanical properties of the composite material.

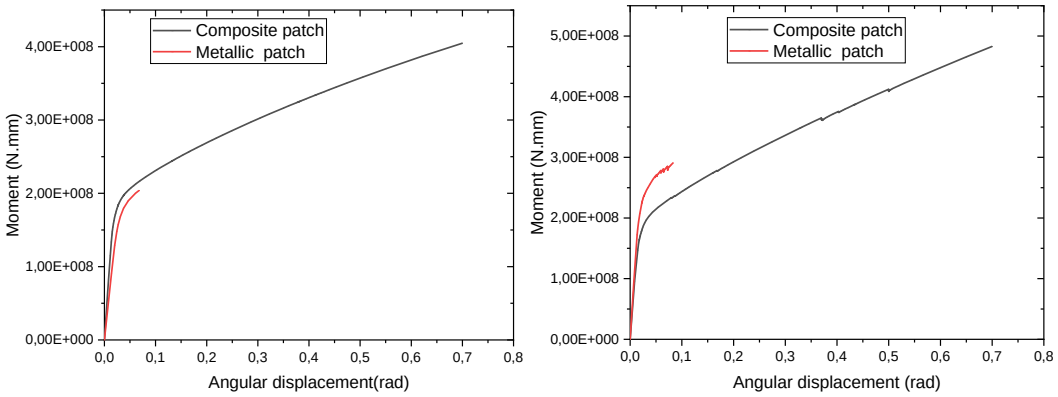

(a) (b)

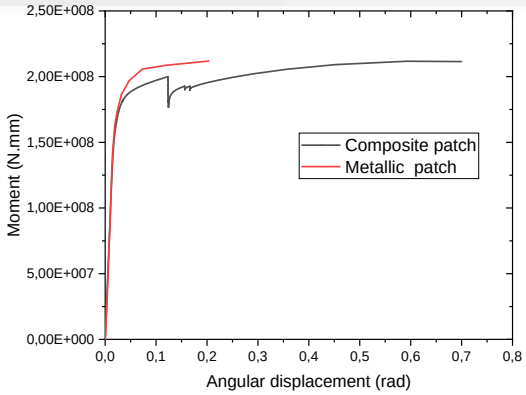

(c)

Figure IV.14: comparison between repair by composite and metallic patch .(a) position 1 with defect at 0°, (b) position 2 with defect at 10° and(c) position 3 with defect at of 45°.

IV.5 CONCLUSION

The numerical study presented effectively describes the behavior of defected pipe elbows at three critical positions, repaired using two methods. The first method involves simply adhering a composite patch to the damaged elbow to improve its resistance. The second technique proposes attaching a metallic patch to the damaged elbow to enhance its limit load. Utilizing the deflection load curve based on instability and collapse load provides reliable results. Repairing defected structures improves the limit load of the defected elbow. The defect's position significantly influences the repair's effectiveness, with the critical moment being smallest when employing two composite bondings. When the defect was at 0°, using four composite bondings yielded a higher enhancement of the critical moment compared to other positions. The most effective method for enhancing the pipe elbow's critical moment was repairing it with eight composite bondings. The metallic patch repair method also significantly enhanced the pipe elbow's critical moment for various defect positions. This study demonstrates that repairing structures using composite bonding is an effective and reliable method for significantly increasing the lifespan of damaged structures.

REFERENCES

[1] ISO/TS 24817:2006: Petroleum, petrochemical and natural gas industries - composite repairs for pipework - qualification and design, installation, testing and inspection. Standard; International Organization for Standardization, Geneva, Switzerland; 2006.

[2] PCC, A.J.N.Y., USA, Repair of pressure equipment and piping. 2006.

[3] Shamsuddoha, M., M.M. Islam, T. Aravinthan, A. Manalo and K.T. Lau, Effectiveness of UsingFibre-Reinforced Polymer Composites for Underwater Steel Pipeline Repairs 2013.

[4] Cruz, C., Vargas, B., Capula, S., Terán, G., Guzmán, I., & Granda, E. Experimental and finite element analysis of a damaged API5L X52 pipeline with longitudinal crack repaired by adhesively bonded metallic patch. Journal of Adhesion Science and Technology, 2021, 35(11):1170-1184.

CONCLUSIONS

CONCLUSIONS

Elbows are widely used in industrial piping systems and power plants due to their flexible mechanical behavior compared to straight pipes, which are more prone to pressure, stresses, and cross-sectional deformation known as "ovalization." Elbows can absorb thermal expansions and other externally induced loads, making them essential components for maintaining the structural integrity of piping systems.

- This study effectively demonstrates the impact of damage using the extended finite element method, considering complex geometric and loading conditions in steel API 5L X60 structures connected by elbows. The findings provide valuable insights into the influence of defect positions on instability and collapse moments:
- The presence of defects exacerbates damage, with their location and the applied bending moment mode playing significant roles. Internal pressure in tubular structures counteracts ovalization during bending moment loading.
- Tubular structures are more susceptible to damage under opening bending moments compared to closing bending moments.
- The relationship between the defect's position and collapse and instability moments exhibits a nonlinear pattern.
- The weakening factor exhibits contrasting trends between opening and closing bending moments, depending on the defect's position.

Regarding the results of the effect of temperature on damage under combined pressure and opening bending moments in steel X60 structures with an elbow, the following conclusions can be drawn:

- The results obtained in this study confirm the findings of a previous study conducted in a soil environment. They found that the X60 steel elbow becomes brittle at room temperature and has a lower load-bearing capacity.
- At low temperatures, the X60 steel elbow exhibits brittle behavior with a maximum limit load. In contrast, at high temperatures, the elbow displays ductile behavior with a minimum limit load compared to low temperatures.
- Temperature plays a significant role in influencing and exacerbating the structural degradation of the pipe elbow resulting from the accumulation of mechanical loads.
- The X-FEM technique, in the numerical prediction of structural damage, enables accurate simulation of the initiation and propagation of cracks under combined loading conditions involving temperature and pressure.

Finally, aggressive flow within a structure has a detrimental effect on its resistance, leading to accelerated damage. This effect becomes more pronounced when considering the temperature conditions of the surrounding environment.

There are various methods for repairing defective pipe elbows, involving two types of repairs: composite bonding and metallic patch. This analysis calculates the limit moment sustained by the defected pipe elbow using the finite element method and studies the enhancement of the limit moment after reparation. The main research results are as follows:

- The study found that the repaired pipe elbow showed an improvement in the critical moment compared to the unrepaired pipe. However, the position of the defect played a significant role in determining the effectiveness of the repair method. Specifically, when two composite bondings were used, the critical moment was found to be the smallest. However, when the defect was located at position 0°, the repair using four composite bondings resulted in a higher enhancement of the critical moment compared to other positions. Overall, the most effective method for enhancing the critical moment of the pipe elbow was found to be repairing it with eight composite bondings.
- The metallic patch repair method was also found to significantly enhance the critical moment of the pipe elbow, considering different positions of the defect.
- When comparing the two methods, the study concluded that repairing with a composite patch was more effective than repairing with a metallic patch in terms of enhancing the critical moment of the pipe elbow.

These results provide valuable insights into the effectiveness of different repair methods, considering the position of the defect and the materials used. The findings suggest that using multiple composite bondings and composite patches can lead to significant improvements in the limit moment of the repaired pipe elbow, outperforming the metallic patch repair method.

LIST OF PUBLICATIONS AND COMMUNICATIONS

List of publications

[1] Arroussi, C., Belalia, A., & Hadj Meliani, M. (2024). Numerical analyses on limit load of X60 pipe elbow in different internal corrosion-damaged positions under combined internal pressure and in-plan bending moment. International Journal on Interactive Design and Manufacturing (IJIDeM), 1-11.

[2] Arroussi, C., Belalia, A. & Meliani, M.H. (2024) Temperature effects on the resistance capacity of API X60 pipe elbow under bending moment using X-FEM method. J Mech Sci Technol. https://doi.org/10.1007/s12206-024-0114-0

[3] Arroussi, C., Belalia, A., & Meliani, M. H. (2023). Effects of composite and metallic patch on the limit load of pressurized steel pipes elbow with internal defects under opening bending moment. Structural Monitoring and Maintenance, 10(3), 221.

[4] Arroussi, C., Mouna, A., Meliani, M. H., & Pluvinage, G. (2022). Proposal Engineering Methods to Repair/Replace Bend Elbow Pipe Contain Internal Corrosion Defect. Procedia Structural Integrity, 41, 752-758.

[5] Amara, M., Arroussi, C., Didouh, H., Meliani, M. H., & Pluvinage, G. fracture mechanics computation to estimate the constraint parameters and crack path orientation proračuni mehanike loma za određivanje parametara ograničenja i orijentacije putanje prsline.

List of communications

[1] C.Arroussi, M.Hadj Meliani, G.Pluvinage. Proposal engineering methods to repair/replace bend elbow pipe contain internal corrosion defect. 2 nd Mediterranean conference on fracture, Catania (Italy), February 16, 2022.

[2] Chaaben Arroussi, Belalia Azeddine, Hadj Meliani Mohammed, Damage prediction of steel pipe elbows subjected to bending and pressure loads ,2nd international seminar on industrial engineering and applied mathematics, SKIKDA(Algeria),October 23&24th , 2022

[3] Chaaben Arroussi, Aicha Benchiha, Hadj Meliani Mohammed. La réparation des plaques des différentes entailles avec patch double, 7eme congrès Algérien de Mécanique, Ghardaïa(Algérie) ,23-26 février 2020.

[4] C.Arroussi, Amara.M, Hadj Meliani, A, Maizia, Guy Pluvinage, hydrogen embrittlement effect On the mechanical properties of X60 elbow pipe steel under bending moment using XFEM numerical method, the first national seminar on green hydrogen for the Algerian industrial sector (NSGH-Al'2022).

[5] Chaaben Arroussi , Belalia Azeddine, Hadj Meliani Mohammed, damage under thermomechanical behavior of pipeline structure, the second doctoral symposium on

Technology process, mechanical and electrical engineering, Chlef (Algeria), October 26&27 th 2022

[6] Chaaben Arroussi , Belalia Azeddine, Hadj Meliani Mohammed, Using the X-FEM method to study the temperature effects on the resistance capacity of X60 Elbow Pipe Steel under combined Opening Bending Moment and pressure , the sixth students symposium on engineering application of mechanics, Chlef(Algeria),30&1 st December 2022.